Cleveland State University
EngagedScholarship@CSU

ETD Archive

Summer 8-5-2022

Mechanistic Understanding Of Phase Stability, Transformation, And Strengthening Mechanisms In Lightweight High Entropy Alloys And High Entropy Ceramics

Ganesh Walunj
Cleveland State University

Follow this and additional works at: https://engagedscholarship.csuohio.edu/etdarchive

 Part of the Mechanical Engineering Commons

How does access to this work benefit you? Let us know!

Recommended Citation

Walunj, Ganesh, "Mechanistic Understanding Of Phase Stability, Transformation, And Strengthening Mechanisms In Lightweight High Entropy Alloys And High Entropy Ceramics" (2022). *ETD Archive*. 1337.
https://engagedscholarship.csuohio.edu/etdarchive/1337

This Dissertation is brought to you for free and open access by EngagedScholarship@CSU. It has been accepted for inclusion in ETD Archive by an authorized administrator of EngagedScholarship@CSU. For more information, please contact library.es@csuohio.edu.

MECHANISTIC UNDERSTANDING OF PHASE STABILITY, TRANSFORMATION, AND STRENGTHENING MECHANISMS IN LIGHTWEIGHT HIGH ENTROPY ALLOYS AND HIGH ENTROPY CERAMICS

GANESH WALUNJ

Bachelor of Engineering in Automobile Engineering

Shivaji University

July 2006

Master of Science in Industrial Engineering

The University of Texas at Arlington

August 2010

Submitted in partial fulfillment of requirements

for the degree

DOCTOR OF PHILOSOPHY IN MECHANICAL ENGINEERING

at the

CLEVELAND STATE UNIVERSITY

AUGUST 2022

We hereby approve the dissertation

of

GANESH WALUNJ

Candidate for the Doctor of Philosophy in Engineering degree.

This dissertation has been approved for the specialization of

Mechanical Engineering

and CLEVELAND STATE UNIVERSITY'S

College of Graduate Studies by

Dr. Tushar Borkar - Dept. of Mechanical Engineering 08/05/2022

Dr. David Schwam - Dept. of Mechanical Engineering 08/05/2022

Dr. Petru Fodor - Dept. of Physics 08/05/2022

Dr. Maryam Younessi - Dept. of Mechanical Engineering 08/05/2022

Dr. Prabaha Sikder - Dept. of Mechanical Engineering 08/05/2022

08/05/2022

Student's Date of Defense

This student has fulfilled all requirements for the Doctor of Philosophy in Engineering degree.

Chandra Kothapalli, Doctoral Program Director

ACKNOWLEDGMENT

First and foremost, I would like to offer my most heartfelt appreciation to my adviser, Dr. Tushar Borkar, for his unwavering support of my Ph.D. studies and research, as well as for his patience, drive, passion, and enormous knowledge. For my Ph.D. studies, I could not have had a greater adviser and mentor than Dr. Tushar. His direction was of great use to me throughout the whole of the thesis's research and writing process.

In addition to my primary supervisor, I would like to express my gratitude to the other members of my thesis committee, Professor David Schwam, Professor Petru Fodor, Dr. Maryam Younessi, and Dr. Prabaha Sikder, for their support and insightful observations.

I want to thank my colleagues at Cleveland State University, Anthony Bearden, Amit Patil, Taban Larimian, and Manoj Mugale, for the enjoyable interactions, the late hours spent working on deadlines, and the productive talks we have had over the last four years. My Makerspace Manager, Mr. Matthew Johnson, deserves my gratitude for changing the timetable as needed and for his courteous assistance during my Ph.D. Thanks to my buddies Balu, Amol, Sharma, Jitin, Kulkarni, and Patwardhan for their support. Thank you for all your help.

Finally, I want to thank my family, including my parents, my brother Bharat, and my sisters, Seema and Meena, for their support and encouragement. Throughout my Ph.D. journey, my daughter Ovi and my wife Sharmishtha have been a source of inspiration and support. I would want to take this opportunity to thank them both.

MECHANISTIC UNDERSTANDING OF PHASE STABILITY, TRANSFORMATION, AND STRENGTHENING MECHANISMS IN LIGHTWEIGHT HIGH ENTROPY ALLOYS AND HIGH ENTROPY CERAMICS

GANESH WALUNJ

ABSTRACT

High-entropy alloys (HEAs) are a novel family of solid-solution alloys that have gained international interest due to their exceptional characteristics. Because of the need from the transportation and defense sectors, lightweight HEAs have attracted researcher's curiosity as prospective advanced materials. Low-weight high entropy alloy synthesizes using arc melting with a mass ratio of $AlCrFeMnTi_{x(0.1,0.15,0.2)}$. The synthesized HEA is comprised of a mixture of body center cubic (bcc) and ordered bcc (L21) solid solution phases. The synthesized HEAs have heat treated at 650C, 800C, and 1150C for 1hr, 4hr after solutionized at 1150C for 2 hr to understand the effect of temperature evaluation in these HEAs. To investigate the role of titanium in improving the strengthening of $Al_{1.5}CrFeMnTi_{x(x=0.1,0.15,0.2)}$ and tailor the mechanical properties via studying strengthening precipitation mechanisms. The results show that the density of the alloy is 5.88 g cm-3, which fulfills the criteria of low-weight HEA; also, from the XRD, the BCC+ L21 phases are available inside the HEA Composition matrix.

Ultra-high temperature ceramics (UHTCs) consist of different ceramics like boride, carbide, diboride, and nitride of the transition metals. The UHTCs show prominent characteristics such as higher melting point, higher oxidation resistance, lower thermal conductivity, higher yield strength, and microhardness. High entropy ceramic (HEC) is a multi-component alloy similar to the high entropy alloy (HEA) specifically developed for

hypersonic vehicles, nuclear reactors, and high temperature applications. In the current study, mechanical alloying(MA) and spark plasma sintering(SPS) were used to develop equiatomic HEC (Hf0.2Nb0.2Ta0.2Ti0.2Zr0.2)N. The HECs were mechanically alloyed using the high-energy ball mill at 500 RPM for 6 hours. The ball to powder (BPR) ratio of 10:1 was maintained during the milling. This mechanically alloyed powder was sintered using SPS for 1800°C, 1900°C, and 2000°C to investigate the effect of temperature on the densification of these HECs. The consolidated samples were further analyzed using SEM, microhardness, XRD, and wear testing to understand the effect of different sintering temperatures on microstructure, phase transformation, and mechanical and tribological behavior of these high entropy nitride ceramics. Oxidation treatments have been performed at 1000°C-1200°C for 2 hours duration.

TABLE OF CONTENTS

Page

LIST OF TABLES

LIST OF FIGURES

Figure Page

CHAPTER I

INTRODUCTION

1.1 Introduction Low Weight High Entropy Alloy

Alloying is the process of mixing metal with one or more additional elements to achieve desired properties. The exploration of new materials like copper, tin, silver, and gold started during the formation of civilized society, and today we can find a different set of materials and their alloys. Michael Ashby illustrated the evolution of material science from 10,000 BC to the current date, as shown in figure 1, "Material section in mechanical design" [1]. The figure shows how the material evolved from the Stone Age, Bronze Age, Iron age till today's age of molecular engineering. The arsenal bronze alloy was discovered accidentally due to fire in the Cave, where copper mixed with arsenic, zinc, and tin. Several different elements were discovered during the industrial revolution that started in the early 18th century. Stainless steel was also discovered by accident because it has been in use for a long time, although carbon as a distinct element was recognized recently. After such significant discoveries, different metal combinations were used to produce alloys with different processing techniques.

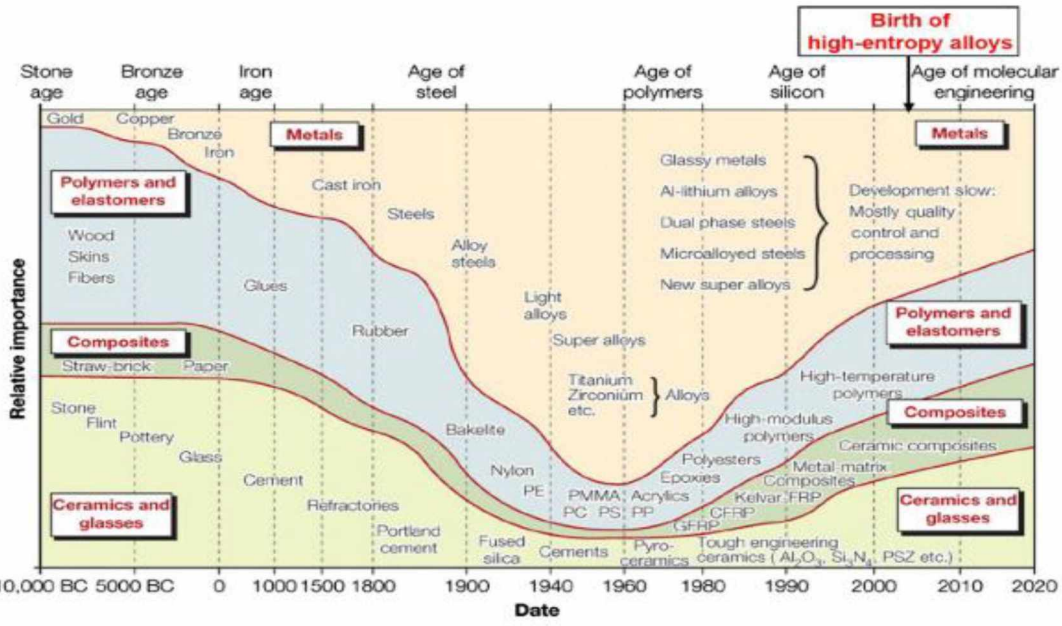

Figure 1 1 Engineering materials' historical development[1]

In the last five decades, extensive research has been conducted in the material science field. The researcher has developed modern alloy systems, intermetallic, metallic glasses, quasicrystal, and composites with specific compositions and processes according to applications. The intermetallic system consists of two or more elements in the compound, and are referred to as solute and solvent. The intermetallic materials developed from nickel (Ni), aluminum (Al), iron (Fe), and titanium (Ti) can be used in aerospace, automobile, and structural applications. Klement et al.[2] observed the Au75Si25 metallic glass when the material rapidly cooled before crystallization, a non-crystalline structure formed called a metallic glass structure. The composites are a combination of metal, and polymer, or metals and ceramics, and it was developed to avoid the limitation of the individual element. Different metal matrix composite (MMC) like Nickel-titanium carbide (Ni-TiC) [3] and low-density materials like aluminum, magnesium, and titanium matrices are currently being used in many aerospace industries and transportation industries[4].

Franz Karl started the investigation of the multicomponent alloy using five to seven elements in the late 18th century; no further study was performed because the initial physical properties were unappealing [5]. Creating an alloy with many different elements with equal atomic percentages was studied by cantor student Alain Vincent where he found a face center cubic (FCC) structure. J. W. Yeh's[6] students started exploring multicomponent alloys, where they created 40 different composites using 20 base materials. They prepared the allow using arc melting considering the high entropy mixing factor radios down the number of phases in the alloy. Their study found some interesting facts about high entropy alloys, such as the alloy having a higher hardness, good corrosion resistance due to large lattice distortion, and stronger bonding.

Therefore in the present work, we are focusing on $Al_{1.5}CrFeMnTi_x$ HEA multicomponent composition, where titanium percentage changes from 0.1, 0.15, and 0.2. The reason behind selecting $Al_{1.5}CrFeMnTi_x$ is because it has a BCC+ L_{21}+laves phase with respect to the temperature. With an in-depth analysis of Al1.5CrFeMnTix, we can determine how to utilize this low-weight high entropy alloy. The preliminary results show that the density of the alloy ranges from 5.2 to 5.5 g cm^{-3}, which fulfills the criteria of low weight HEA; also, from the XRD, the BCC+ L_{21} phases are available inside the HEA matrix.

1.2 Introduction to High Entroy Ceramic

High entropy ceramic(HAC) is a new solid solution material class using five-plus elements of nitride[7], carbide[8][9], boride[10], diboride[11] and oxide[12]. The transition metal nitride is currently used in cutting tools and protective coating due to its higher hardness, melting point, excellent thermal conductivity, and good chemical

stability[13]. The addition of more elements at equiatomic percentage reduces the Gibbs free energy and increases the configurational entropy. Therefore, the new alloy is thermodynamically more stable at higher temperatures and has unique properties that can be utilized for many applications. Moreover, the transition metal nitride compound has a nitrogen -3 oxidation state, exhibiting superior strength, hardness at high temperatures, higher oxidation resistance, electrical conductivity, and chemical stability [7].

Superalloy has been used in high temperatures applications to achieve higher efficiency, such as gas turbines and power plants. The major drawback of superalloy is that it shows low strength and corrosion resistance at a higher temperature for longer working hours. To improve the efficiency of the superalloy, thermal barrier coating of ceramic and oxide is used to increase the material's life span also achieve higher efficiency[14], [15]. High entropy ceramics(HEC) is a multicomponent alloy similar to the high entropy alloy (HEA) specifically developed for a wide set of applications. The material scientists found that high entropy ceramics have an excellent thermoelectric Seebeck coefficient and low thermal conductivity; therefore, they can be used in many applications where a low thermal coefficient is required[16]–[18]. The HEC exhibits unique properties that have been found in recent publications, such as transition metal oxide (Mg, Co, Ni, Cu, Zn)O fabricated using field-assisted sintering technique shows the single-phase salt rock microstructure[19]. Several applications where high entropy ceramics can play a vital role include cutting tools, thermal spray coating, high-temperature application, gas turbine, die and mold, and an aerospace application[15], [20]–[23].

This study investigates the phase stability and processing technique of high entropy nitrides derived from HEA and becomes a new set of Ultra high-temperature ceramics

(UHTCs) . In the present work, five equimolar metal nitrides produce using mechanical alloying and spark plasma sintering. The Ultra high-temperature ceramics (UHTCs) consist of different ceramic elements like (Hf-Nb-Ta-Ti-Zr)N of the transition metals nitride. The UHTCs show prominent characteristics such as higher melting point, higher oxidation resistance, lower thermal conductivity, higher yield strength, and microhardness. The oxidation resistance and the microhardness of the individual material processed via similar technique is far less than the HEC. The Gibbs free energy is minimized by adding a number of elements that increase the entropy, and the lower valency (VEC<10) of transition metal nitride improves the thermodynamic stability at high temperatures and increases the material's hardness [23], [24].

This research aims to learn more about high entropy alloys and investigate two unique types of high entropy alloys for different applications. The first goal is to find out low-weight high entropy alloy for transportation applications where weight is a prime concern for improving the efficiency. The second goal is to develop high entropy ceramics (HEC) that can be used in areas where high-temperature applications including gas turbines, reactors, and cutting tools.

CHAPTER II

LITERATURE REVIEW

2.1 Introduction

Initial definitions of high-entropy alloys (HEAs) included solid solution alloys with more than five primary elements present in equal or nearly equal atomic percent. Every component's atomic fraction is typically larger than 5 at %. However, this theory has finally changed as additional multi-element concentrated alloys have been studied and explored. These alloys represent a technological breakthrough in terms of the way that newer alloy systems are researched and developed compared to earlier research, which primarily focused on conventional alloys and did not take entropy into account as a significant influencing element in establishing the equilibrium phases. Thus, entropy is crucial for the stability of the final phases, but the ultimate result may not always be a single solid solution phase; rather, it may be decided by the interaction and competitiveness between enthalpy and entropy.

HEAs have drawn considerable attention as a result of their unique compositions, microstructures, and adaptable characteristics. Cantor et al. [25], who are regarded as the inventors of these alloy systems, gave these alloys their names and characterized them as HEAs. According to Cantor et al. [25], a typical approach for alloy creation results in a vast knowledge about alloys made up of only one or two primary components, but little to

no information regarding alloys made up of multiple main components that are distributed almost equally. Alloys with one or two primary components have been the focus of theoretical and experimental research on the formation, morphology, and characteristic of crystalline phases. As a result, the comprehension and knowledge of alloys around the corners of a multi-component phase diagram are considerably developed, whereas the middle of the phase diagram is much less well-known. For ternary alloys, this difference is noticeable, but it gets more obvious as the number of constituents rises. Except for certain HEA systems that have recently been described, knowledge regarding alloys towards the center of the phase diagram for quaternary and other higher-order alloys is almost nonexistent. Therefore, researching HEA not only adds new dimensions to the creation of unique alloys, but also offers a fascinating field for scientific research.

The Boltzmann equation from statistical thermodynamic use to calculate configurational entropy[26]. The definition of an entropy alloy comes from the mixing of multiple elements in such a way that it should have higher configurational entropy and a stable solid solution state [27].The high entropy alloy combines five or more elements with a 5% to 35% atomic percentage [6].

$$\Delta S_{conf} = k \ln w = -R \ln \frac{1}{n} = R \ln n \qquad (1)$$

Where,

k Boltzmann constant

w number of different ways energy can mix R

R is gas constant =8.314 J/Kmol

ΔS_{conf} = 1.10R,1.61R, 1.79R, 2.20R, 2.57R for equiautomic alloy containing 3, 5, 6, 9, 13 elements.

Based on the configuration entropy calculation

$\Delta S_{conf} \leq R$ called low entropy alloys

$1R \leq \Delta S_{conf} \leq 1.5R$ called medium entropy alloys

$\Delta S_{conf} \geq 1.5R$ called high entropy alloys

The high entropy alloy consists of many elements; therefore, several factors affect the microstructure, phases, and mechanical properties[27]. The four major factors contribute to the significant impacts: high entropy effect, severe lattice distortion, sluggish diffusion, and cocktail effect[27].

2.2 Core Effects of HEA

The terms "high entropy effect", "lattice distortion effect", "sluggish diffusion", and "cocktail effect" are often used to describe HEAs [26], [27]. For properties, a cocktail effect brings excess to the quantities predicted by the mixture rule due to mutual interactions of different atoms and severe lattice distortion. In the next following section, we will explain these factors in detail.

2.2.1 High entropy effect

The high entropy effect is a significant contribution to the formation of solid solution and microstructure. Due to the multi-component in the alloy, there would be different interactions between different elements, causing binary, ternary, and quaternary intermetallic phases. According to the thermodynamic law, the equilibrium state in a solid solution state has the lowest free energy through numerous possibilities of different states. The Gibbs free energy of mixing calculate as

$$\Delta G_{mix} = \Delta H_{mix} - T\Delta S_{mix} \quad (2)$$

where ΔH_{mix} is the enthalpy of mixing and it measures energy under constant pressure and volume, and ΔS_{mix} is entropy of mixing and it measures configurational entropy. An increasing number of elements in the HEA system causes an increase in entropy and a decrease in free energy. The HEA consists of a solid solution and intermetallic compound; $\Delta H = 0$ is assumed to be an ideal solid solution, whereas $\Delta H = 0$ is ideal for intermetallic compounds

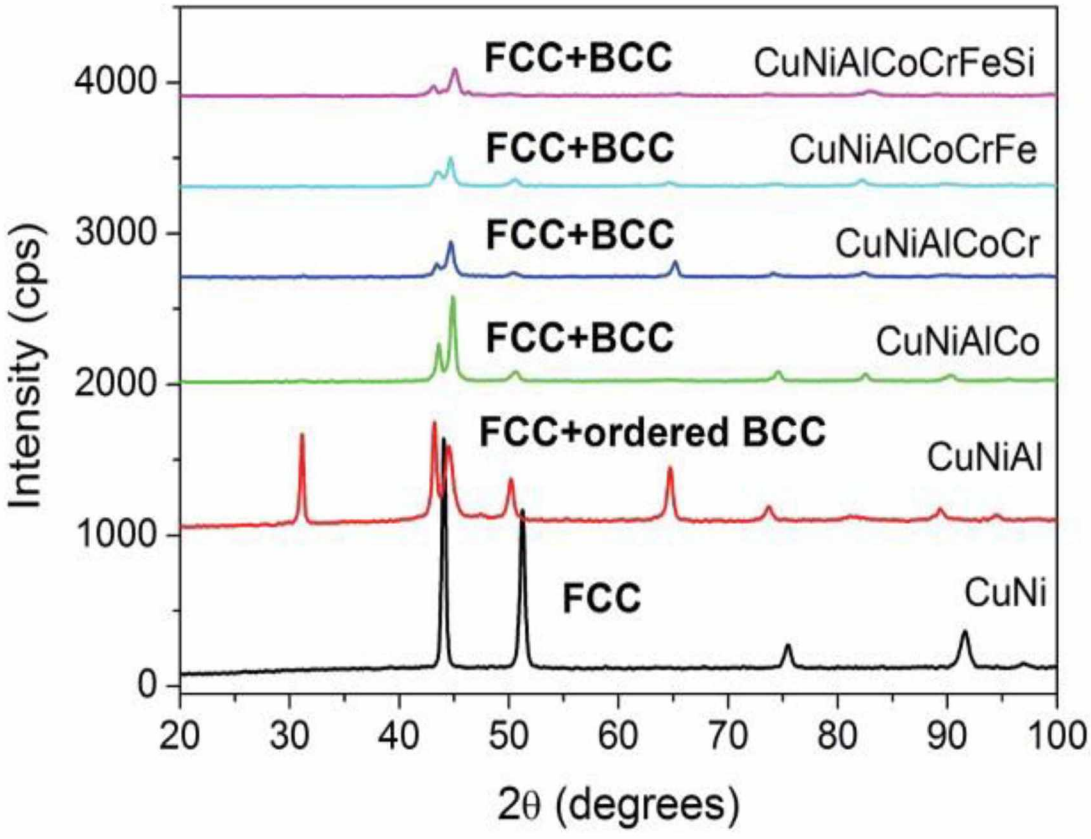

Figure 2 1 Series alloy XRD patterns created by the successive addition of one more element to the preceding one [11]

A sequence of binary to multi element alloys is shown in XRD patterns in Figure 1, where this effect may be seen in action. As more elements are added, the phase transition from FCC to FCC+BCC is observed. The higher entropy of a solid solution phase with

several random scattered elements (Five or more elements) is responsible for the high-entropy effect. This impact reduces the Gibbs free energy, which results in the phase being more stable. It is proposed that it is the element that leads to the creation of HEAs in the work that Yeh [27] and his team discussed. A more in-depth examination of the laws of thermodynamics indicates that the predicament is far more complicated. Phase Solid solution (SS) and intermetallic (IM) phases are delicately interrelated in the stabilization process, where slight changes between matrix contributed by distinct phases with varying compositions have a substantial impact. Further research has shown that kinetic stabilization of the basic crystalline structure and SS phase may play a significant role in the alloy formation.

2.2.3 Severe lattice distortion effect

The severe lattice distortion effect is prevalent in high entropy alloys because of the number of elements present inside the matrix. The different components inside the matrix have a different atomic size which causes lattice strain and stress. Individual atoms' bonding energy and crystal structures cause severe lattice distortion because of nonsymmetrical binding and electronic structure around the atoms. Lattice distortion causes changes in the mechanical and thermal properties; the microhardness increases drastically compared to the mixture rule, whereas it reduces thermal and electrical conductivity[6], [28], [29]. During the lattice distortion, electron scattered causes a reduction in electrical conductivity, and electron contribution to the thermal conductivity reduces, which causes a decrease in thermal conductivity[30]. The Vicker hardness of CoCrFeMnNi FCC equiatomic alloy is 1192 MPa, far higher than 864 MPa obtained by the mixture rule[26]. On the other hand, the MoNbTaVW BCC equiatomic alloy has a three

times higher hardness than the mixture rule [31]. The BCC structure has higher distortion strain and solution hardening than the FCC structure, and the difference in the atomic size also significantly contributes to lattice distortion.

The severely deformed three-dimensional unit cell of a five-component BCC lattice is shown in Figure 2. Smaller peak intensity is caused by the deformed atomic planes' increased x-ray diffuse scattering effect[27]. In addition to causing electron scattering, lattice distortion may significantly reduce the electrical conductivity of a material. Because

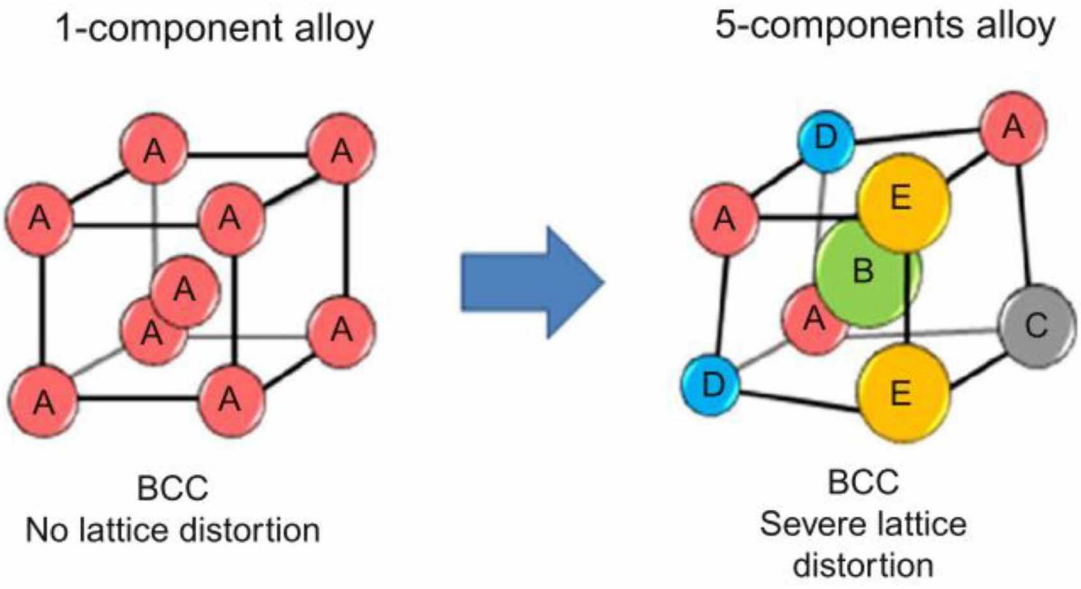

Figure 2 2 Graphic image illustrating the five-component BCC lattice's presence of significant lattice distortion [2]

of this, the electron contribution to the thermal conductivity that is caused by electron conduction is decreased. The thermal conductivity is reduced due to phonon scattering, amplified in the deformed lattice [30]. It has been discovered that none of these characteristics of HEAs are very temperature sensitive. For instance, HEAs have relatively low-temperature coefficients of resistivity. This is due to the fact that the lattice distortion

brought on by the thermal vibration of atoms is not nearly as severe as the lattice distortion brought on by other factors [6].

2.2.3 Sluggish diffusion effect

It was suggested that HEAs had slower diffusion and phase transition kinetics than conventional equivalents [32][33]. The atoms surrounding each location in the HEA matrix are distinct from one another in several ways. This means that the neighbors of an atom before and after jumping into empty space will be distinct. Due to the fact that each location has its own unique atomic configuration, the resulting bonding and hence the local energies are unique to that location. A low-energy site traps an atom, making it less likely to leap out of that site in the future. To put it otherwise, a high-energy site is more likely to allow the electron to return to its original location. The rate of the diffusion process is slowed down in any of these two cases. It is important to keep in mind that the local atomic configuration both before and after leaping into a vacancy is, the vast majority of the time, exactly the same in ordinary alloys with a low solute concentration. Tsai et al. calculated the impact of local energy variation on diffusion using a seven-bond model [34]. They demonstrated that the mean potential energy difference between lattice sites for Ni atoms diffusing in Co–Cr–Fe–Mn–Ni alloys is 60.3 meV and this value is almost fifty percent greater than the value observed for Fe–Cr–Ni alloys [34]. Because of this disparity in energy, low-energy sites have a substantially longer occupancy period than high-energy sites.

Sluggish diffusion effects in a HEA happened due to different elements present inside the matrix, causing lattice distortion and lattice potential energy(LPE). Tsai et al.[34] stated that the diffusion rate is slower in high entropy alloy because of the more significant

activation energy required for the movement of the atoms due to higher lattice potential energy. The vacancies available inside the HEA matrix required competition between the number of different atoms to fulfill that vacancy; therefore, more elements present inside the matrix slower the diffusion[34]. The sluggish diffusion effect phases inside the matrix, green growth, precipitation, and end re-crystallization temperature. The lower the mass flow between the elements creates smaller precipitates inside the matrix that restrict the grain growth and particle coursing rate[6], [35].

2.2.4 Cocktail effect

The cocktail effect is the terminology used by professor Rangarajan to describe the impact of different elements. The word cocktail effect does not refer to a particular structural or thermodynamic logic; instead, it is a phrase that refers to the collaborating effects that may occur unexpectedly and are more significant than their components. Despite this, it illustrates a small portion of the large compositional space that is open to multi-component composites and shows evidence that unexpected effects may be produced by non-linear correlations as well as odd combinations of components and microstructures. Depending on its composition, lattice distortion, and diffusion, the HEA may have a single phase or several phases. Yeh et al.[6] explain the importance of aluminum inside the AlxCoCrCuFeAl; increasing the percentage of aluminum changes the solid solution from FCC phase two to FCC+BCC and BCC phase. Zhang et al. [36] studied the soft magnetic HEA CoNiFe(AlSi)0.2 with good corrosivity, electrical resistance, and higher yield strength that can be used in different applications in the future. The cocktail effect can be utilized for many future applications, but choosing different elements and compositions is the key in designing HEAs to use the alloy's full potential. For example, the cocktail effect

in the AlxCoCrCuFeAl alloy is shown in Figure 3 [6], which results in the phase change from FCC to BCC when the Al concentration is above the critical threshold.

2.5 Non-Equilibrium HEA Approach

The design philosophy of HEAs is the maximization of configurational entropy (CE) to lower Gibb's free energy [37]. This leads in simple-structured phases instead of brittle ordered intermetallics [25], [38], [39]. As a result, HEAs were first described as containing at least five primary elements in concentrations ranging from 5 to 35 percent to optimize CE and enable the formation of solid solutions. Yet, several current studies have questioned the CE's dominant function independent of the mixing enthalpy, and it has been

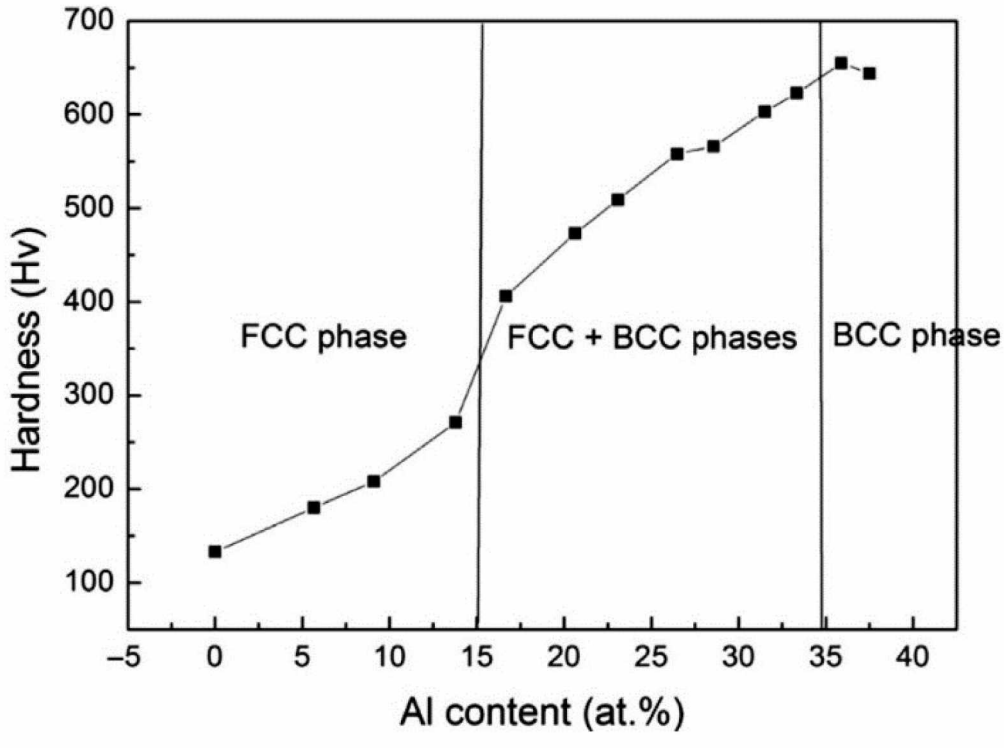

Figure 2 3 The AlxCoCrCuFeAl alloy's component elements' interaction produces a "cocktail effect." [2]

emphasized that the Gibbs free energy is an important factor for phase structure, even in circumstances of high CE [40], [41]. Although the function of the CE is yet unknown, most

of the studied HEAs have near-equiatomic ratios. Surface morphology shows that most of the HEAs investigated so far are not single-phase structures and often comprise intermetallic phases [40], [42]–[44]. Intermetallic phases often affect most major mechanical properties, including as ductility, wear resistance, and hardness. As a result, alloys with intermetallic phases often exhibit poor properties compared to single-phase non-equiatomic alloys.

It is more necessary to avoid the development of intermetallic compounds than to maximize entropy when producing homogenous single phase crystalline solid solutions [40], [41], [45], [46]. The equiatomic combination of CoCrFeMn alloy reported a complex multiphase microstructure with many intermetallic phases, while a similar component with a non-equiatomic ratio Co10CrFe40Mn10 forms a homogenous fcc single phase that has outstanding phase stability and tensile ductility [45], [46]. As a result, it is critical to determine the probabilities of intermetallic compounds instead of merely the configurational entropy in the phase diagram considering an aspect of thermodynamics. Another consideration is that non-equiatomic compositions, which generally occur in multi-component systems, have lower vapor pressure changes, which reduces segregation and enhances casting characteristics. The use of a non-equiatomic mixing criterion would therefore open up a substantially greater compositional space for the synthesis of intermetallic phase-free lightweight high entropy alloys.

2.5 High Entropy Alloy Physical Properties

As previously mentioned, the quantity of alloys that may be found using the typical alloy design technique based on one and occasionally two primary elements is relatively restricted. Just about around 30 alloy systems for typical applications were identified

throughout thousands of years of investigation, according to the ASM Metal Handbook. The compositional space of alloys may be significantly increased by going from the narrow band of sides and boundaries to the wide middle zone in phase diagrams using the multi-component design technique. Cantor et al. cautious assessment put the total number of potential alloys that could be formed out of 60 viable components in the range of 10^{100}[25], [26], [39]. HEAs and their variants, such as interstitial and medium-entropy alloys, undoubtedly provide a path to covering a considerable amount of unexplored alloys systems. Improved materials with better mechanical properties are needed to meet the ever-growing demand for sophisticated applications. These three dimensions of composition, crystalline structure, phase transformation, and grain size are used to optimize mechanical properties. High-entropy alloys are an exciting new class of metallic materials that have a large variety of compositional and phase-structure permutations as well as a variety of structure-property combinations [39], [44], [47]–[51]. Despite holding significant concentrations of five or more elements with distinct crystal structures, this novel class of alloys may form a single phase structure or multiphase giving them their unique properties [31], [36], [52]–[55].

HEAs have piqued the interest of researchers owing to their improved mechanical and physical qualities, sometimes superior to commercially optimized and utilized alloys. For instance, it was discovered to have an ultrahigh fracture toughness [11], [38], [56], [57], fatigue resistance [49], [57], [58], oxidation [59]–[62] and corrosion [39], [63]–[66], superconductivity [67], magnetic properties [24], [68], [69], high-temperature strength and toughness [70]–[73], chemical properties [74]–[77]. The better features of HEAs are often argued in the literature as a direct result of the four core effects high entropy effect, slower

diffusion, severe lattice distortion, and cocktail effect [40], [44], [45], [72]. A universal rule for all multi-element systems may not be achievable or scientifically true due to many problems in summarizing.

The anticipated development of multi-component alloys will certainly present several opportunities for creating diversified microstructures and improved mechanical and structural properties. In fact, numerous unique, previously unexplored properties were recently revealed. For instance, Yield strength and ultimate tensile strength both increased by replacing Ti and Nb with Al and Ni [78]. Mechanical alloying and Spark plasma sintering was used to create NbTaTiV refractory high-entropy alloys when the Vickers hardness improved, and the sintering temperature rose from 1500 to 1700 °C [79]. TiAlVNbMo has been found to have a lower density 6g/cm^3, than nickel-based superalloys and other refractory high-entropy alloys, as well as excellent strength and acceptable plasticity at high temperatures [80].

2.6 Low-Weight High Entropy Alloy

HEAs are described as alloys of four or more primary metallic elements, each with an atomic percentage of between 5% and 35%[2]. The conventional alloy systems, such as iron or aluminum-based, are built on a single major element that serves as the system's matrix, with various other elements added to improve certain attributes. The majority of HEA research, in the beginning, was focused on single-phase HEAs. However, most HEAs described in the literature incorporate multiple phases rather than a single solid-solution phase.

Lightweight materials are in high demand for transportation and energy-saving applications. The main disadvantage of the existing lightweight materials is their

inadequate properties or excessive production costs. As a result, scientists are working hard to produce new forms of lightweight alloys that are low-cost and capable of meeting property criteria. Most designed HEA has a high density of over 10 g cm^{-3} because it was first developed to replace superalloys[81][53]. Senkov et al[82], [83]. developed a Cr-Nb-Ti-V-Zr refractory alloy system to reduce the weight of HEA to 6.49 g cm^{-3} in order to develop lighter materials with superior strength at higher temperatures and further reduced to 5.5 g cm^{-3} by replacing Cr with Al. Furthermore, as a potential approach of manufacturing LWHEA using porous architectures to lower the density of already created HEAs for biomedical and transportation industries.

Low-weight design is critical in developing and advancing next-generation structural materials that are high-performing, efficient, and environmentally friendly. High-entropy or multi-component alloys have transformed the conventional alloy design technique and sparked significant interest because of their appealing extensive mechanical properties. There is now a wide range of HEAs available, including face-centered-cubic (FCC) HEAs with excellent ductility [51], [52], [84], body-centered-cubic (BCC) HEAs with high strength [47], [53], [85], and hexagonal-close-packed structure (HCP) HEAs combined with rare-earth alloy elements [5], [86], [87], or transformation-induced-plastic These studies highlight HEAs' excellent research potential. However, further study is required to create advanced HEAs with greater strengths.

Due to the high weight of the element, The alloy systems development was limited. As a result, various research has concentrated on the design of low-density HEAs. In addition, another form of low-density HEA is used for lightweight refractory HEAs composed of refractory elements such as Ti, Zr, Nb, and V, as well as Al, Cr, and Si have

BCC phase [88]. The effect of Al element on the NbTiVTaAlx HEAs alloys, which present BCC structures with excellent compression ductility exceeding 50% without the breakage. Among them, the NbTiVTaAl0.25 HEA shows the highest yield strength at around 1330 MPa [88]. In addition, a low-density Cr-Nb-Ti-V-Zr system was also investigated. With the addition of low-density refractory alloy elements, the NbTiVZr and NbTiV2Zr HEAs form disordered BCC structures, and the Cr element promotes the formation of the ordered Laves phase, thereby improving the hardness of these alloys [38], [82]. The addition of the Al element can enhance the yield strength of the AlxNbTiMoV HEAs [89], and Al is an element that can increase the stability of BCC or B2 structures [74], [90]. In addition, the AlTiNbV, AlNbTiVZr0.5, and AlTiVCr low-density HEAs display single BCC structures, high specific strengths, and an improved ductility with the addition of Zr [74], [91], [92].

Several studies have indicated that adding Al can increase the strength of the Zr50Ti35Nb15 alloy, and the Alx(Zr50Ti35Nb15)100−x HEAs present high strength and excellent plasticity [93], [94]. The Cr and Mo can improve the high-temperature properties of the BCC HEAs [95], [96], and the Si can also promote some Laves phase to enhance the properties [97]. Therefore, the present work investigates the effect of the Cr, Mo, and Si on microstructures and properties of the Al-Zr-Ti-Nb HEAs and attempts to demonstrate the influence of these elements on the phase formation of low-density BCC HEAs.

Another method for reducing density is to increase the percentage of lighter elements while retaining mechanical properties, such as the Al concentration in traditional AlCoCrFeNi alloys. A further option is to include two or more light components like Al and Ti; a lighter material is described in this study as have a density of less than 5 g/cm3. The phase forms of HEAs with at least two light elements described in the literature were computed in this

work utilizing a CALPHAD technique and thermodynamic databases. The analyses included HEAs with relatively significant quantities of light elements Al and minor amounts of light elements with different Ti percentages, such as $AlCrFeMnTi_{x(0.1,0.15,0.2)}$. The computed outcomes then confirmed our experimental findings to (1) comprehend the fact impact of low-density elements; (2) investigate the potential relevance of CALPHAD to phase predictions in Alloying elements manufactured using various processing procedures, such as traditional casting; and (3) discuss methods to incorporate low weight material to form LWHEA.

2.7 High Entropy Ceramic

Ultra-high temperature ceramics, or UHTCs, that has a high melting point (>3000 °C), excellent hardness, resistance to thermal shock, and oxidation resistance [98]. Because of the synergistic impact of these characteristics, UHTCs have the potential to be used as prospective candidates for structural applications such as the next generation of hypersonic vehicles, nuclear reactors, leading edges in airplanes [99], [100]. To meet rising demands for materials performance, advanced structural materials must be selected and designed to outperform standard UHTCs in terms of selection and design. As a result, this UHTC has started to follow metallurgy in its analysis of multi-component alloy systems.

The compositional space of metallurgy has recently advanced owing to the production of high entropy alloys (HEA) with outstanding thermo-mechanical characteristics, such as high strength, wear, and oxidation resistance in the room as well as at extreme temperatures previously created [39], [100], [101]. High entropy ceramics (HEC), which were motivated by the idea of HEA, have attracted a lot of attention in the past five years for use in temperature insulating material in hypersonic vehicles, nuclear

reactors, and other high-temperature applications [98], [102]. The mass production of HEC, including oxides, silicides, nitrides, borides, and carbides, began in 2015, and scientists in 2016 discovered a new kind of UHTC known as high entropy ceramic, but their study of these materials is only beginning [22], [103]–[105]. In the literature, Similar processes like arc melting [106], hot press [8], spark plasma sintering [100], [107] are used to produce HE-UHTCs, which have four or five elements with 1:1 molar ratios.

The preliminary research on high-energy ultrahigh temperature ceramics yielded lower densities due to a higher percentage of impurities formed during the high-energy ball milling process, which included the formation of oxides [108]. After this, the scientists were forced to adopt reactive synthesis techniques to synthesize HECs, resulting in improved relative densities of more than 99 percent and characteristics [109]. The densification of >98% was also accomplished while synthesizing HE-carbides using the ball mill method [107]. The solid-solution ternary metal carbide (Nb,Zr,Ta)C has also been synthesized using the polymer-derived ceramic technique, which has low oxygen impurity of about 2.56 at.% but considerable carbon impurity concentration 10.24 at.% [47]. The two-step processing method, which combines self-propagating high-temperature synthesis (SHS) and SPS to process a single-phase solid-solution of (Hf, Nb, Ta, Ti, Zr)B2, has made further advancements in the production of HE-UHTCs [29]. The (Hf, Nb, Ta, Ti, Zr)B2 system published the first report on reducing the experiment to a single step by processing metal oxide precursors smoothly [110]. As a result, the bulk of current HEC research focuses on improving processing pathways to obtain high density by solid solutions with desired properties.

This article provides a viewpoint on an important scientific subject about the real function of entropy in stabilizing and increasing the high temperature mechanical properties of a high entropy (HEC) system. A novel family of ultra-high temperature ceramics is projected to have remarkable mechanical, chemical, and corrosive resistance compared to standard UHTCs. Although, little attention is paid to the role of entropy in HEC's improved characteristics, which are linked to the multi-component system. The configurational entropy of thermodynamically stable HECs may be determined using high throughput first-principle computations, which may prove to be an important tool in solving this conundrum. The mechanical properties of HEC have been shown to improve well above the anticipated rule of the mixture, and this cannot be explained by a simple impact of solid solution formation. Isothermal oxidation investigations of HECs that were confined to furnace testing show that the oxide scale exhibited extraordinary oxidation resistance. This remarkable oxidation resistance was ascribed to the passivity of the complex, layered structure of the oxide scale. There must be an investigation into whether or not all of the HEC components react concurrently or whether selective oxidation occurs. The development of thermal insulation for high temperature applications has been proposed to handle all of these difficulties using an integrated computational and experimental approach. If this strategy is successful, it will open up new prospects in the compositional space of high-energy ultrahigh temperature compounds that have customized features.

CHAPTER III

PROCESSING TOOLS AND EQUIPMENT

3.1 Introduction

This chapter describes the equipment used to synthesize, prepare, and analyze the high entropy alloy systems considered in this research. For the synthesis of HEAs, several processing procedures, including melting and casting, powder metallurgy, and deposition processes, have been utilized to synthesize HEAs. HEAs in different shapes have been created using melting and casting procedures, and the most popular melt processing techniques are vacuum arc melting. The other form of synthesizing is powder metallurgy is mechanical alloying followed by sintering. The LWHEA were synthesized using vacuum arc melting, and high entropy ceramics were synthesized using mechanical alloying followed by spark plasma sintering. Following are the types of equipment used to conduct current research.

3.2 Fabrication Methods

3.2.1 Arc melting

An arc furnace was used to melt the $Al_{1.5}CrFeMnTi_X$ ingots (x = 0.10; 0.15; 0.2) which refer as alloy 1, alloy 2 and alloy 3. After the raw materials of all elements in the

required quantity mentioned in Table 1 had been loaded into the electric arc furnace, the mechanical pump was turned on to begin the process. As soon as the vacuum meter registered 10^{-1} Pa, the shut-off valve was opened. The vacuum meter had to be closed to open the air-filled valve, and the ionization unit had to reach a pressure of $3x10^{-3}$Pa. In order to initiate vacuum-arc melting, the air-filled valve was shut when the pressure gauge read at least $6x10^{-2}$Pa. Pure Titanium was first melted during the melting process to absorb oxygen and other contaminants in the environment. The quality of the argon gas was maintained through the vacuum arc melting furnace. Metal pieces (purity more than or equal to 99.9%) were put in respective proportions, added to a copper crucible and arc melted in an inert argon atmosphere. The alloy specimens were flipped at least three times to achieve a homogeneous composition and remelted many times.

Table 1 Nominal wt. % of all elements in LWHEA

Element	Alloy 1	Alloy 2	Alloy 3
Al	19.46	19.23	19.02
Fe	26.84	26.54	26.24
Cr	24.99	24.71	24.43
Mn	26.41	26.11	25.81
Ti	2.3	3.42	4.5

3.2.2 Mechanical alloying (MA)

The term "mechanical alloying," or "MA," refers to a method of powder processing that enables the development of homogenous products by beginning with blended elemental powder combinations [111]. MA is defined as the repetitive welding and

fracturing of powder particles entrapped between milling mediums, the ball-to-powder ratio and milling duration determined by the mechanical properties of powder ingredients [3], [112][111]. The actual method of MA begins with combining material powders in the appropriate amounts, followed by loading the powder mixture into the mill, where it is ground with the medium (different material balls). After this, the mixture is milled for the necessary amount of time until a steady state is attained. The study state occurs when the material composition of all particles are identical, which would be an essential processing time to carry out the milling process. Consolidation using the different process of the MA powder are then used to get the appropriate material characteristics. The purity materials powder, milling machine, and the process parameter like the ball to powder ratio, cooling time, and length of the milling process are therefore crucial elements of the mechanical alloying process.

Elemental powders of Hafnium Nitride-HfN (99.5% pure, -325 Mesh), Niobium Nitride-NbN(99.8% pure, -325 mesh), Tantalum Nitride-TaN (99.8%, 1-5micron APS), Titanium Nitride-TiN(99+%, -325 mesh), and Zirconium Nitride-ZrN (99.8%, 10 micron APS) were purchased from Atlantic equipment engineers, NJ, USA. The powder was blended in several different nominal compositions with varying atomic weight percentages of elements. The blend of these elemental powders was then mechanically alloyed using high-energy planetary ball milling equipment.

FRITSCH Pulverisette 7 premium line planetary ball mill was utilized for mechanical alloying. The milling was performed using 3 mm diameter Tungsten carbide (WC) milling media with a Ball to Powder weight ratio (BPR) of 10:1. The blend of the powder mixture was ball milled at 500 rpm for 6 hours in 80 ml Tungsten carbide milling

vial. The mechanical alloying was carried out in an inert argon atmosphere to prevent the powder mixture from oxidizing. To prevent contamination of the powders milling vessel and the milling medium of the same material was selected. In order to avoid excessive temperature rise and welding during milling, 30 mins of milling were followed by a cooling interval of 30 mins. 2 wt % of the total powder weight of stearic acid ($C_{18}H_{36}O_2$) was added to the powder charge as a process control agent in order to prevent cold welding of the powder mixture inside the milling vial during the alloying process.

3.2.3 Spark plasma sintering (SPS)

A new method for manufacturing metal or non-metal composites synthesize at low temperatures and quicker processing than standard conventional casting methods is spark plasma sintering (SPS) [113]. In the SPS process, impurities and gases between the material particles activate the spark discharge, which produces high-temperature states in a gap, causing condensation and melting on the powder interface to make a completely dense composite material. SPS uses uniaxial force and DC pulse current for a fast sintering process for conductive and non-conductive materials. This large AC transmission and dispersion of the joule heat effect across the specimen result in quick and comprehensive heat transfer, providing high homogeneity and constant precipitate densities. SPS can consolidate nanopowders without significant grain development due to higher heating rates and temperature quicker sintering process [114]. The SPS process is broken down into four primary steps 1) Vacuuming and removing all gasses, 2) applying pressure, 3) heating DC pluses 4) cooling in the fourth stage.

The mechanically alloyed powder was then consolidated using the spark plasma sintering technique. SPS 10-3 by Thermal Technologies LLC was used for sintering the as-

obtained powder. The SPS process was programmed with specific operating instructions in the Itools software. Parameters including temperature set points, applied load, heating rate, the rate at which uniaxial load is applied, and holding time were set in the program. The alloyed powder was loaded in cylindrical graphite die of 20mm and lined with a graphite foil. The SPS process was carried out at 1800^0C-2000^0C with heating ramped at 100 ^{0}C/min and a uniaxial load of 50 MPa for a hold time of 5 minutes. An optical pyrometer was employed to monitor the temperature inside the die.

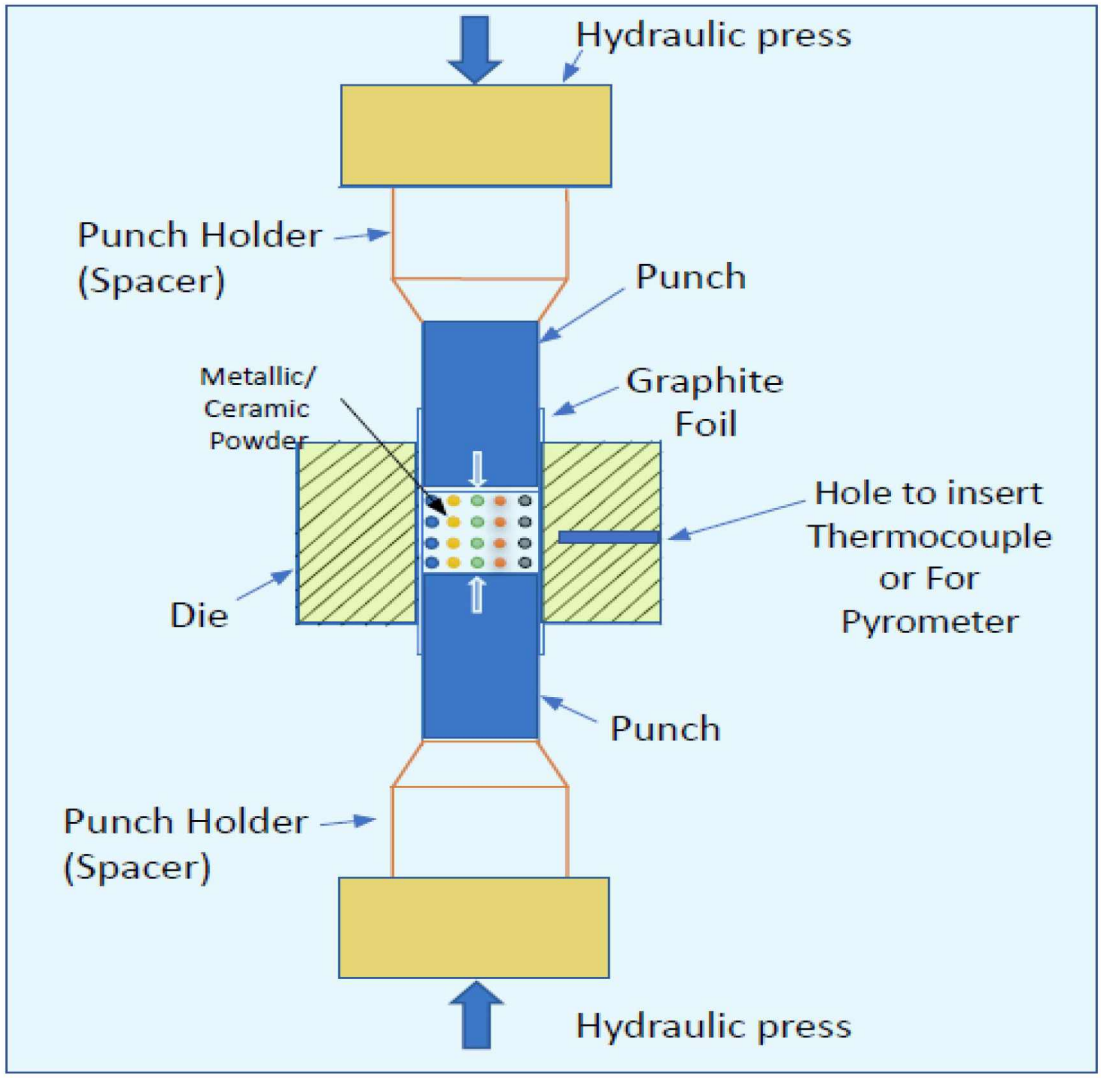

Figure 3 1 Spark plasma sintering schematic

3.3 Heat Treatment

A collection of thermal and metallurgical procedures are used to change a material's physical and sometimes chemical properties. Heat treatments are carried out for various reasons; some methods soften the metal, others harden it also it can alter electrical and thermal conductivity. Heat treatment is the process of heating metal to a certain temperature, maintaining it there, and then cooling it again. During the procedure, the material's microstructure changes, which will help to change the mechanical properties of the metal component. The variety of factors includes the heating duration, holding time, heating and cooling rate, cooling medium, and the environment.

In the present work, Diamond saws or electric discharge machines were used to cut the ingots of alloy into the desired forms (EDM). The samples were placed in an argon-filled quartz tube to avoid oxidation. Tube and box furnaces from carbolite (from verder scientific Inc.) were used for heat treatment of the alloy samples. Various heat treatment procedures have been carried out, including annealing, water quenching, and normalizing. The various heat-treatment conditions are detailed in their own chapters.

3.4 Electric Discharge Machine (EDM) and Liner Precision Saw

The arc melted metals were cut into the required dimensions before heat treatments using a Buehler isomet 4000 liner precision saw and a Fanuc robocut alpha-1iD Wire EDM. The wire EDM machine cuts the sample by sending a high voltage through a wire, resulting in exact dimensional tolerances. The example is cut using CNC machine algorithms written in general code (G) and machine code (M) codes. Electrical discharge machining, often known as EDM, is a procedure that does not need any physical contact and can cut components despite the hardness of the materials. In this procedure, a thin wire is inserted

into a flowing di-water, along with a conductive material (specimen). DI-water functions as an insulator until ionized by a high voltage and gap, allowing a current to flow to the substrate.

3.5 Characterization Tools

3.5.1 Scanning electron microscopy (SEM)

All of the high entropy alloys investigated here were subjected to microstructural development, evaluations of precipitates, crystal structure, compositional characterization, and area fraction analysis utilizing an Inspect F50 FEI equipped with a field emission gun (FEG). The Everhardt Thornley Secondary-Electron Detector is used to analyze the fracture surface (ETD). The SEM will be carried out using a high-energy electron beam of 100-30000 electron volts, and it employs a cold emitter for the beam generation that relies on field emission. SEM images employ both secondary and backscattered electrons. The secondary and backscattered electrons will be collected if a positive voltage is applied to the collector screen. Only BSE will be collected when a negative voltage is given to the collector screen. The presented information is affected by the gun's electron voltage mode. Good surface information in scan images is available if low voltage 5kV is used. On the other hand, the high acceleration voltages from15 to 30 kV go below the surface and give interior information about the sample.

3.5.2 X-ray Diffraction (XRD)

XRD is a non-destructive method for examining the material structure, spacing between atoms, grain orientation, and finding unknown material. In this XRD investigation experiment, we used a Rigaku Ultima III diffractometer with a Cu-K frequency of 1.5418 to identify phase, crystal structure, and lattice parameters. The XRD system was set to run at a voltage of 40kV and a current of 44mA. The data was collected in a 2Θ range of 20°-90° with a step size of 0.01° at a rate of 0.5°/minute. XRD is based on the idea of nanoscale wavelengths. When the x-ray interacts with the sample surface having structure at generates a pattern of low and high frequencies wavelengths. This is basically comparable to the multicolored patterns created by soap bubbles, where various hues are observed from different orientations. The XRD generates a diffraction pattern that provides interior details of structure on a length scale (0.1-100nm).

The X-Ray Diffraction works on the concept of Bragg diffraction,

$\lambda n = 2d\sin\Theta$,

where,

n = order of reflection integer (1,23..), λ= wavelength of the X-ray, d = lattice spacing distance, and is the Θ = incidence angle of the X-rays. In the bcc system, the summation of Miller indices (hkl) is an equal number, whereas for the fcc system, either all even or odd.

3.6 Microhardness

Materials resistance for plastic deformation is called material hardness. A Vicker harness is an indentation hardness tester to measure the hardness of a small section of any material, composite, or alloy. A diamond indenter is used to deliver a load to the specimens,

resulting in an indent impression on the sample. The measurement of the specimen's hardness is determined by the depth of the indentation in the material. Typically, the harder material has a smaller impression. The procedure for the test consists of pressing a diamond indenter into the sample surface that is being evaluated. The diamond indentor is a square base with a pyramid shape on the top with an angle of 136 degrees with an opposite side. The tester typically applies pressure to the sample for 10-15 seconds and has a load range of 1-100kgf. The hardness (Hv) is calculated using the force/Area, where force is the applied load and the area is the average of two diagonal lengths. The SPS consolidated samples' microhardness values were determined using a standard Wilson Vickers microhardness tester. The measurements were made with a 5N load and a dwell period of 10 seconds. For each sample, ten separate microhardness measurements were taken into consideration, and the average result was given.

3.7 Wear Testing

Wear is the material removal process when two surfaces contact each other. Therefore, it is feasible to modify the surface properties rather than entirely replacing the alloy with one with higher wear resistance. Dry (unlubricated) wear tests were performed at room temperature on a ball-on-disc tribometer manufactured by NanoveaTM and located in Irvin, California, in the United States. The standard test technique for wear testing pin-on-disc equipment was adhered to throughout the process [115]. The ball was held against the counter body and made of a silicon nitride (Si3N4) with a 3mm diameter. Three major parameters were used under the wear testing: load, speed, and distance. During the experiment, all the parameters were kept constant throughout the test. In order to conduct the wear tests, a load of 1 newton, a sliding velocity of 200 revolutions per minute, a track

diameter of 5 millimeters, and a total sliding distance of 200 meters were used in a dry environment with a relative humidity of 45-50 percent.

CHAPTER IV

LIGHT WEIGHT HIGH ENTROPY ALLOY(LWHEA)

4.1 Abstract

High-entropy alloys (HEAs) are a novel family of solid-solution alloys that have gained international interest due to their exceptional characteristics. Because of the need from the transportation and defense sectors, lightweight HEAs have attracted researcher's curiosity as prospective advanced materials. Low-weight high entropy alloy synthesizes using arc melting with a mass ratio of $AlCrFeMnTi_{x(0.1,0.15,0.2)}$. The synthesized HEA is comprised of a mixture of body center cubic (bcc) and ordered bcc (L21) solid solution phases. The synthesized HEAs have heat treated at 650C, 800C, and 1150C for 1hr, 4hr after solutionized at 1150C for 2 hr to understand the effect of temperature evaluation in these HEAs. To investigate the role of titanium in improving the strengthening of $Al_{1.5}CrFeMnTi_{x(x=0.1,0.15,0.2)}$ and tailor the mechanical properties via studying strengthening precipitation mechanisms. The growth and coarsening of the L_{21} phase by the change in percentage of Ti and temperature for annealing were investigated using SEM and tailored the microstructure using heat treatment to improve mechanical properties from precipitation hardening. The results show that the density of the alloy is 5.88 g cm-3, which fulfills the criteria of low-weight HEA; also, from the XRD, the BCC+ L21 phases are available inside the HEA Composition matrix.

4.2 Introduction

The high entropy alloy (HEA) is a multi-component alloy system that has five or more elements with 5-35% equiatomic, nearly equiatomic, or mixed in small quantities [26][116]. The HEA exhibit unique physical and mechanical properties such as high fracture toughness[117], [118], fatigue resistance[58], [63], oxidation resistance[38], magnetic properties[77], higher mechanical strength at elevated temperatures [31] The HEA materials with such extraordinary set of properties have gained considerable interest in the research community. The HEA comprises several elements that generate curiosity and raise questions about the role of entropy inside the material matrix, phase stability, vacancy, diffusion rate, and prediction of the multidimensional phase diagram. The four primary effects are the high entropy effect, sluggish diffusion, severe lattice distortion, and cocktail effect contributing to superior properties[26][25], [27], [36], [39], [104], [119]. Due to the presence of many elements in the material, one rule for designing HEA is not possible, but it provides several opportunities to tailor the microstructure and phases as per the desired properties according to the required application.

Light weight HEAs (LWHEAs) have lately gained popularity for transportation and energy savings. Aluminum and titanium, as well as their alloys, have been utilized in the chemical transportation, nuclear, and energy sectors for decades. They are lightweight and exhibit exceptional corrosion and chemical oxidation resistance, biocompatibility, high-temperature strength, and creep resistance. The Ti-6Al-4V alloy has a density of around ~4.43 $g.cm^{-3}$ and is the most popular titanium-based alloy for biomedical applications[120]–[123]. On the other hand, titanium-based alloys are not meeting high-temperature creep, wear, and oxidation resistance requirements [120], [121], [123]–[125].

As a result, low-density alloys with good mechanical and oxidation properties are required to replace certain high density superalloys. Senkov et al[82], [83]. developed a Cr-Nb-Ti-V-Zr refractory alloy system to reduce the weight of HEA to 6.49 g cm-3 with excellent high-temperature strength in order to develop lighter materials with superior strength at higher temperatures and was also able to further reduce the density to 5.5 g cm -3 by replacing Cr with Al.

The HEAs system reveals new materials with unique properties to replace lightweight materials. The research in high entropy alloy systems can provide a new set of exclusive materials with the opportunity to replace traditional materials in different industries. The current challenge of the aerospace, automobile, and space industries is to reduce the material's weight to improve performance and efficiency with increased payload. Chain et al. [12] studied "The Material and Energy Impacts of Passenger Vehicle Weight Reduction in the US." discussing about how weight reduction is still a very cost-effective measure to reduce fuel consumption and carbon dioxide footprint. The researcher has made an effort to reduce high-density materials like steel and iron and replace them with low-weight materials such as aluminum and magnesium. The current lightweight materials are expensive and have limited physical and mechanical properties, with higher manufacturing costs. To fulfill the current requirement of low weight alloy with higher mechanical properties and lower cost, we have selected low-weight materials like aluminum and titanium to reduce the cost of manganese and iron alloy.

The transportation and aerospace industries are designing lightweight materials to reduce energy consumption without increasing manufacturing costs. The superior properties of HEA provide new possibilities for developing lightweight material with

promising performance. An effort has been made the replacement of high-density iron base materials with newly developed composites from aluminum(Al), Titanium(Ti), and magnesium(Mg) [83], [126]–[128]. Youssef et al.[87] develop a close-packed nanocrystalline single-phase structure of $Al_{20}Li_{20}Mg_{10}Sc_{20}Ti_{30}$ HEA using mechanical alloying reported density 2.67 g/cm^{-3} and hardness similar to ceramic. Feng et al.[126], [129] designed a new low-cost, lightweight HEA $Al_{1.5}CrFeMnTi$ with a BCC+L21 structure and a density of less than 6 g/cm^{-3}. Recent research shows that the high entropy alloy has high microhardness[83], wear resistance[119], multiphase microstructure and precipitate[130], soft-magnetic properties[131], and exhibit good mechanical properties and corrosion resistance. Moreover, the HEA has multi-elements inside the matrix; therefore, the mixing entropy of the alloy is generally higher than conventional alloy, making the alloys more stable at high temperatures. In designing lightweight HEA, several elements with a lower density like Magnesium (Mg), aluminum (Al), and lithium (Li) are used inside AlLiMgZnSn HEA in different atomic percentages, causing the density of the alloy to range from 3.08 to 4.23g cm^{-3}[48]. The high entropy refractory alloy design using Cr-Nb-Ti-V-Zr has a lower density of 6.49 g cm^{-3} with higher stability at elevated temperatures[82]. Stepanov et al. redesigned the Cr–Nb–Ti–V–Zr [82]refractory alloys by replacing chromium with different percentages of aluminum in $Al_xNbTiVZr$ (x=0,0.5,1,1.5) to reduce the density from 6.49 to 5.55 g cm^{-3}[92].

The present research aims to create LWHEAs with excellent Mechanical and tribological properties and oxidation resistance for use in transportation, defense, and space applications. Previously, several material scientists created LWHEAs utilizing low-density non-transition metals such as Li, Mg, Al, and Si and observed a weight of less than 4 g

cm3 [86], [87], [127], [128]. This paper focuses on $Al_{1.5}CrFeMnTi_x$ HEA multi-component composition, where titanium atomic percentage changes from 0.1, 0.15, and 0.2. The reason behind selecting $Al_{1.5}CrFeMnTi_x$ is because it has a BCC+ L21 +laves phase with respect to the temperature. With an in-depth analysis of Al1.5CrFeMnTix, we can provide a new glimpse on how this low-weight high entropy alloy can be utilized.

4.3 Materials and Methods

Al1.5CrFeMnTi0.1 and Al1.5CrFeMnTi0.15 and Al1.5CrFeMnTi0.2 alloys, referred to as Alloy 1, Alloy 2, and Alloy 3, respectively, were prepared at the South Dakota School of Mines and Technology by vacuum arc melting (VAM). Three different alloys with variation in the nominal composition (as listed in Table 1) of distinct elements Al, Cr, Fe, Mn, Ti (99.9%) pure were processed via Vacuum arc melting. The corresponding mixture of the elements were arc melted within a copper chamber that was cooled by water. The remaining oxygen, nitrogen, and hydrogen were removed using pure titanium. Each alloy was solidified and remelted five times to obtain a homogenous distribution of all elements in the alloys, flipped for each melt, and remained liquid for about 5 minutes for each melting event. The prepared sample ingots had a 100 mm diameter and a 30 mm width. The Energy dispersive spectroscopy (EDS) was utilized to identify the alloy composition, and the corresponding results are listed in Table 2.

Table 2 Material specification

Sr. No.	Powder Name	Purity (*%)	Manufacturer	Physical State	Density (gm/cm^3)	Melting point
1	Iron Metal	99.9+	Atlantic Equipment Engineers	Granules	7.874	1539
2	Titanium	99.99	Alfa-Aesar	Granules	4.5	1668
3	Manganese	99.9	Alfa-Aesar	Broken Plate	7.26	650
4	Chromium Metal	99.99	Atlantic Equipment Engineers	Flake	7.19	1907
5	Aluminum	99.7	Atlantic Equipment Engineers	Granules	2.7	661

A small section of the ingot was cut from the VAM processed sample using electrical discharge machining (EDM), and then it was encapsulated inside of an enclosed Argon backfilled quartz tube for conducting heat treatment at 1200°C for one hour, which was then followed by water quenching. Heat treatment was used to arc-melting the sample and chemically homogenize the material; this is called solutionization treatment. After solutionization, the samples were isothermally annealed for 1 hour, 4 hours, and 16 hours at 650 °C, 800 °C, and 1150 °C followed by water quenching.

The as-processed and the heat-treated samples was successfully mounted using conductive mold material, polished (using an AutoMet 250 from Buehler, Illinois, in the United States), and subsequently polished using grinding paper with grit sizes ranging from 120 to 1200 to obtain a flat surface. The last step was to polish the samples using colloidal silica so that they would have a flat surface. In the last step, the samples were polished using the microcloth with a 0.04mm colloidal silica solution to obtain a metallographic finish surface characterization. Finally, these samples were cleaned via ultrasonication in ethanol for further characterization.

The microstructures of as-casted and heat-treated well-polished specimens were analyzed using scanning electron microscopy (SEM) and electron dispersive spectroscopy (EDS) (Inspect F50, Manufacturer: FEI now ThermoFisher Scientific, Hillsboro, OR, USA). The program known as ImageJ was used to take measurements, and the results of those measurements, together with an average of 50 grains, are presented in this study. The phase composition of the as-casted and heat-treated specimens was investigated and analyzed using the X-ray diffraction (XRD) technique. The 1.54 Cu K line of a Rigaku Ultima III x-ray diffractometer was used characterization on each as a processed sample. A typical Vickers microhardness tester (Wilson, Chicago, IL, USA) with a diamond indenter was used to evaluate the microhardness of as-casted and heat-treated samples. The microhardness values were evaluated under the load of 0.5 Kgf and the dwell time of 10 s. The average value of ten microhardness readings for the individual sample is reported.

4.4 Results and Discussion

The following experiment will be described for conventionally cast HEAs, involving arc or induction melting and casting. The impacts of light elements Al and Ti were fabricated using arc melting. The chemical composition of an alloy was measured using energy dispersive spectroscopy (EDS), which is mentioned in table 3. There is a 4% deviation observed in actual vs. theoretical values. In LWHEA, the phase diagram (Figure 1) of $Al_{1.5}$CrFrMnTi reveals three primary phases bcc, L21, and laves C14 at different titanium percentages. This experiment focuses on the BCC+ L21 phase, which resembles a superalloy microstructure (γ/γ') with two phases and exhibits excellent mechanical properties to a single-phase alloy.

Table 3 Nomial vs. Actual composition

	Nominal wt%			Actual wt%		
Element	**Alloy 1**	**Alloy 2**	**Alloy 3**	**Alloy 1**	**Alloy 2**	**Alloy 3**
Al	19.46	19.23	19.02	18.34	18.1	18.29
Fe	26.84	26.54	26.24	26.94	27.78	27.15
Cr	24.99	24.71	24.43	23.61	24.93	23.98
Mn	26.41	26.11	25.81	28.9	25.85	26.3
Ti	2.3	3.42	4.5	2.21	3.34	4.28

Figure 1 demonstrates that the BCC L21 phase is available from 0.1 to 0.5 atomic percent of Ti, according to CALPHAD modeling. As a result, three distinct ingots with Ti atomic percentages of 0.1, 0.15, and 0.2 were cast utilizing arc melting for investigation. The phase diagram shows that the bcc phase is stable above 800C and that the bcc L21 phase is stable below this temperature. As a result, this research aims to modify the

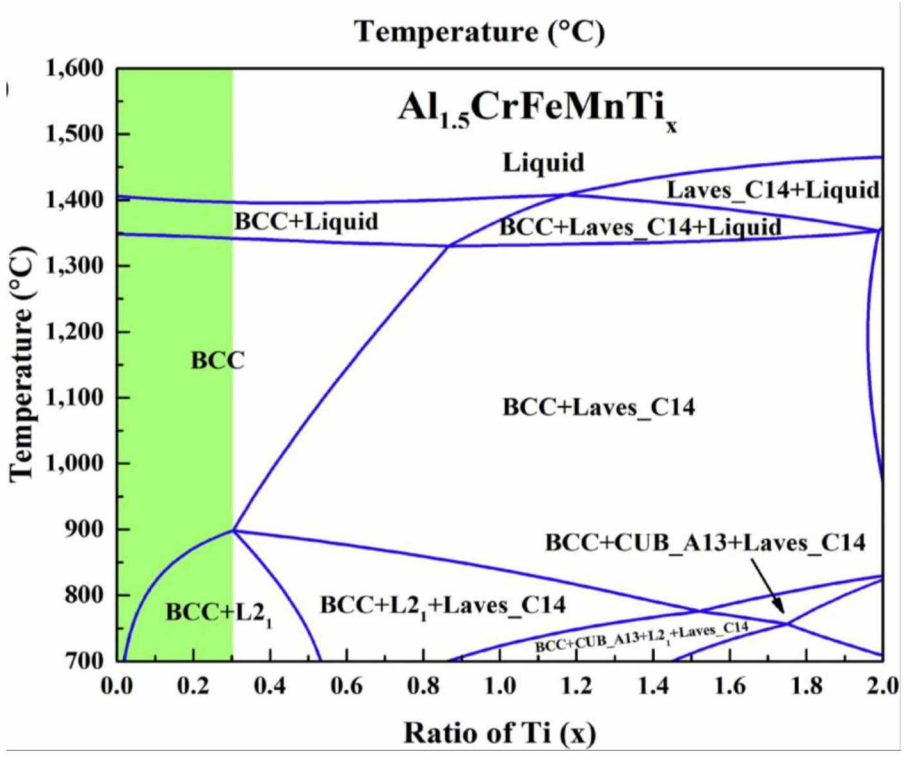

Figure 4 1 CALPHAD modeling of $Al_{1.5}CrFrMnTi_x$ [28]

microstructure of order L21 by applying various heat treatments and then investigate whether these changes will impact the material's mechanical properties.

Figure 2 illustrates the X-ray diffraction (XRD) patterns of arc-melted Al1.5CrFrMnTi0.1, Al1.5CrFrMnTi0.15, and Al1.5CrFrMnTi0.2 alloys in their as-cast conditions. The XRD analysis verifies that all of the alloys, when analyzed at room temperature, exhibit bcc and L21, which is consistent with the phase diagram. Although the L21 phase cannot be seen on SEM images, two small peaks in the XRD data indicate that L21 phase particles are nanosized. Precipitate hardening and improved ductility may be achieved by accumulating the L21 phase, which may change the microstructure.

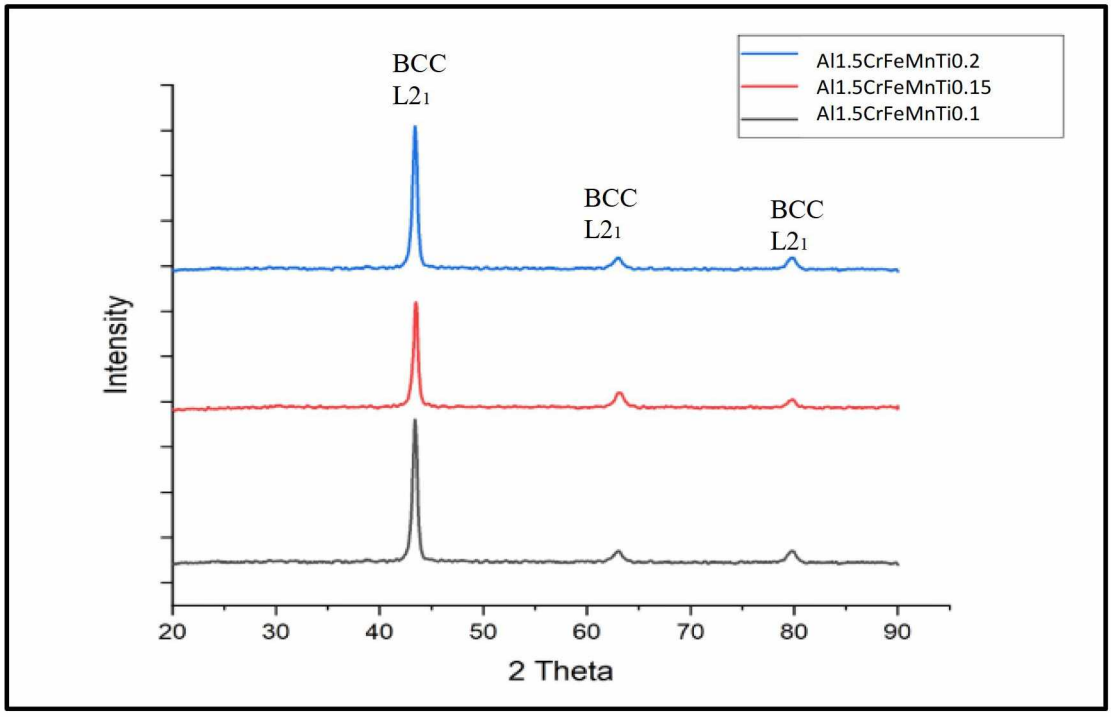

Figure 4 2 XRD graph and peak index Al1.5CrFeMnTi0.1, Al1.5CrFeMnTi0.15 and Al1.5CrFeMnTi0.2

We used the Archimedes technique to determine the weight of each of these three alloys since our investigation is focused on creating a low-density high entropy alloy. Aluminum and titanium have a density of 2.7 and 4.5 g.cm-3, respectively, but iron, manganese, and chromium all have a weight that is more than 7.1 g.cm-3. Therefore, a higher proportion of aluminum results in an overall weight that is lower than 6 g cm-3. The aim is to create alloys with a density of less than 6 g.cm-3 that could be achieved by all of the possible compositions. The densities of Al1.5CrFrMnTi0.1, Al1.5CrFrMnTi0.15, and Al1.5CrFrMnTi0.2 vary from 5.886 g cm^{-3} to 5.889 g cm^{-3}.

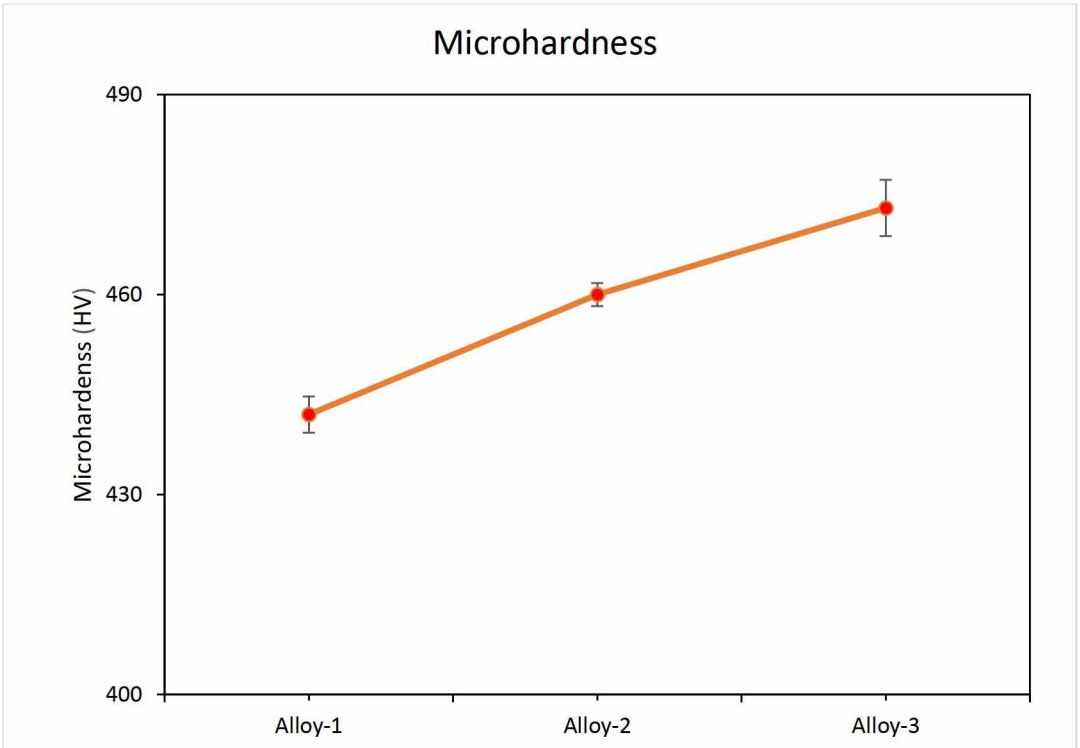

Figure 4 3 Density and the microhardness of LWHEA

Figure 3 shows the correlation between density and microhardness, and our analysis reveals that as the percentage of titanium in an alloy increases, the density, and the microhardness

increase. Titanium is a harder material, and an increasing percentage of titanium increases an alloy's microhardness.

Scanning electron microscopy (SEM) and Energy dispersive spectrometry (EDS) were used further to examine the microstructure and morphology of the alloy. Figure 4 shows the backscattered SEM image and details the microstructure of three separate alloys. There is no evidence of L21 precipitation seen in any of the images. Figure 5 shows the results of the EDS mapping performed on LWHEA. Here, it is possible to see that all of

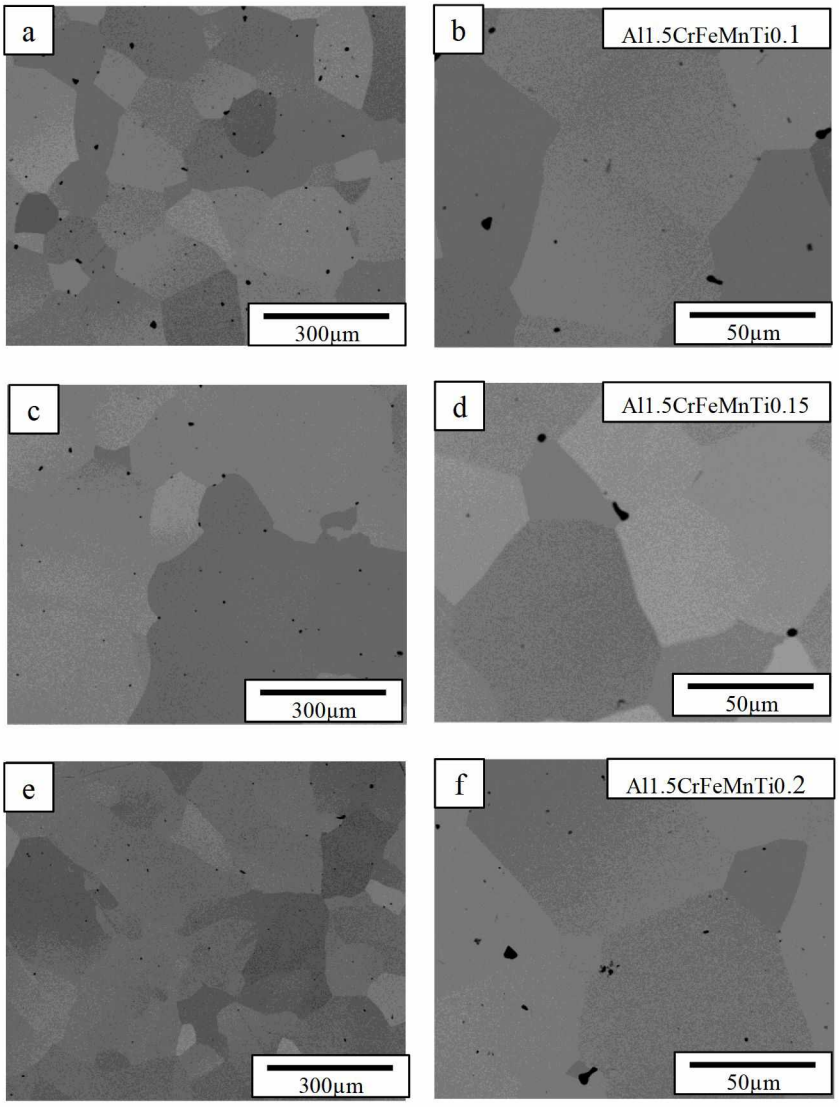

Figure 4 4 SEM images of $Al_{1.5}CrFrMnTi_{0.1}$, $Al_{1.5}CrFrMnTi_{0.15}$ and $Al_{1.5}CrFrMnTi_{0.2}$

the components have been dispersed evenly inside the matrix, and the L21 +BCC phase is combined. The L21 particles are distributed inside the BCC matrix, and it is a classical representation of nickel superalloy structure γ/γ'. Feng et al.[126] was investigated the L21 phase, and DF imaging was used to determine the nano-scale particle size of the L21 phase.

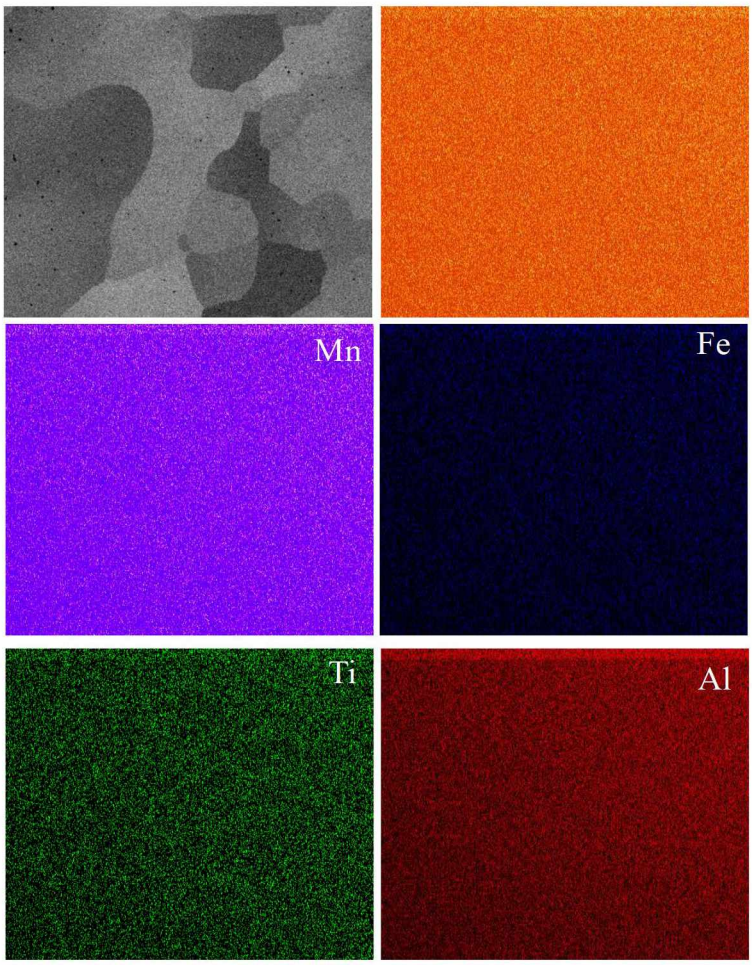

Figure 4 5 EDS mapping of $Al_{1.5}CrFrMnTi_{0.15}$

In order to increase the performance of an alloy, it is necessary to change the microstructure of LWHEA further using the L21 phase as the γ' phase, similar to nickel superalloy. Therefore, our objective is to design thermal processing or heat treatment technics that can improve the alloy's properties. A differential scanning calorimetry (DSC) experiment

shown in figure 6 was conducted at a heating rate of 10 °C/min up to 1400 °C to explore the phase stability of synthesized HEA. The recrystallization of the phase is represented by two exothermic peaks on the DSC curve, which are seen at 797 °C and 1100 °C, respectively. At approximately 797°C, the L21 recrystallization occurred, and the HEA matrix recrystallization occurred at around 1100°C. The DSC analysis reveals that the microstructural and phase changes occurred at 797°C and 1100°C, corresponding to the two different temperatures where the partial and complete recrystallization occurred.

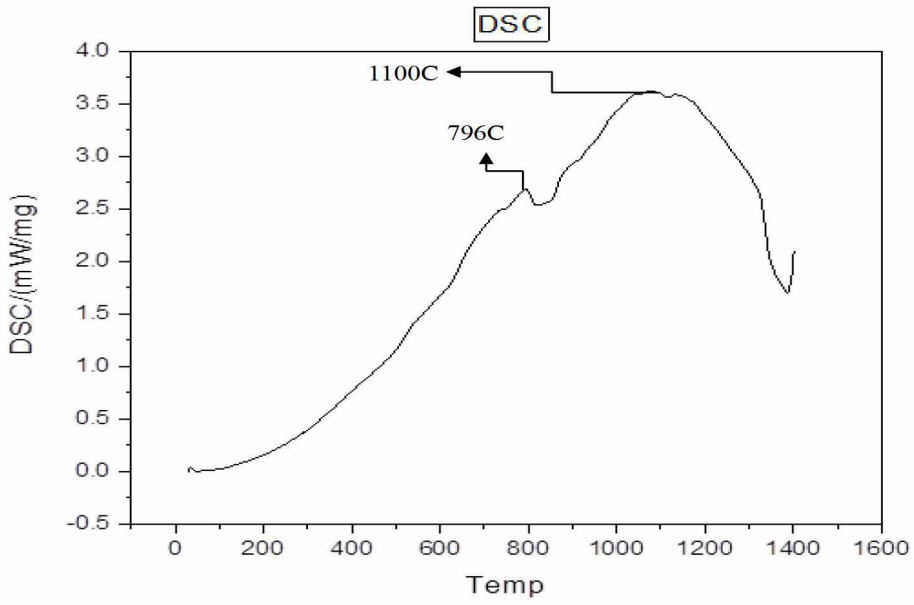

Figure 4 6 DSC Curve of $Al_{1.5}CrFrMnTi_{0.15}$

In accordance with the results of the DSC investigation, new heat treatments were developed. The as-cast $Al_{1.5}CrFrMnTi_{0.15}$ alloy was annealed at 650 °C, 800°C, and 1150 C for 1, 4, and 16 hours in an encapsulated quartz tube and water quench subsequently to evaluate the influence of annealing on phase formation. SEM images are shown in Figures 7,8 and 9 of annealed $Al_{1.5}CrFrMnTi_{0.15}$ HEA show the impact on microstructure and

hardness after heat treatments at 650°C, 800°C, and 1150°C for 1,4 and 16 hours. The images obtained from scanning electron microscopy show that the grain size increases as temperature and time increase. However, there have been slight microhardness changes, meaning the precipitation accumulation is not happening with the respective time. Therefore we can say that a long hour of heat treatment would be required to see any changes in the microhardness and microstructural. Also, the L21 precipitation needs to be studied in detail to make further changes in the heat treatment or the alloy composition to get better results in terms of mechanical properties.

The bcc alloy is often brittle and has a greater hardness. The present LWHEA alloy is brittle, and nanosized L21 precipitation may be one of the factors leading to this brittleness. The mechanical property may be significantly influenced by the phase stability, phase evolution, and precipitation properties of L21 precipitates in the BCC matrix[53] [73], [129]. As a result, we will now describe these behaviors as follows: The alloy's compositions strongly influence the creation of the L21 phase. The L21 phase is high in Fe and Ti and low in Cr, or the BCC matrix is high in Cr but low in Fe and Ti [129]. As for the L21 prediction, Feng et al. [132]observed the highest enthalpy of $AlFe_2Ti$ in his $Al_{1.5}CeFeMnTi$ alloy. Also, Cr and Mn are observed in the L21 phase creating quinary $Al(CrFe)_2Ti$, $Al(CrMn)_2Ti$, $Al(FeMn)_2Ti$, and When Mn is present, Cr solubility in the L21 phase is limited. Substituting Cr for Fe in $AlFe_2Ti$ raises the enthalpy, indicating that this replacement is energetically adverse; therefore, the Cr substitution in the L21 phase is the less favorable of these 5 components; thus, its solubility in the L21 phase should be limited[132].

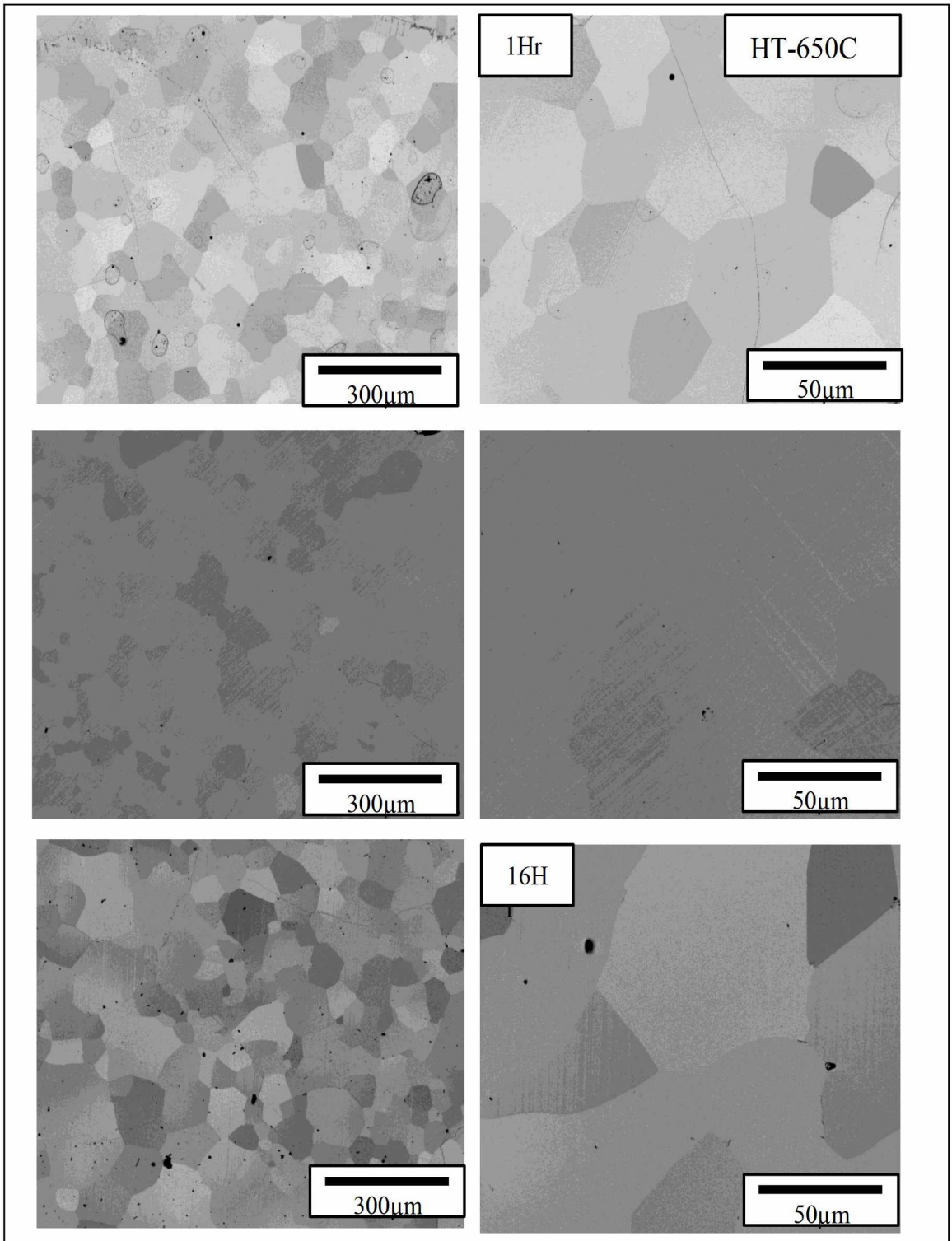

Figure 4 7 SEM image for annealing heat treatment for 650C for 1,4 and 16hour

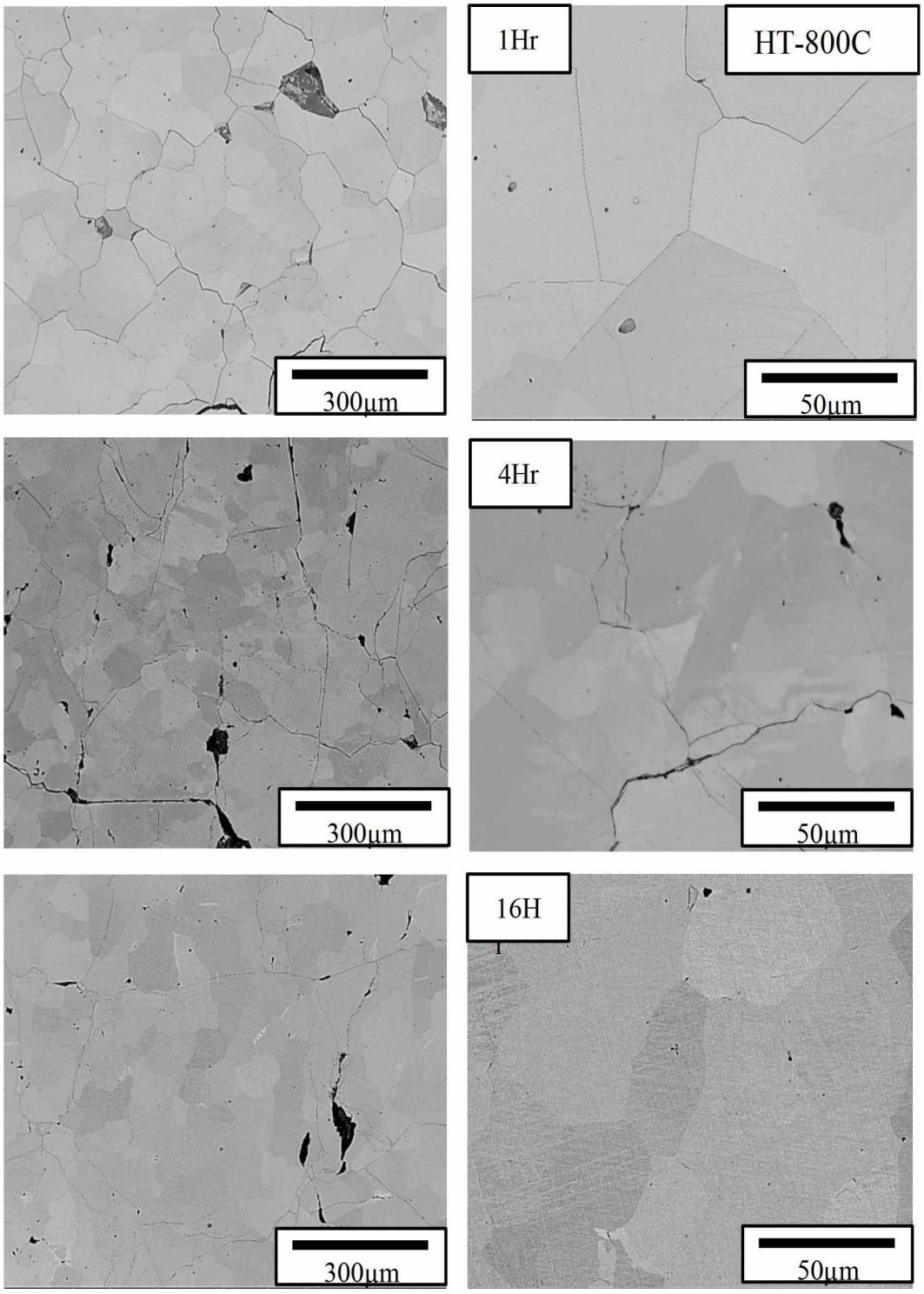

Figure 4 8 image for annealing heat treatment for 800C for 1,4 and 16hour

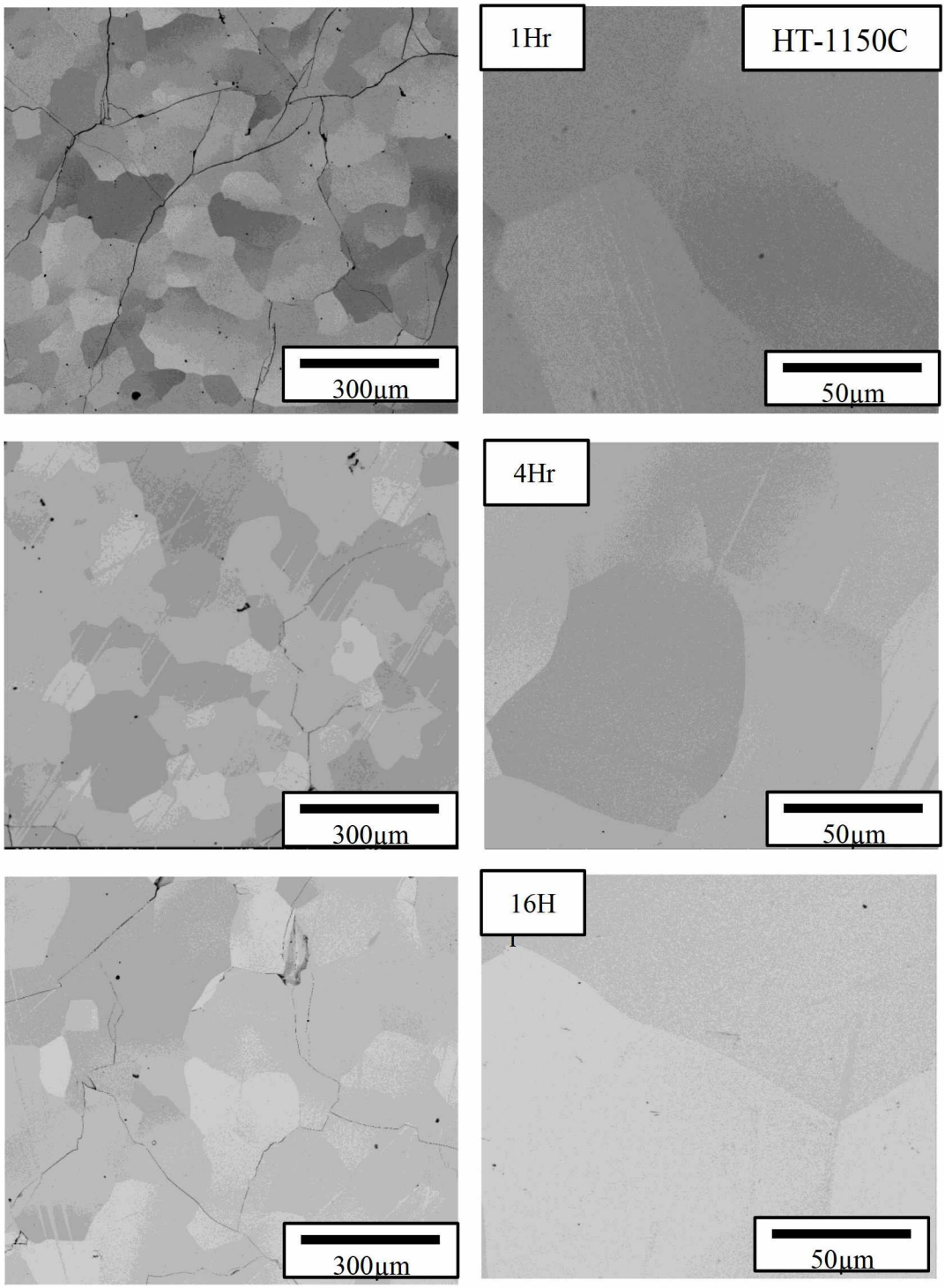

Figure 4 9 SEM image for annealing heat treatment for 1150C for 1,4 and 16hour

Additionally, it has been discovered that when Ti is added to the alloy, the D03 structure of Fe3Al may transform into the L21 structure of AlFe2Ti as a consequence of the Fe sites being replaced by Ti [133], [134]. Due to the limited solubility of Cr and the need for Ti in the L21 phase, the diffusion behaviors of Ti and Cr will play a crucial role in developing the L21 phase. The partitioning of Cr to the BCC phase and Ti and Fe to L21 show the existence of a molecular driving force for the development of the BCC and L21 phases. The establishment of the L21 phase is most likely driven by clustering and ordering processes [135]. However, the L21 phase offers benefits for nucleation considering the low interaction energy between the L21 and BCC phases, which is the consequence of a smaller lattice distortion[136], [137]. This gives the L21 phase the advantage. During precipitation, the balance between elastic-strain energy (Eel) and interfacial energy (Es) determines the equilibrium form of the L21 precipitates[138].

The graph (figure 10) shows the relation between the grain size and the microhardness. We have observed that with increasing heat treatment, the grain size of the alloy increase, and the microhardness decreases. However, there has been a good increment in the grain size, but there is a very slight change in microhardness. A slight change in microhardness also shows that there has been very less impact on the strengthening mechanism in the alloy. Or there will not be any accumulation of precipitate causing a very slight change in microhardness. The sample heat treated at 800C shows an increase in brittleness. A recrystallization peak at 797 °C is also shown in the DSC data, which could be related to this process. Also, we can say that the recrystallization of the L21 phase occurred between 600-800C. The annealing at 1150C reveals that the BCC and L21 phases re-crystallize at

around 1150C showed in the DSC curve, resulting in the lowest microhardness and largest grain size.

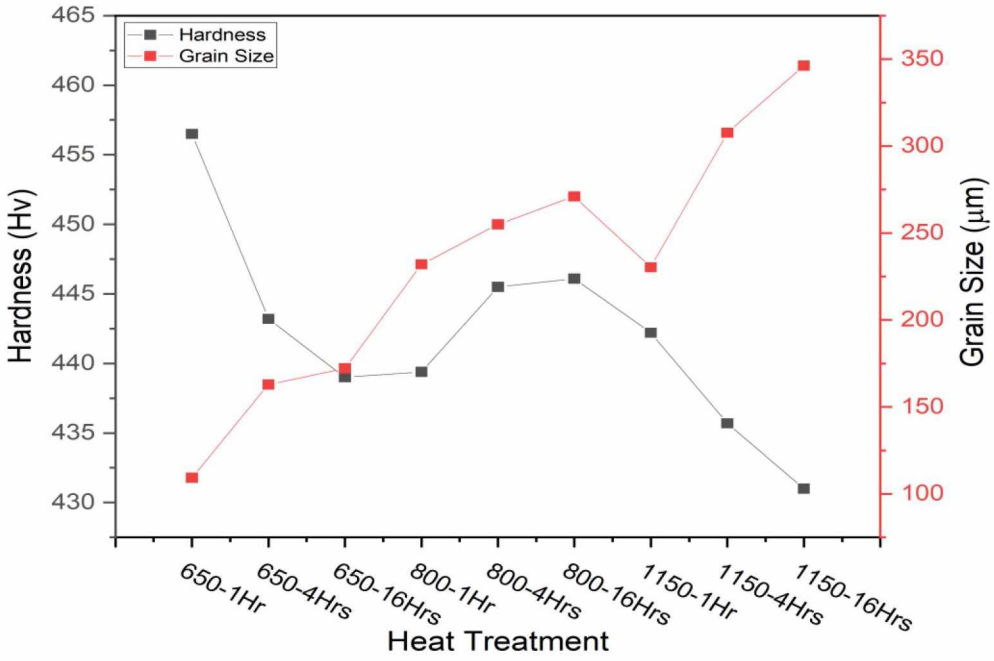

Figure 4 10 Grain size and the microhardness of LWHEA

During water quenching, the solutionized alloy appeared to have decomposed the high-temperature single phase into BCC and L21 phases. The CALPHAD demonstrates the presence of L21 at or above 796 °C, indicating high-temperature phase over 800 °C is most likely a single-phase BCC. The high-temperature phase splits result in an interlinkage between BCC and L21 phases, and such a linked network is not anticipated in the case of nucleation and growth processes. Furthermore, the phase transition caused by the spinodal decomposition process varied in composition during annealing isothermal heat treatment. Furthermore, unlike the nucleation and growth processes, the volume percentage of the phases seems to be more or less constant.

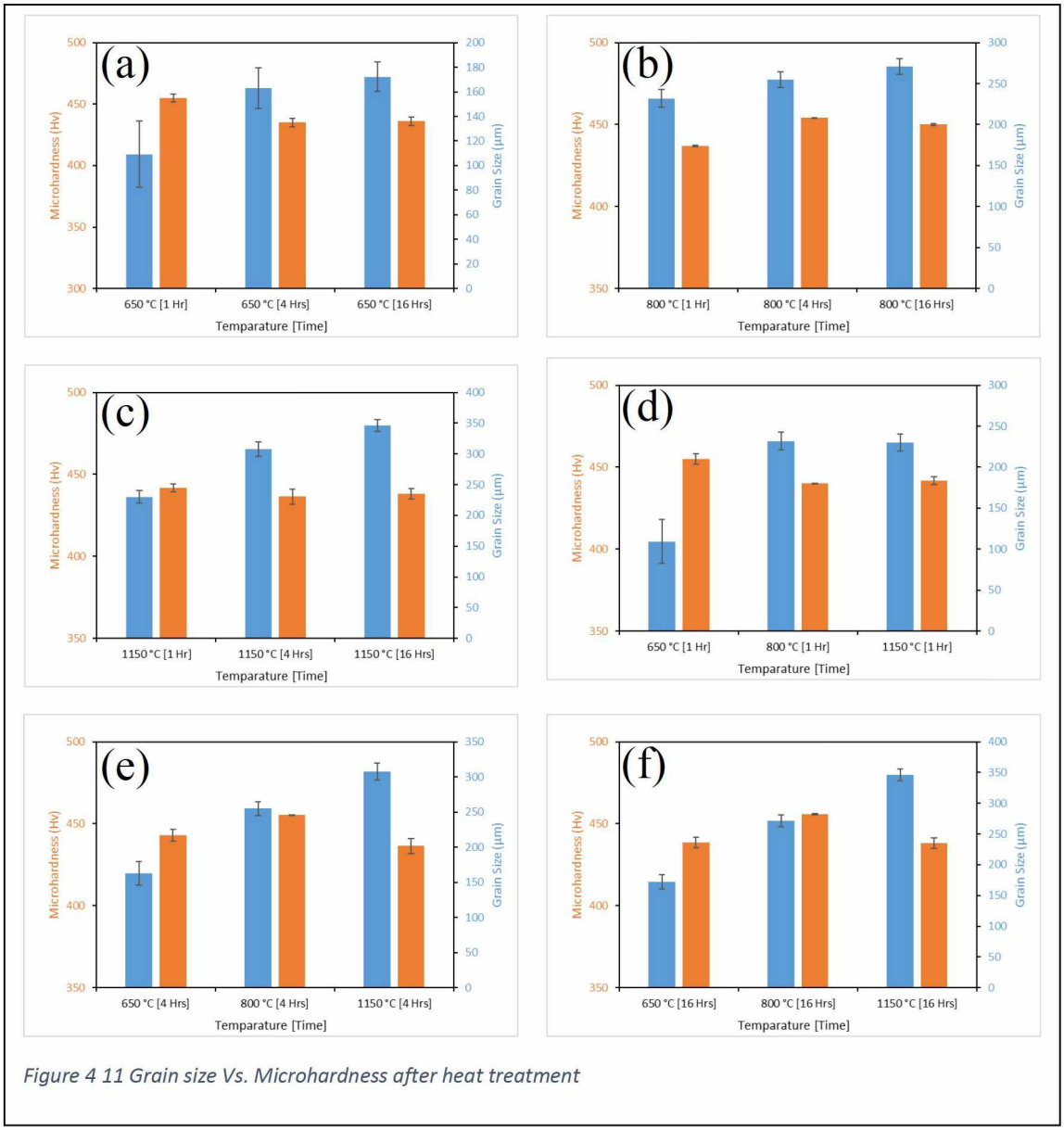

Figure 4 11 Grain size Vs. Microhardness after heat treatment

Figure 11 shows the in detail analysis of microhardness and grain size after heat treatment at different times and temperatures. We have observed that the strengthening mechanism of precipitate hardening does not impact the mechanical properties. That means the effect of heat treatment is minimal due to multiple reasons that need to be verified in the future study of the formation of the order phase and restructuring of the order L21 phase.

4.5 Conclusion

In this research, a novel LWHEA $Al_{1.5}CeFeMnTi_{x(0.1,0.15,0.2)}$ with a low density of 5.88 g cm^{-3} was successfully developed and synthesized arc melting. The arc melted sample have a BCC+L21 structure. To modify and alter the l21 structure in the BCC matrix, we have carried out different heat treatments at different temperatures and times to investigate the effect on the mechanical properties of the $Al_{1.5}CeFeMnTi_{1.5}$ alloys. Different heat treatments were carried out at temperatures of 600 °C, 850 °C, and 1150 °C for periods of 1,4, and 16 hours, respectively. Variations in the alloy's structure and mechanical characteristics were investigated using hardness tests, SEM, XRD, and EDS. The overall investigation leads to the following conclusions:

1. The density of an as-cast sample of alloy 1, alloy 2, and alloy 3 is 5.886, 5.887, and 5.889 g cm^{-3} respectively. Because Al is lighter than Ti , increasing the proportion of titanium in an alloy will result in a decrease of the amount of aluminum in the alloy. This will cause the density of the alloy to increase.
2. The grain size of alloy 2 was measured using image j software during several different heat treatments. The results show that an increase in grain size can be seen with an increase in temperature; however, even at the same temperature, there is a very slight variation in grain size when the duration of the heat treatment is changed.
3. Although the grain size changes with increasing temperature, there has been a slight microhardness change. Therefore, the strengthening mechanism does not significantly impact the alloy's mechanical properties.

CHAPTER V

HIGH ENTROPY NITRIDE

5.1 Abstract

Ultra-high temperature ceramics (UHTCs) consist of different ceramics like boride, carbide, diboride, and nitride of the transition metals. The UHTCs show prominent characteristics such as higher melting point, higher oxidation resistance, lower thermal conductivity, higher yield strength, and microhardness. High entropy ceramic (HEC) is a multi-component alloy similar to the high entropy alloy (HEA) specifically developed for hypersonic vehicles, nuclear reactors and high temperature applications. In the current study, mechanical alloying(MA) and spark plasma sintering(SPS) were used to develop equiatomic HEC (Hf0.2Nb0.2Ta0.2Ti0.2Zr0.2)N. The HECs were mechanically alloyed using the high-energy ball mill at 500 RPM for 6 hours. The ball to powder (BPR) ratio of 10:1 was maintained during the milling. This mechanically alloyed powder was sintered using SPS for 1800°C, 1900°C, and 2000°C to investigate the effect of temperature on densification of these HECs. The consolidated samples were further analyzed using scanning electron microscopy (SEM), microhardness, x-ray diffraction (XRD), and wear testings to understand the effect of different sintering temperatures on microstructure, phase transformation, mechanical, and tribological behavior of these high entropy nitride

ceramics. Oxidation treatments have been performed at 1000°C-1200°C for 2 hours duration. According to the findings, the oxidation behavior of all HEC samples follows a parabolic rate low at temperatures 1000-1200°C.

5.2 Introduction

Materials research has always been at the cutting edge of technological developments that have led to the progress of human civilizations from the beginning of time. The traditional alloy design process involved adding one or more components to the parent metal to achieve desired properties, including higher mechanical properties, chemical resistance, and wear resistance. Multi-principal element alloys (MPEAs) with a high configuration entropy that is created from more than 5 elements with equiatomic or more than 5-35 at.% are often referred to as high entropy alloy (HEAs) [6], [25], [26]. Entropy is a thermodynamic indicator that describes the degree of disorder and the many configurations that influence it, including magnetic moment, atomic vibrations, and crystal structure [104]. Until recently, when the notion of high-entropy alloys (HEAs) was created, entropy was not regarded as useful as enthalpy for material design [37][25]. Simultaneous research by Yeh et al.[116] and Cantor et al.[25] introduced the concept of HEAs, which discovered a novel family of multi-component alloys following some previous ground research. These HEAs' composition, microstructure, and characteristics are unique [40], [47], [50], [52], [69], [126].

The high entropy ceramics are derived from the high entropy alloy with two different material families for different applications. The transition metal nitrates currently used for the application required higher hardness, thermal stability, and chemical resistance. Transition metal nitride shows rocksalt structure including HfN[139],

NbN[140], TaN[141], TiN[142], ZrN[143], MoN[144], WN[145], FeN[146] and VN[147]. These metal nitrides show high hardness and fracture strengths than regular HEA because of their phase structure and electron valence[148]. Balasubramanian et al.[24] explain the role of valence electron concentration(VEC); ductility increases with increasing VEC, and transition from brittle to ductile occurs at VEC=10 for rocksalt structure in binary and ternary systems. High-entropy ceramics (HEC), like HEAs, are described as a solid solution with a high configuration entropy of five or more cations or anions sublattices [149]. HECs are a type of ceramic material with a melting point of more than 3000°C and can retain stable physical and chemical characteristics in high-temperature conditions[150]. Today, high-entropy ceramics encompass various materials such as carbides, nitrides, and borides of Group IV and V transition metals [151]. HEC showed better results in terms of hardness, fracture strength, wear resistance, and corrosion resistance [7], [11], [109], [152]–[155]. As a result, technologies like nuclear reactors, jet engines, cutting tools, and aerospace applications are the only materials that can protect components subjected to severe working conditions. Even after this, a suitable diffusion for similar materials class has yet to be achieved due to their poor fracture toughness, insufficient high-temperature oxidation characteristics, and the problems faced in synthesizing extremely dense structures.

Shen et al. [59] studied high entropy nitride(HEN) film coating using reactive sputtering because nitrides have high hardness and oxidation resistance. Each transition-metal nitride has its own set of characteristics, which would undoubtedly expand materials properties by synthesizing with a mix of transition metals. Due to their higher chemical and mechanical properties, metal nitrides, a vast family of metal compounds with nitrogen

in the formal oxidation state of -3, have received a lot of interest [7], [156]. Understanding the general patterns in interactions between nitrogen and other relevant elements is necessary to address phase stability and bonding in multi-component nitride materials. Transition metal's capacity to create thermodynamically stable nitride compounds varies with strong nitride formers occurring in groups 4–6 (Y, Ti, Zr, Hf, V, Nb, Ta) and poorly nitride producing Groups 7–11(Cr, Mo, Mn, Fe, Ru, Co, Ni) [157]. Transition metal nitrides are often interstitial compounds in which the nitrogen fills spaces in the metal's closed packing structure. The interstitial nitrides contain a combination of covalent, metallic, and ionic bonding, giving them desirable features such as high hardness, high electrical and thermal conductivities, and comparable chemical stability [157].

Mechanical alloying (MA) is a powder processing methodology that facilitates synthesizing homogenous products from combined elemental powder mixtures. MA is defined as the repetitive welding and fracturing of powder particles entrapped between milling mediums, the ball to powder ratio and milling duration determined by the mechanical properties of powder ingredients [3], [112][111]. The technique was successfully applied to a wide range of materials, including metal matix composites, solid solution alloys, amorphous material, and HEAs [111]. MA has the added benefit of enhanced solid solubility, even in insoluble materials, in addition to nanomaterials processing. Solid mixing of nanoparticles before alloying using milling increases diffusion rates, and higher configurational entropy, also improving the stability of solid solution phases in HEAs. The microstructure and characteristics of high entropy alloys significantly change as milling parameters such as a ball to powder ratio (BPR), milling speed, and milling duration are varied. This technique has previously been utilized to create plasma-

sprayed HEA coatings[3], [158], [159], and it would be perfect for large-scale processing of nanocrystalline HEAs.

A new method for manufacturing metal or non-metal composites synthesize at low temperatures and quicker processing than standard conventional casting methods is spark plasma sintering (SPS) [113]. In the SPS process, impurities and gases between the material particles activate the spark discharge, which produces high-temperature states in a gap, causing condensation and melting on the powder interface to make a completely dense composite material. SPS uses uniaxial force and DC pulse current for a fast sintering process for conductive and non-conductive materials. This large AC transmission and dispersion of the joule heat effect across the specimen result in quick and comprehensive heat transfer, providing high homogeneity and constant precipitate densities. SPS can consolidate nanopowders without significant grain development due to higher heating rates and temperature quicker sintering process [114]. Even while SPS is beneficial for a wide variety of powder treatment processes, there is a particular focus on nanocrystalline materials at the moment. SPS also allows for producing near-net form components with symmetrical and simple geometry in a single phase.

In this study, we first investigated the formation possibility of $(Hf_{0.2}Nb_{0.2}Ta_{0.2}Ti_{0.2}Zr_{0.2})N$ high entropy nitride (HEN) effectively consolidated using the SPS process at 50Mpa pressure 2000°C temperature. The phase development and crystal structure of consolidated HEN were examined for their mechanical, wear properties also oxidation behavior. The SEM micrographs and XRD (X-ray diffraction) patterns of high-entropy nitride ceramic verified the development of an Fcc structure in which transition metal elements(Hf, Zr, Ta, Ti, Nb) occupy a cation place and nitrogen N element holds the

anion position. Furthermore, (Hf0.2 Zr0.2 Ta0.2 Nb0.2 Ti0.2)N gets their mechanical and wear properties from the binary nitride ceramics. High-entropy nitride (HEN) ceramics are an excellent choice for aerospace and automotive applications, including gas turbines and spacecraft, because to their superior properties.

5.3 Experimental Methods:

5.3.1 Materials

The commercially available ceramic powder of Hafnium Nitride-HfN (99.5% pure, -325 Mesh), Niobium Nitride-NbN(99.8% pure, -325 mesh), Tantalum Nitride-TaN (99.8%, 1-5micron APS), Titanium Nitride-TiN(99+%, -325 mesh), and Zirconium Nitride-ZrN (99.8%, 10 micron APS) were purchased from Atlantic equipment engineers, NJ, USA. The high entropy ceramics of equiatomic composition (HfN: NbN: TaN: TiN: ZrN = 1:1:1:1:1) were synthesized with the help of SPS.

5.3.2 Mechanical alloying(MA) and SPS:

The powder was added into Tungsten Carbide (WC) 80ml bowl under an inert (Ar) atmosphere for MA. The WC material balls (Ø3 mm) were used to prevent cross-contamination during the mechanical alloying process. The ball-to-powder (BPR) mass ratio was 10:1, and the stearic acid ($C_{18}H_{36}O_2$) of 2% was added as a process control agent (PCA) to prevent the excess welding effect throughout the MA process. The mixture of equiatomic powder along with PCA was mechanically alloyed at 500 rpm for 6hrs duration using the high-energy planetary ball mill (Model Pulverisette 7, Fritsch GmbH). The effect of the temperature rise was prevented by providing a cooling period of 30 min after every 30 min of ball milling.

This mechanically alloyed powder's sintering was done with the help of Spark Plasma Sintering (SPS) (Model SPS 10-4, Thermal Technologies). The mixture of ball-milled powder was placed inside the Ø20 mm graphite die (inner diameter), and the thin graphite foil was used to easily remove the sintered part and to avoid any reaction between powder and die. The sintering of the powder was carried at 1800°C, 1900°C, and 2000°C and 50Mpa uniaxial pressure in argon, and the heating rate was 100°C/min with a dwell period of 5 minutes.

The temperature within the die was measured using an optical pyrometer. The compacted sample was mounted on conductive material using hot press mounting, polished (AutoMet 250, Buehler, IL, USA), and sanded successfully in different grit (120 to 1200) sandpaper. To complete the process, samples were polished using colloidal silica to remove any remaining grit. To obtain a better glossier metallographic finish, samples were polished on micro cloth with 0.04mm colloidal silica solution, and lastly, these samples were cleaned ultrasonically in ethanol.

5.3.4 Characterization

Scanning electron microscopy (SEM) and Electron Dispersive Spectroscopy (EDS) were used to examine the microstructures of all sintered and well-polished specimens (Inspect F50, Manufacturer: FEI now ThermoFisher Scientific, Hilsboro, OR, USA). In order to assess the phase composition of the spark plasma sintered specimens, XRD was used. The 1.54 Cu K line of a Rigaku Ultima III x-ray diffractometer was used in order to conduct a phase analysis on each sintered sample. Additional isothermal oxidation heat treatments at 1000, 1100, and 1200°C were used to examine the oxidation behavior of the sintered samples.

5.3.5 Measurement of hardness and tribological properties

The microhardness of the as-sintered (Hf0.2Nb0.2Ta0.2Ti0.2Zr0.2)N samples was measured using a standard Vickers microhardness tester (Wilson, Chicago, IL, USA) with a load of 0.5 Kgf for 10 seconds. For each sample, the level of hardness is determined by taking the average of 10 separate measurements. Dry (unlubricated) wear tests were performed at room temperature on a ball-on-disc tribometer manufactured by NanoveaTM and located in Irvin, California, in the United States. The standard test technique for wear testing pin-on-disc equipment was adhered to throughout the process [115]. The counter body was made of a silicon nitride (Si3N4) ball with a 3mm diameter. In order to conduct the wear tests, a load of 1 newton, a sliding velocity of 200 revolutions per minute, a track diameter of 5 millimeters, and a total sliding distance of 200 meters were used in a dry environment with a relative humidity of 45-50 percent.

5.4 Results and Discussion:

5.4.1 Microstructural analysis

The SEM images of $(Hf_{0.2}Nb_{0.2}Ta_{0.2}Ti_{0.2}Zr_{0.2})N$ samples sintered at different temperatures are shown in figure 1. For brevity, samples sintered at 1800°, 1900°, and 2000° C refer to HEC-1, HEC-2, and HEC-3, respectively. The SEM micrographs illustrate that with increasing temperature, the densification of the sample is increased due to significantly less porosity for the sample sintered at 2000°C. The lower magnification SEM images show the black-spotted area observed over the sample sintered at 1800°C and 1900°C. The black-spotted are nothing but porosity, confirming that the 1800°C and 1900°C were inadequate for HEC consolidation.

The HEC-3 was selected for further study due to its better compactness, relative density, and microhardness than the other two HEN samples. The EDS mapping of the well-polished surface of HEC-3 was performed, and the corresponding elemental maps of Hf, Nb, Ta, Ti, Zr, and N are shown in figure 2. These metal nitrides are evenly distributed in the formed solid solution of High entropy ceramic (HEC-3). All the elements are evenly distributed inside the alloy, a secondary phase of (Hf, Zr)N is present, and Hf clusters are also noticed (shown in figure 2b,f). HEC-3 shows a homogenized microstructure compared to other refractory HEA complex microstructures with dendrites and intermetallic phases confirmed using XRD.

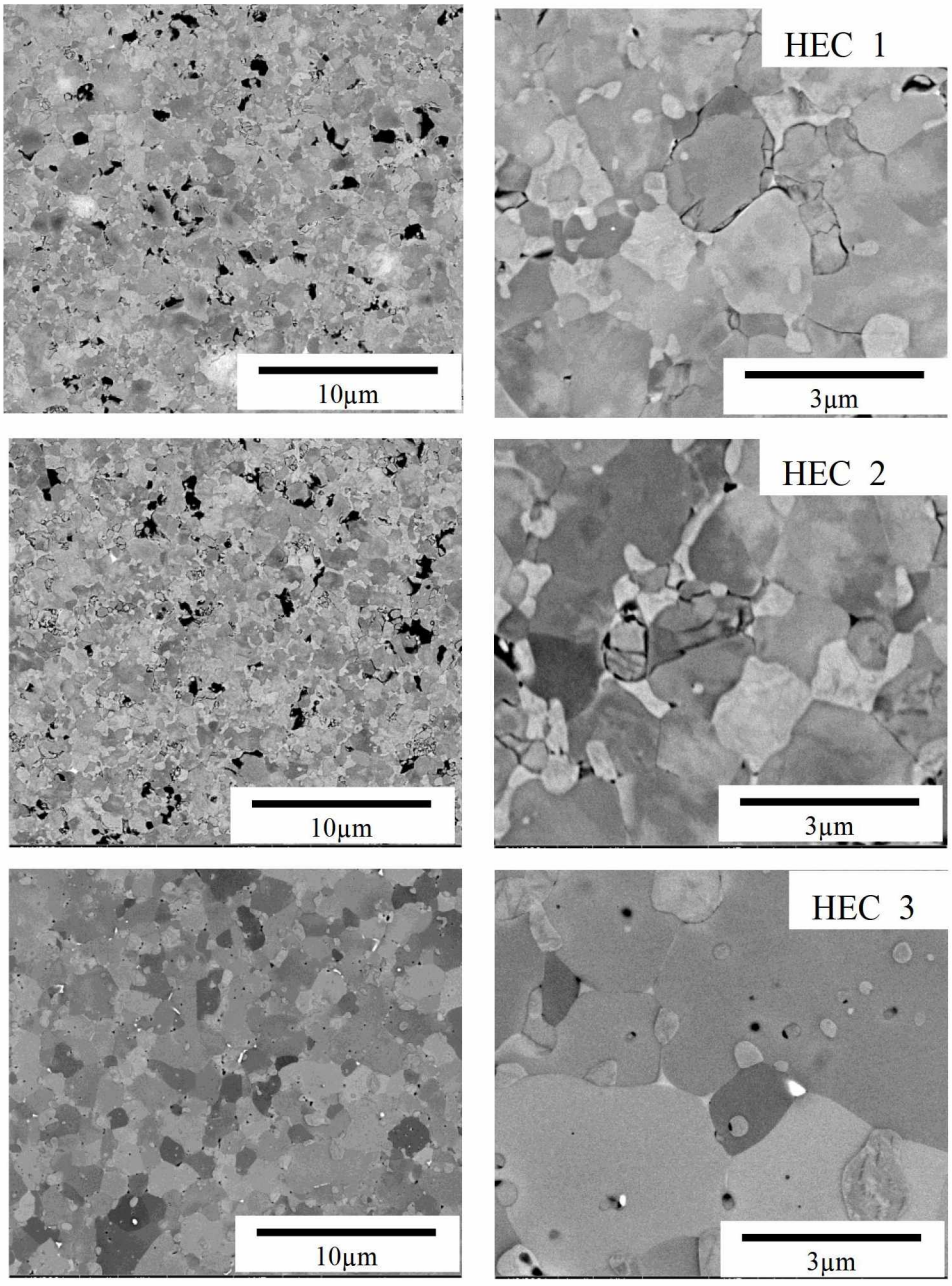

Figure 5 1 SEM of HEC sample sintered at HCE-1 1800C, HEC-2 1900C and HEC-3at 2000C

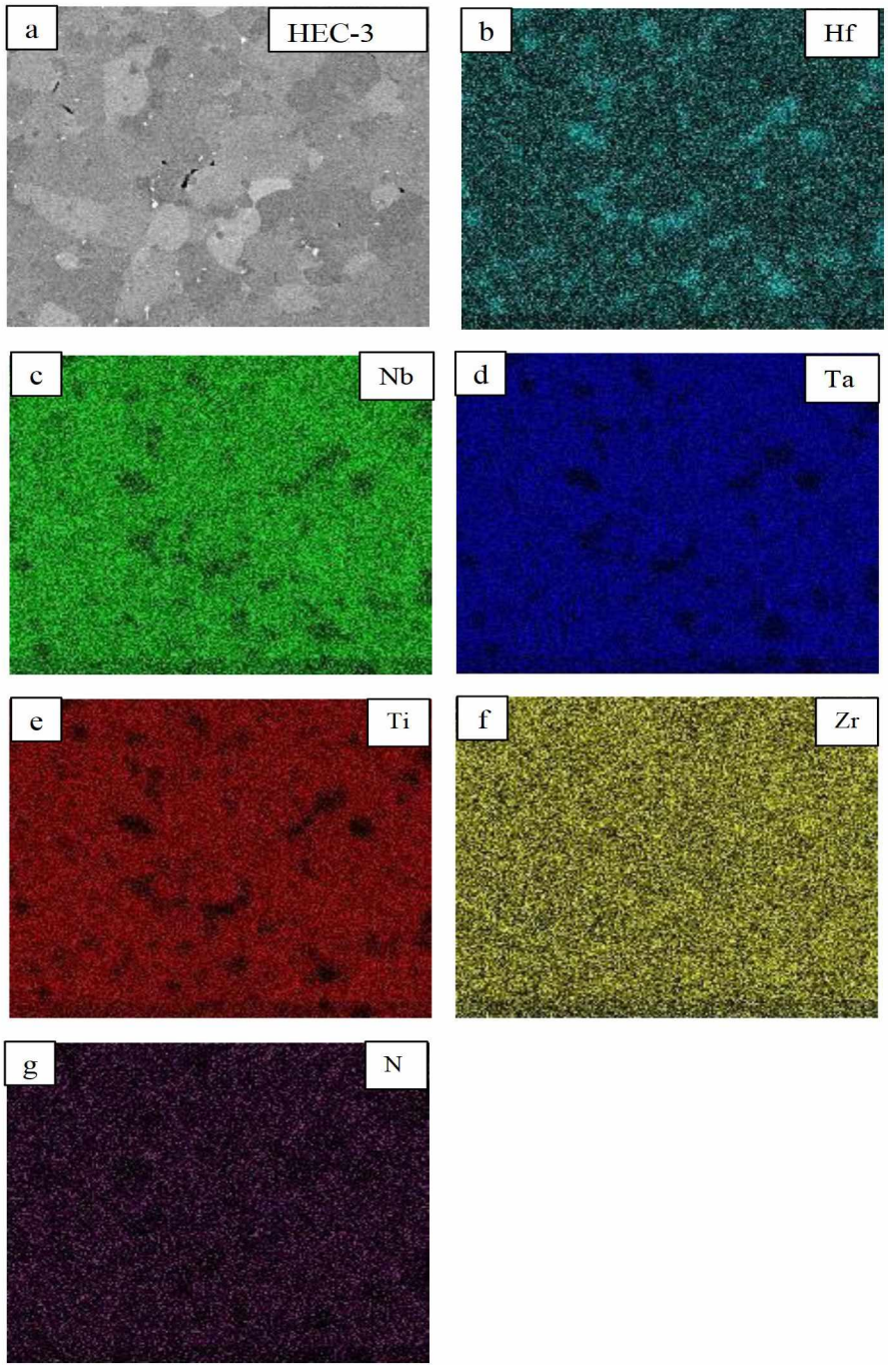

Figure 5 2 EDS mapping of the sintered sample at 2000 ℃ (HEC-3) (a) Electron Image and Elemental analysis of (b) Hafnium,(c) Niobium (d) Tantalum (e) Titanium, (f) Zirconium, and (g) Nitrogen

Figure 3 shows the X-ray diffraction patterns of a sample obtained after mechanical alloying and SPS. Only the peaks of a single FCC structure have been seen in the XRD graph after spark plasma sintering, showing that the system has progressed toward a solid solution. A similar FCC structure has been observed in the HEN processed using

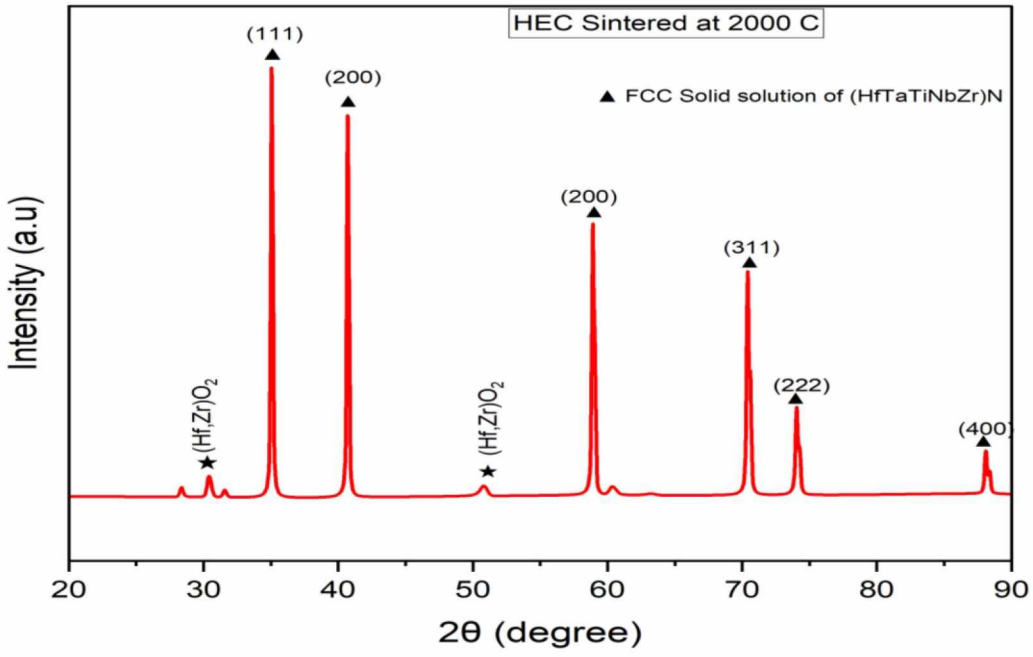

Figure 5 3 XRD graph and peak index of HEC sintered at 2000 ℃

exothermic combustion [148]. The potential of transition metals to create thermodynamically stable nitride compounds where nitrogen occupies the voids (interstitial position) varies along various elements and groups of elements that are high nitride formers [157], such as groups 4 and 5, both of which were employed in this experiment. The high entropy effect and diffusion growth during the phase formation in multi-component ceramics greatly assist in stabilizing the solid solution phase [160].

5.4.2 Microhardness

Figure 4 shows the relation between microhardness and sintering temperature for the HEC sample sintered at 1800°C, 1900°C, and 2000°C. From this figure, we have observed that the increasing temperature will help improve an alloy's microhardness. The porosity inside the samples was also observed in SEM images shown in figure 1 for samples sintered at 1800°C and 1900°C, whereas the 2000°C sample shows the highest densification due to higher densification. Therefore, the sample sintered at 2000°C shows the highest hardness.

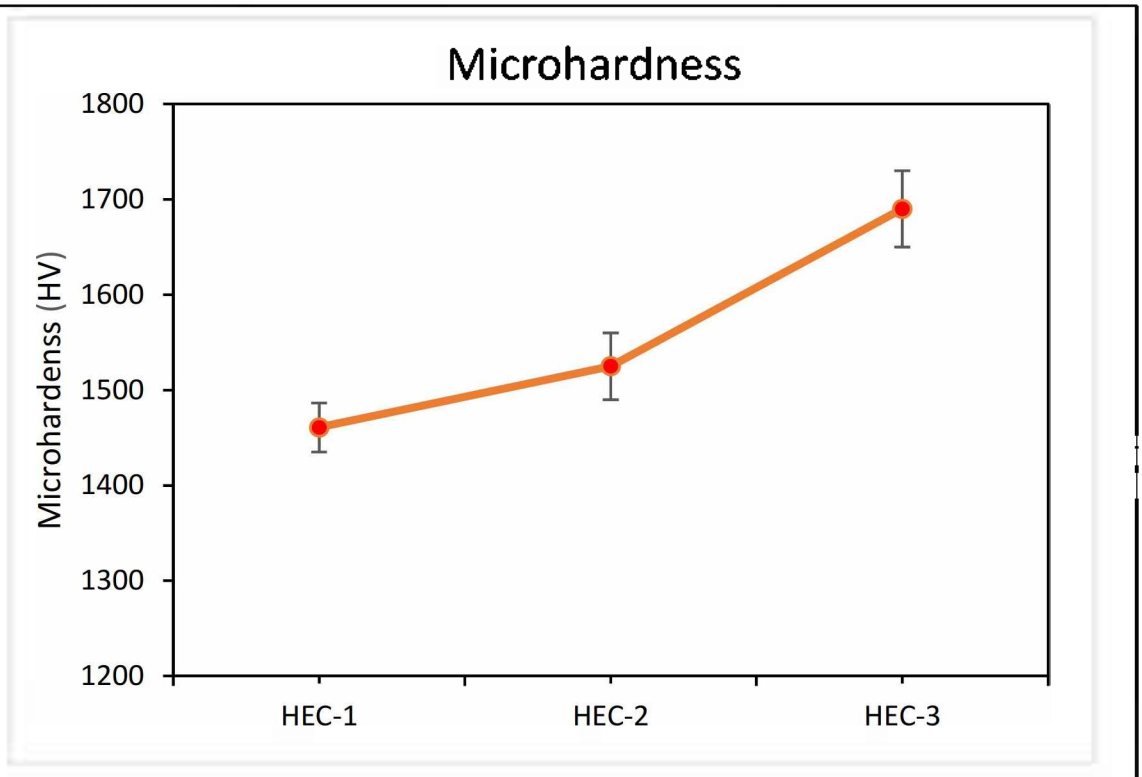

Figure 5 4 Microhardness of spark plasma sintered samples at 1800 ℃(HEC-1), 1900 ℃(HEC-2), and 2000 ℃(HEC-3)

The high entropy effects significantly impact the hardness of these high-entropy nitrides more than the average performances of individual metal nitrides. Due to valency, the hardness should be crucially dependent on microstructures, porosity, and point defects [24], [33]. As a result, we evaluated single-phase HEC SPS sintered at 2000°C and HfN,

NbN, TaN, TiN, and ZrN specimens SPS sintered at 1800°C. Individual metal nitride dense samples obtained at 1800°C were observed in many studies [76], [140], [141], [161]. to compare the microhardness of selected HEC, we have sintered individual nitride samples at 1800°C that may be utilized to compare the high entropy nitride. The microhardness reading of high entropy ceramics $(Hf_{0.2}Nb_{0.2}Ta_{0.2}Ti_{0.2}Zr_{0.2})N$ is shown in figure 4. There is a significant improvement of 150 + HV in the hardness of the sintered sample at 2000°C compared to 1900°C. Therefore, the highest density (98.1% relative density of HEC-3) and higher hardness HEC-3 sample were comparable to the binary nitrides HfN, NbN, TaN, TiN, and ZrN, as shown in Table 4. The HEC-3 sample has a better hardness of 1690 HV than the average of respective binary nitride 1325 HV, confirming that hardness increases due to high entropy effects.

The transition metal nitrides are often challenging to synthesize experimentally. Many researchers reported nitrogen loss at high temperatures though nitride has a high kinetic barrier and leads to point defect [38]. As a result, different hardness values are obtained in different studies due to the processing parameters, valency, and temperature. The calculated hardness differs by 49%-87% experimentally measured values of binary carbide, nitride, and carbonitride if the valency is greater than ten [24], [162], [163]. Free cation energy increases with temperature, while nitrogen vacancies decrease with it; as a consequence, to get successful results for transition metal nitride with rocksalt structure, we should determine the temperature range at which cation and nitrogen are stable [75]. Microhardness levels fluctuate due to the point defect caused by nitrogen loss at high temperatures, as has been reported in the literature.

The SPS sintered (Hf0.2Zr0.2Ta0.2Nb0.2Ti0.2)C has a much lower thermal conductivity and microhardness than the binary carbides may be the consequence of the considerable phonon scattering that occurs at its deformed anion sublattice [164]. Demirskyi et al. [165] synthesized in situ tantalum nitrides utilizing SPS processing and obtained 20.8Gpa hardness at 1800°C. Lee et al. [76] investigated that the pressure considerably influences densification, and increasing pressure reduces nitrogen dissociation from ZrN; they observed 97% densification at 1700°C SPS temperature with appx mean 1200 to 1300Hv hardness. TiN ceramics sintered at higher SPS temperatures under nitrogen flow hardness, reaching up to 20 GPa at 1600°C. Many factors contribute to its hardness: significant densification, the absence of titanium oxides, and twins in its microstructure. [70]. In the instance of NbN, the hardness began to decrease as soon as the eutectic phase of NbN began to form after the 1130 °C sintering temperature [166].

Table 4 Microhardness of individual nitride sample and HEC-3 sample.

Materials	**Hardness (HV)**	**Density ($g.cm^{-3}$)**
(Hf0.2Zr0.2Ta0.2Nb0.2Ti0.2)N	1690	9.375
HfN	994	11.00
TaN	2036	13.3
TiN	868	5.75
NbN	1568	8.47
ZrN	1251	7.09

5.4.3 Tribological Analysis

The coefficient of friction (CoF) plots of High entropy nitride ceramic are shown in the figure(figure 5a,5b.) The results show that the sample sintered at 2000°C has a better wear performance compared to samples sintered at 1800°C, and for 1900°C, the Cof is higher at the beginning but reaches a constant value with sliding distance. The grain

refinement and densification of the sample sintered at a higher temperature result in improved wear resistance. The SEM (Figure 1) images also confirm that the sample sintered at 2000°C has less porosity, resulting in a lower coefficient of friction. This result is reinforced by the increase in the microhardness of the sample. The highest CoF of ~0.95 is observed for HEN-1, and the lowest CoF of ~0.732 is observed for HEC-3. Figure 5b shows wear testing results with the HEC-3 samples with individual nitride samples, where we have observed that the HEC-3 sample has the lowest CoF except for ZrN and HfN, which have CoF of 0.65. The average coefficient of friction (CoF) of HEC-3 is 0.732 and HfN, NbN, TaN, TiN, and ZrN,CoF is 0.65,0.74,0.77,0.83, 0.65 respectively.

According to Ahn et al. [167], the brittle nature of ceramic and abrasive wear is the primary reason to low wear resistance. Recent discoveries found that improved fracture toughness and higher hardness of the material help to increase wear resistance[103]. The HEC-3 sample outperformed the other samples based on SEM and microhardness measurement, and this was further confirmed by wear analysis on both the individual sintered sample and HEC-3.

EDS mapping of the HEC-3 sample is shown in figure 6, which is used to understand and investigate the behavior of the high entropy ceramic in further detail. The ceramic's brittleness and increased hardness value are likely to reason for its abrasive wear behavior, which we have seen. Additionally, as illustrated in figure 6, there is more debris visible on the wear track. It also explains that the Si_3N_4 balls wear more as a result of the ceramic's higher hardness value since the silicon particles are left outside the track. The oxidation that has built up over the wear track can be seen rather obviously. As a result,

the most important wear mechanisms of as-cast HEC-3 alloys were abrasive wear and adhesive wear caused by the oxidized nanoparticles.

Vacancies significantly influence transition metal nitride's mechanical, structural, and tribological properties. Vacancies may cause significant changes in mechanical properties, such as an increase or decrease in elastic modulus in and the formation of a stable cubic structure from an unstable structure [151], [162], [168], [24]. Early transition metal stoichiometric nitrides typically form in the rocksalt structure, while hexagonal phases have also been found, demonstrating that growth factors such as temperature and pressure impact the crystal structure[75]. Therefore, we have sintered all other powders initially for analysis of the HEC- 3 samples. All samples such as HfN, NbN, TaN, TiN, and ZrN are sintered at 1800°C for 5 min holding time. A similar wear analysis was performed on all samples to find out the effect of multi-component alloy. During this analysis, we have observed that HfN has the lowest coefficient of friction, whereas ZrN, TiN, TaN, and NbN have the more friction coefficient.

(a)

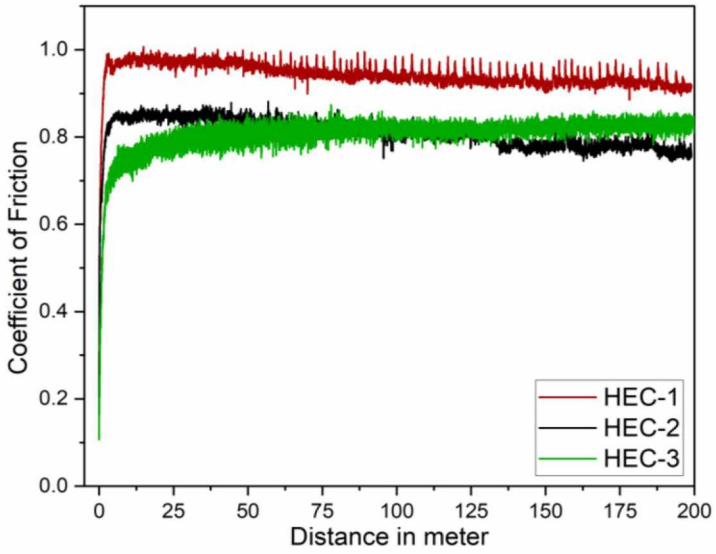

(b)

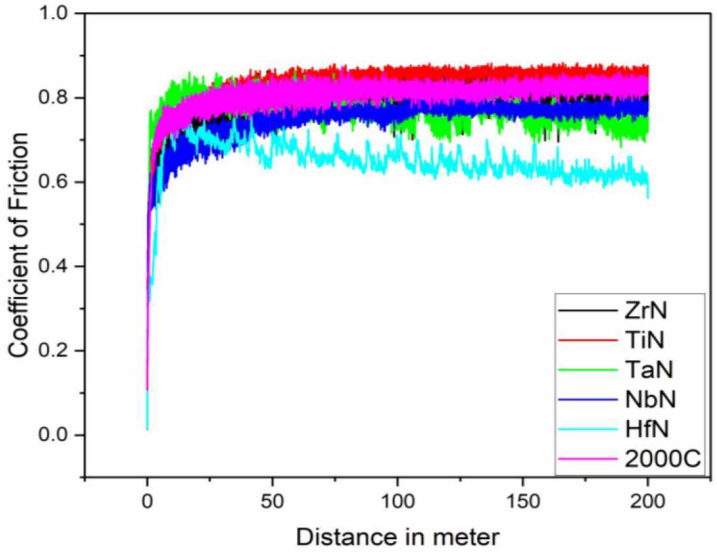

Figure 5 5 Coefficient of Friction vs. Distance (200 m) (a) Sintered at 1800, 1900, and 2000 ℃, (b) all nitride and HEC-3

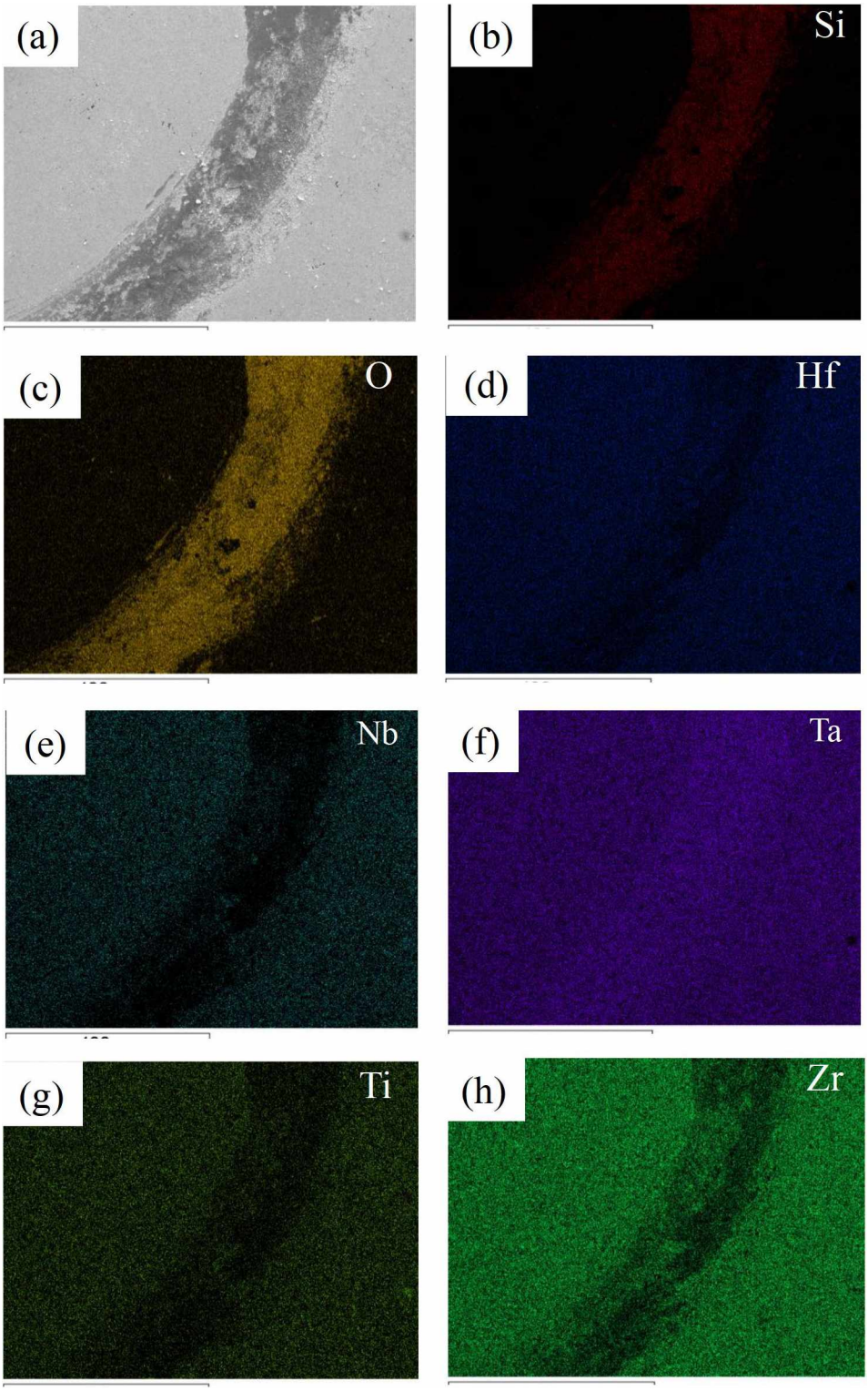

Figure 5 6 SEM/EDS analysis of wear track/tribology behavior at 2000C

5.4.4 Oxidation behavior

Figure 7 illustrates the weight gained graph of (Hf0.2Nb0.2Ta0.2Ti0.2Zr0.2)N HEC-3 samples at different temperatures after the isothermal oxidation process at 1000–1200°C in air. Due to rapid oxidation of the sample at elevated temperature, the sample's weight increases. There is a solid linear correlation between the specific weight change and the oxidation temperature, indicating that the oxidation behavior of HEC-3 samples at 1000-1200°C is similar to the parabolic rate law.

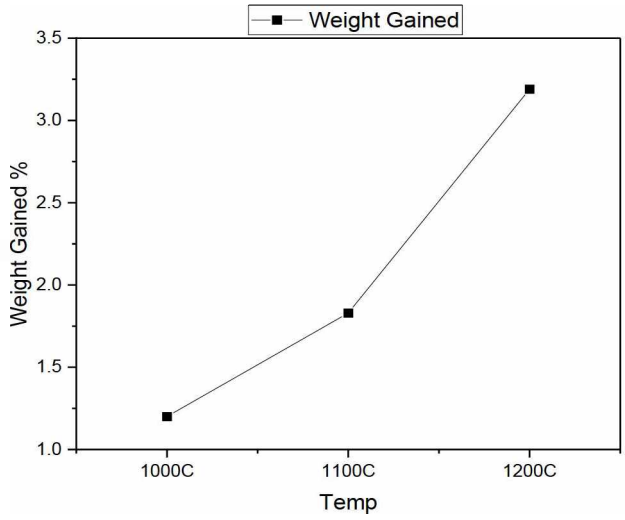

Figure 5 7 Weight gained (%) of isothermal oxidation at 1000, 1100, and 1200 °C samples

SEM surface images of HEC-3 samples following isothermal oxidation testing at different temperatures are shown in Figure 8. The size of the microcracks in the produced oxide layer can be observed under lower magnification SEM images shown in figure 8(a,c,e). After isothermal oxidation experiments at 1000°C, 1100°C, and 1200°C, higher magnification SEM morphology (Figure 8(b, d, f)) shows that the thick oxide layer is developed, and with increasing temperature of oxidation, the thickness of the oxide layer

increases. At 1200°C oxidation temperatures, tiny hole oxide granules are evident on the surface of the developed oxide layer, as illustrated in Figure 8(f). Similar phenomena reported by Ye et al. [154] in high entropy carbide oxidation investigation demonstrate that as oxidation temperature increases, the surface morphology of the oxide sample becomes granular until 1173k, and then with increasing temperature begins to form a compact oxide layer.

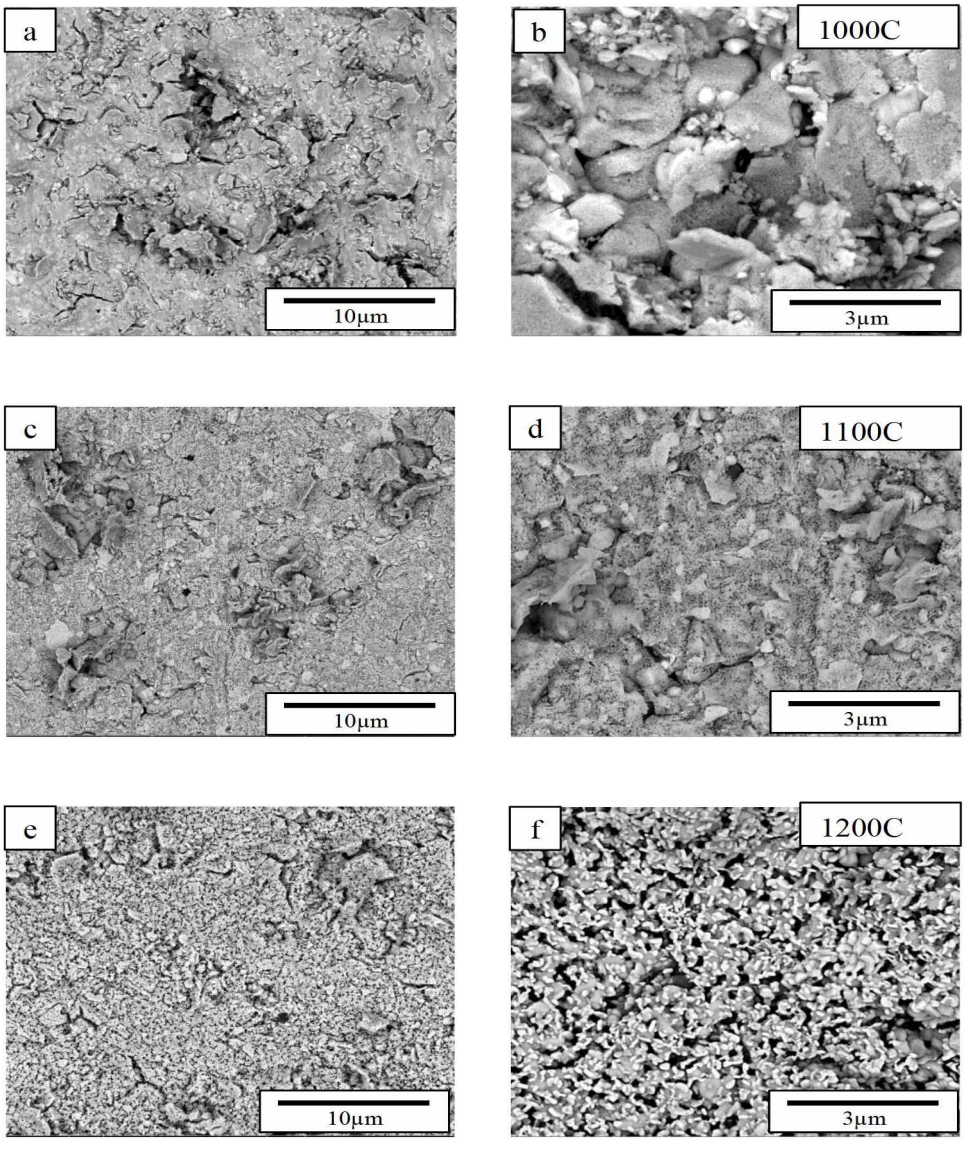

Figure 5 8 SEM images of Isothermal oxidation behavior at (a,b)1000 °C, (c,d) 1100 °C, and (e,f)1200 °C samples.

The EDS analysis (Figure 10-13) reveals that all of the produced oxide layers include Hf, Zr, Ta, Nb, Ti, and O elements, having very homogeneous distributions throughout the whole cross-section region of the oxide layers. Figure 2 shows the XRD characterization of HEC-3 samples carried out at 1000°C,1100°C, and 1200°C to explore the phase compositions of these oxidation products. According to the XRD graph in Figure, Titanium, Tantalum, and Niobium begin to diffuse outward at 1000C, and when mixed with oxygen that has begun to diffuse inward, these elements produce TiO_2 and $(TaNb)O_5$ at lower temperatures. These already formed oxides combine with newly diffused elements from the substrate to form new oxides, which can be clearly seen from the XRD graph as these, TiO_2 and $(TaNb)O_5$ peaks disappear at higher temperatures. As the temperature increases, further diffusion of elements from the substrate will occur. And recently developed diffraction peaks in XRD patterns may be indexed to the $Ti(NbTa)O_7$, $(TaNb)(Zr_3Hf_3)O_{17}$, and $(ZrHf)TiO_4$, phases.

In general, oxygen combines with the substrate metal to generate the metal's oxides. When the temperature increases, the oxide coatings start to develop cracks, which supports in the metal's further oxidation. [169]. Consequently, atmospheric oxygen gets a passage to propagate within the nitride ceramics due to this crack formation there is further oxidation of samples. With increasing temperature, we can easily observe the change in oxide layer thickness from the SEM/EDS electron images. The oxide layer thickness varies with the varying temperature. The oxide layer thickness is the lowest in the 1000°C isothermal oxidation test samples. Oxygen diffusivity increase with increasing oxidation temperature and even detect crakes.

Due to the low diffusivity of oxygen at lower temperatures, samples at 1000°C have much lesser oxidation as compared to samples heated to 1200°C. Figure 9 shows the increase in oxidation thickness with increasing temperature. At lower temperatures, a certain percentage of nitrogen is entrapped at the outer layer of the oxidation region. But at elevated temperatures, this entrapped nitrogen is completely released, thus providing easy passage to inward diffusion of oxygen [161]. Ti's distribution is not uniform, with larger concentrations near the surface, moderate concentrations in the center, and lower concentrations in the interior layer due to Ti's small atomic radii compared to its other constituent elements [170].

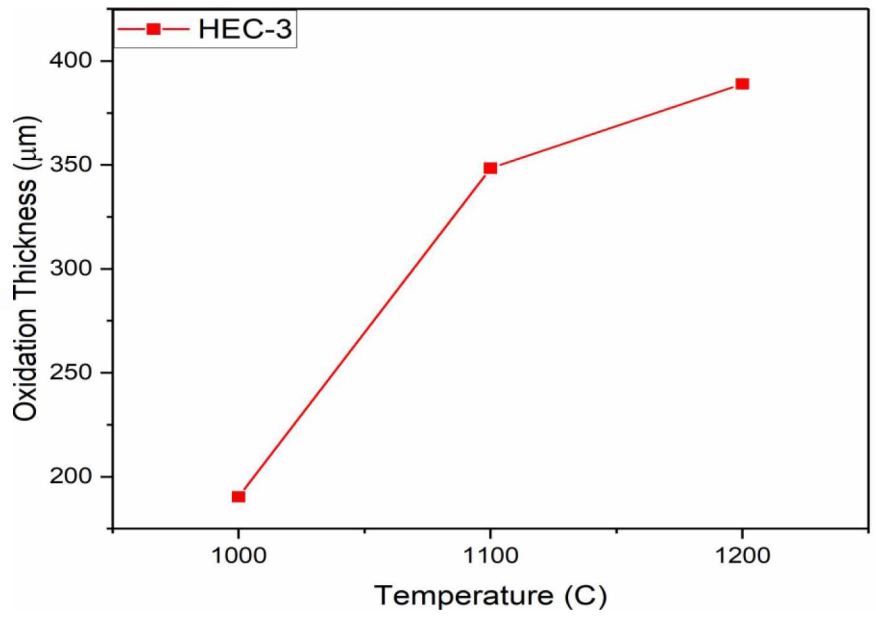

Figure 5 9 Oxidation Tickness Vs Temperature

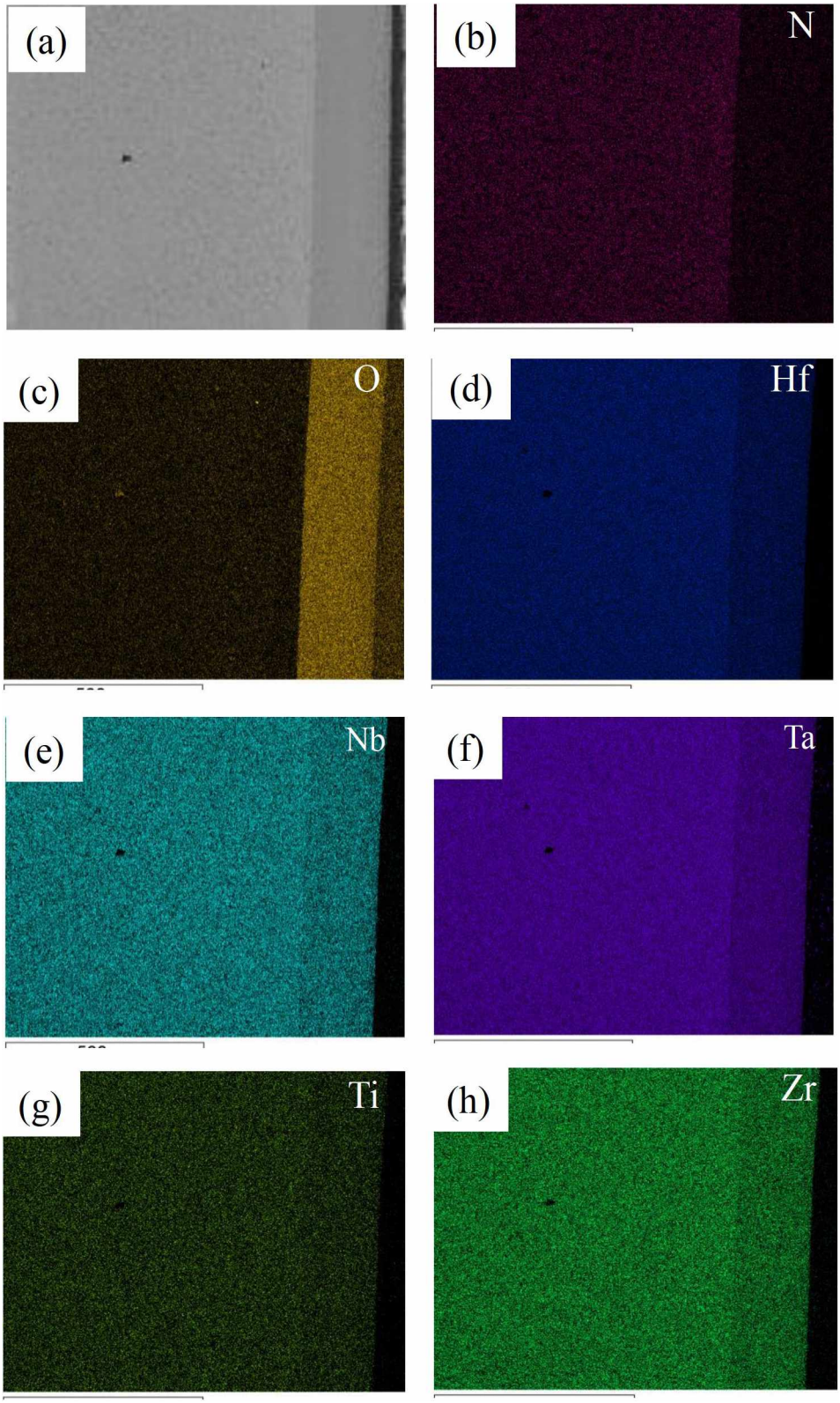

Figure 5 10 SEM/EDS analysis of isothermal oxidation at 1000 °C

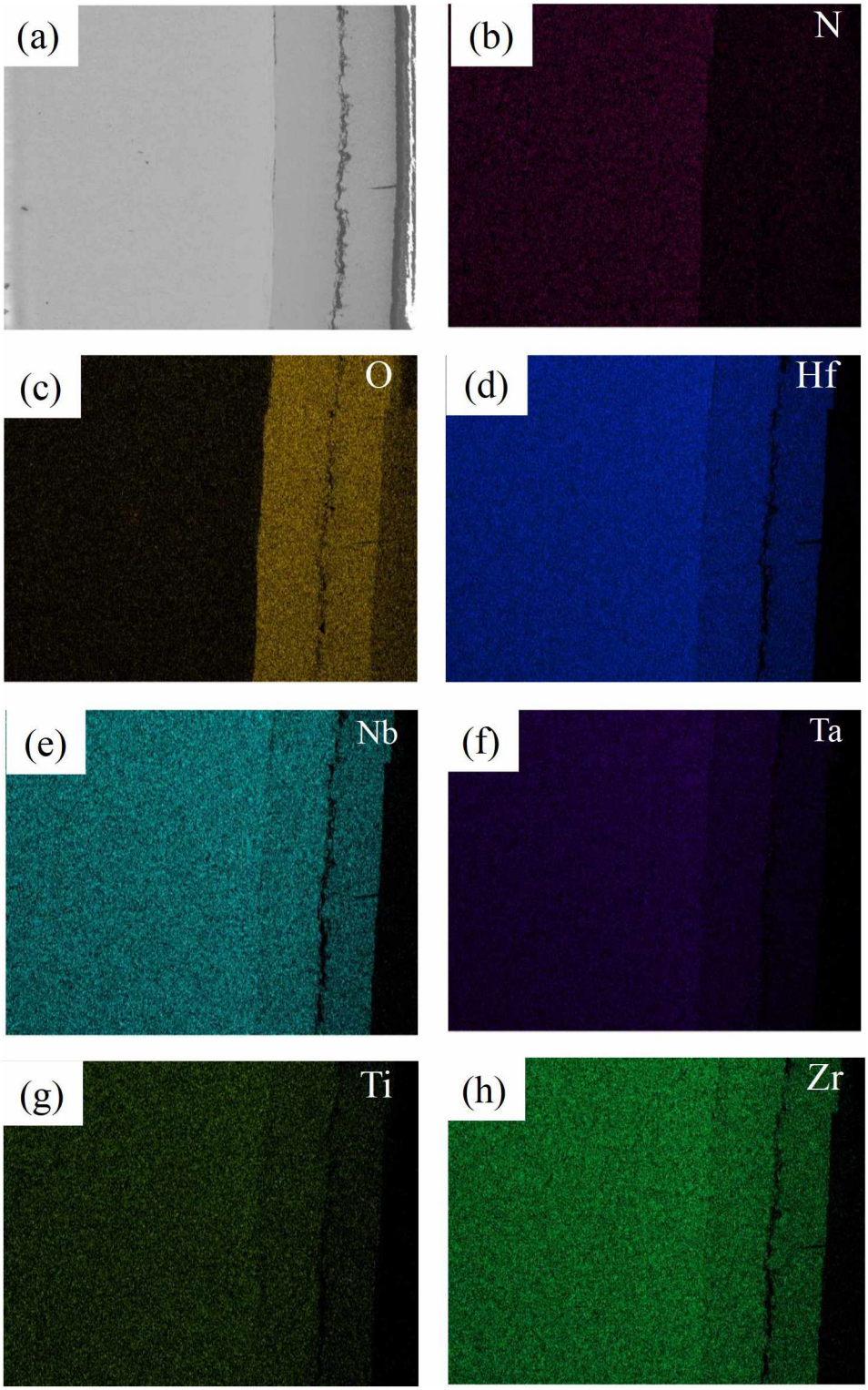

Figure 5 11 SEM/EDS analysis of isothermal oxidation at 1100 ℃

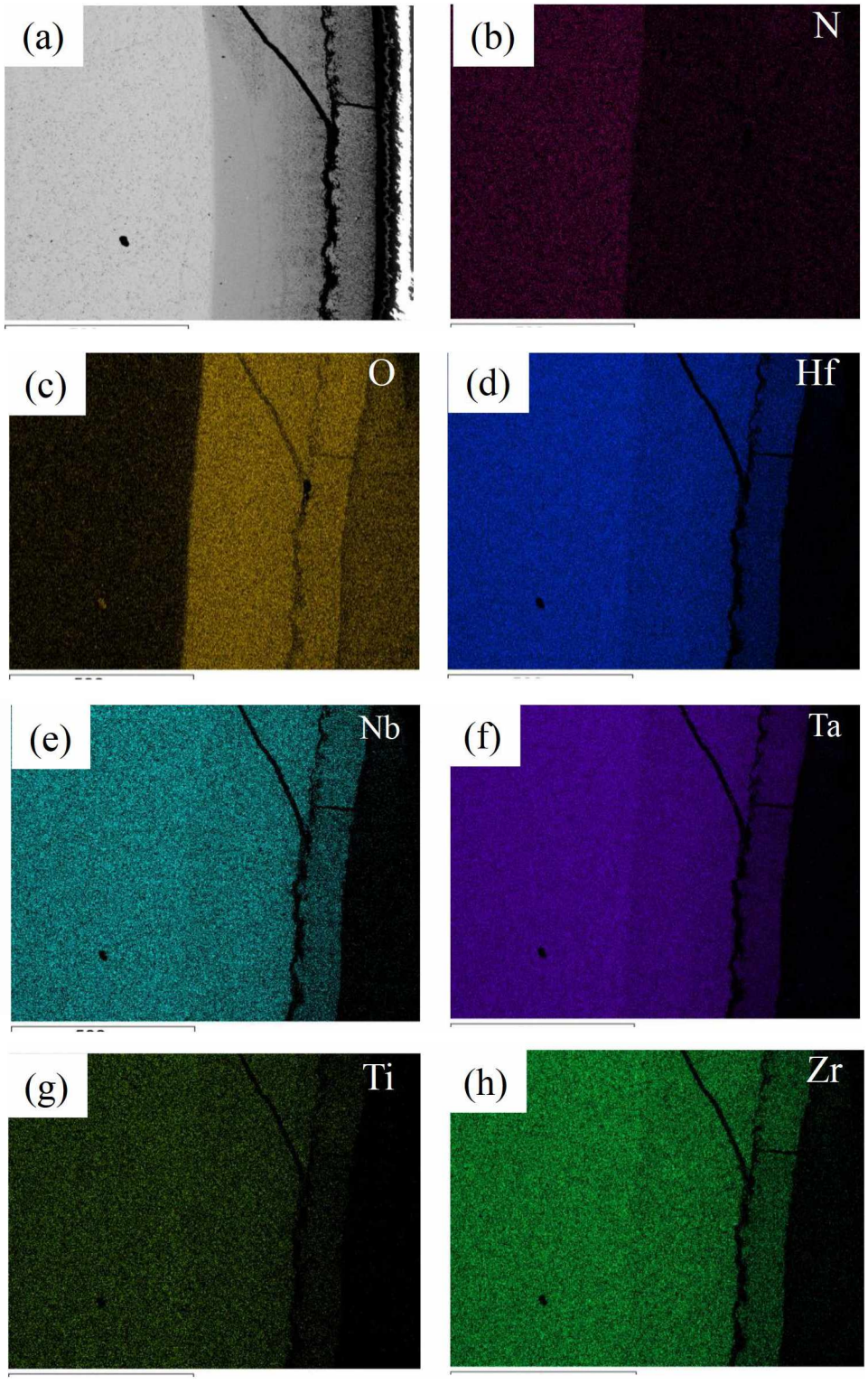

Figure 5 12 SEM/EDS analysis of isothermal oxidation at 1200 °C

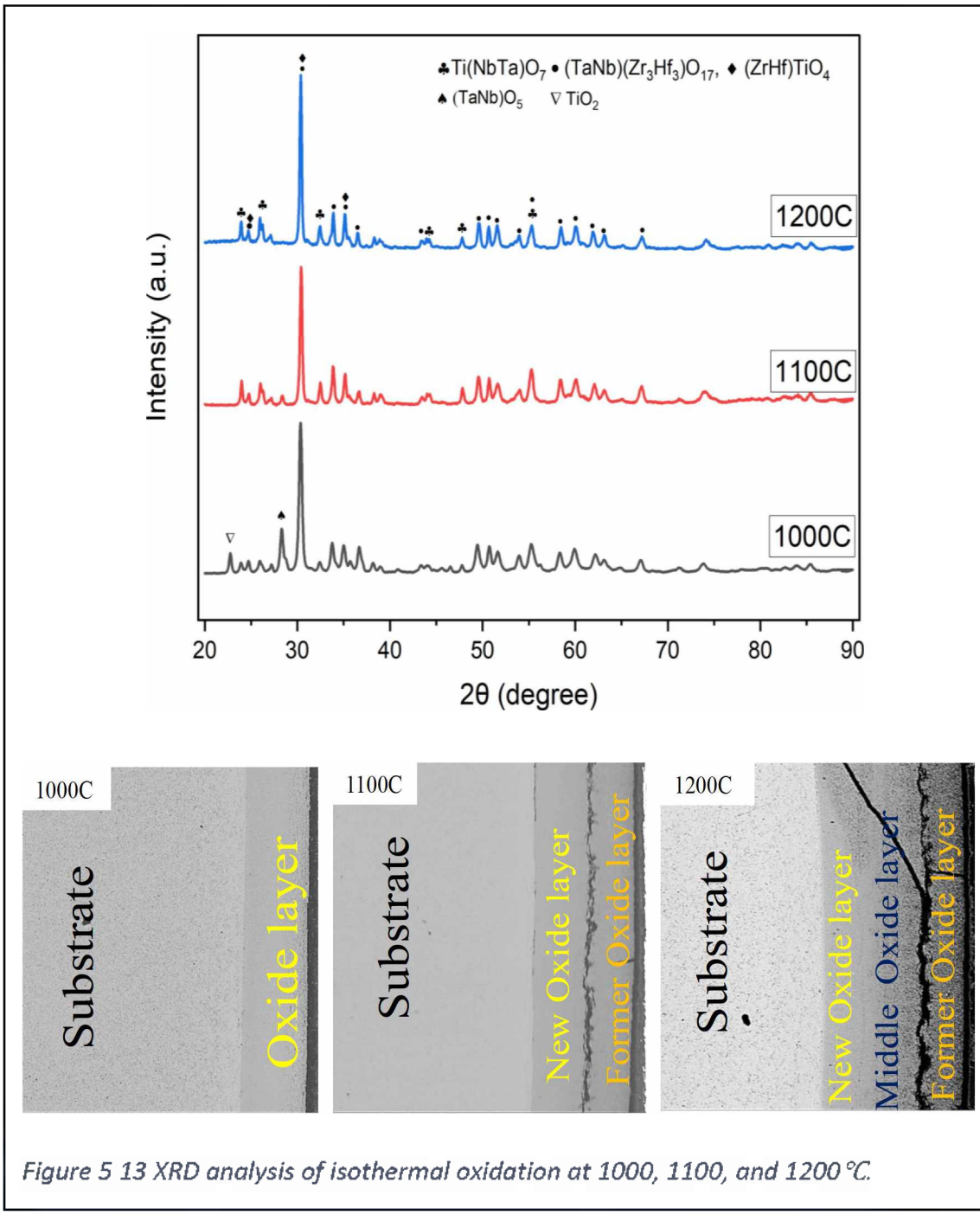

Figure 5 13 XRD analysis of isothermal oxidation at 1000, 1100, and 1200 ℃.

5.5 Conclusion

Single phase High entropy ceramic synthesized $(Hf_{0.2}Nb_{0.2}Ta_{0.2}Ti_{0.2}Zr_{0.2})N$ ceramics with equiatomic composition from mechanical, followed by spark plasma sintering. HEC ceramics were studied in terms of their microstructure, mechanical, and tribological characteristics, and the following conclusions may be obtained.

1. The SCM and XRD analysis show this single rocksalt phase in high entropy nitride. The microhardness of SPS sintered sample Increases with the increasing sintering temperature. We have a 98.2% relative density using 2000 degrees Celsius sintering temperature. The HEC-3 sample shoes higher hardness compared to all individually sintered nitride accept TaN.
2. The processing parameter, pressure, temperature, and nitride synthesis method affect the mechanical and tribological properties of the high entropy ceramic. Valency, the stability of cations and nitrogen at high temperatures, is viewed as a crucial influencer that changes the mechanical property.
3. The fact that the microhardness of the HEC-3 sample is 1690Hv, which is more than the average hardness of all elements, demonstrates that the high entropy effect is advantageous.
4. The high entropy ceramic follows the parabolic rate law of oxidation because of its isothermal oxidation behavior weight, and oxide layer thinness increases with temperatures. At lower temperatures, 1000C titaniums begin to oxidize, and at 1200C, all other elements of the matrix begin to oxidize; as a result, Ti peaks disappear at high temperatures and create multielement oxide peaks.

5. The friction coefficient does not change significantly, as shown in the HEC-3 sample and the individual nitride sintered samples. The greater hardness and bitterness of the ceramic material led to the abrasive wear characteristics that were reported in HEC.

CHAPTER VI

FUTURE SCOPE

6.1 Light Weight High Entropy Alloy

Different alloying procedures, which are derived from classical metallurgy, are required in order to enhance the mechanical characteristics of potentially useful HEAs. In order to prevent dislocation motion, these methods use as substantial barriers. These design processes for creating new alloys significantly depend on an alloy's mechanical properties and weight. The CALPHAD technique is the best strategy to try to estimate the phase stability in multi-component systems like HEAs, as has been shown in the current study and earlier investigations. There are three different approaches to hardening HEAs, and each one is founded on the inclusion of relevant components to generate certain microstructures in the final product.

1. Computer modeling CALPHAD
2. Enhance the formation of multi-phase HEAs;
3. Controlled nano-precipitation in a compositionally complex solid solution

Substantial gains in strength might be accomplished by carefully controlling the precipitation, that is, by ensuring the precipitates are homogeneous and evenly spread throughout the matrix. A focused technique for LWHEAs that is very similar to that explored in duplex γ/γ' superalloys may lead to the investigation of hardened bcc LWHEAs

that include nanosized reinforcing phases. There have been intriguing findings with the generation of $AlFe_2Ti$ type precipitates with the L12 structure in the disordered bcc matrix of Al1.5CeFeMnTi based systems [132]. Regulated thermo-mechanical treatments, a uniform distribution of nanosized ordered L12 γ/γ' precipitates. Thermodynamic studies show that such precipitation will occur across a wide range of compositions, but the actual two-phase bcc + L21 domain is quite restricted owing to the chemical complexity of the alloying system. In alloys containing nano-scale L21 $Al(CrFe)_2Ti$, $Al(CrMn)_2Ti$, $Al(FeMn)_2Ti$, precipitates [132], precipitation hardening is regarded to be the primary strengthening process at room temperature.

Developing very stable intermetallic compounds between alkali metal (Al) and late TMs (such as Mn and Fe) synthesizing single-phase HEAs with high Al and/or Ti concentrations is challenging. Because of this, the overall number of single-phase light-weight HEAs is relatively low, and their densities are often more than 5.5 $g.cm^{-3}$. On the other hand, multi-phase microstructures are often preferred to balance different material characteristics, notably the outstanding combination of strength and ductility, and the alloy compositions do not necessarily need to be equimolar or close to equimolar ratios for practical applications. An application-oriented strategy for developing future light-weight HEAs with densities below 5 $g.cm^{-3}$ may be summarized as follows:

- The goal qualities demand that identify the key alloying elements in addition to the dominating principle element (such as Ti, Al, or Cr).
- Adjust the bulk composition using the high-entropy principle in order to enhance the solubility of important strengthening (improve ductility) alloying components.

- Develop optimal processing and heat-treatment methods to improve the microstructure and predict phase stability using the CALPHAD approach, DFT modeling and/or experimental criteria.
- Manufacture and characterize the microstructures and mechanical characteristics of the down-selected alloys.
- Repeat the following steps to refine the design of the alloy further.

6.2 High Entropy Ceramics

There are many compositional possibilities in a solid solution phase due to the complexity of a multi-component compositional space. Therefore, using the usual materials science methods may not be sufficient in this case. Due to the increasing amount of conceivable permutations and combinations and the complicated interaction between phases, microstructure, and functionalities, the work at hand might be described as both massive and complicated. If we use the conventional approach to materials science, it will take a very long period before we see any results. A novel strategy that fuses contemporary computation approaches with established experience and understanding approaches is required.

This work does not consider the structural complexity of high entropy ultra high temperature ceramic such as point defects, VEC, dislocations, and grain boundaries. In the not too distant future, HECs will be able to accommodate more universal deep learning potentials capable of precisely characterizing chemical and structural complexities. Then, it is believed that strong approaches like these may provide a profound understanding of HECs.

REFERENCE

[1] Michael F. Ashby, *Materials Selection in Mechanical Design*, Fourth Edi. Butterworth-Heinemann, 2011.

[2] Klement W; Willens R; Duwez P., "Non-crystalline Structure in Solidified Gold-Silicon Alloys," *Nature*, vol. 187, no. 4740, pp. 869–870, 1960.

[3] A. Patil *et al.*, " Tribological Behavior of in situ Processed NI-Ti-C Nanocomposites ," *Tribology Transactions*, vol. 0, no. 0, pp. 1–13, 2020, doi: 10.1080/10402004.2020.1800880.

[4] F. H. Froes, "Advanced metals for aerospace and automotive use," *Materials Science and Engineering A*, vol. 184, no. 2, pp. 119–133, 1994, doi: 10.1016/0921-5093(94)91026-X.

[5] Michael C. Gao; Jien-Wei Yeh; Peter K. Liaw; Zhang Yong, *High-entropy alloys Fundamentals and Applications*. 2016. doi: 10.1007/978-3-319-27013-5_12.

[6] J. W. Yeh, "Recent progress in high-entropy alloys," *Annales de Chimie: Science des Materiaux*, vol. 31, no. 6, pp. 633–648, 2006, doi: 10.3166/acsm.31.633-648.

[7] T. Jin *et al.*, "Mechanochemical-Assisted Synthesis of High-Entropy Metal Nitride via a Soft Urea Strategy," *Advanced Materials*, vol. 30, no. 23, pp. 1–5, 2018, doi: 10.1002/adma.201707512.

[8] B. Ye, T. Wen, D. Liu, and Y. Chu, "Oxidation behavior of (Hf 0.2 Zr 0.2 Ta 0.2 Nb 0.2 Ti 0.2)C high-entropy ceramics at 1073-1473 K in air," *Corrosion Science*, vol. 153, no. April, pp. 327–332, 2019, doi: 10.1016/j.corsci.2019.04.001.

[9] B. Ye, T. Wen, K. Huang, C. Z. Wang, and Y. Chu, "First-principles study, fabrication, and characterization of (Hf 0.2 Zr 0.2 Ta 0.2 Nb 0.2 Ti 0.2)C high-entropy ceramic," *Journal of the American Ceramic Society*, vol. 102, no. 7, pp. 4344–4352, 2019, doi: 10.1111/jace.16295.

[10] J. Gild, K. Kaufmann, K. Vecchio, and J. Luo, "Reactive flash spark plasma sintering of high-entropy ultrahigh temperature ceramics," *Scripta Materialia*, vol. 170, pp. 106–110, 2019, doi: 10.1016/j.scriptamat.2019.05.039.

[11] P. H. Mayrhofer, A. Kirnbauer, P. Ertelthaler, and C. M. Koller, "High-entropy ceramic thin films; A case study on transition metal diborides," *Scripta Materialia*, vol. 149, pp. 93–97, 2018, doi: 10.1016/j.scriptamat.2018.02.008.

[12] S. Zhou *et al.*, "Microstructure and dielectric properties of high entropy Ba(Zr0.2Ti0.2Sn0.2Hf0.2Me0.2)O3 perovskite oxides," *Ceramics International*, vol. 46, no. 6, pp. 7430–7437, 2020, doi: 10.1016/j.ceramint.2019.11.239.

[13] S. M. Aouadi, "Structural and mechanical properties of TaZrN films: Experimental and ab initio studies," *Journal of Applied Physics*, vol. 99, no. 5, 2006, doi: 10.1063/1.2178394.

[14] X. Q. Cao, R. Vassen, and D. Stoever, "Ceramic materials for thermal barrier coatings," *Journal of the European Ceramic Society*, vol. 24, no. 1, pp. 1–10, 2004, doi: 10.1016/S0955-2219(03)00129-8.

[15] D. R. Clarke, M. Oechsner, and N. P. Padture, "Thermal-barrier coatings for more efficient gas-turbine engines," *MRS Bulletin*, vol. 37, no. 10, pp. 891–898, 2012, doi: 10.1557/mrs.2012.232.

[16] J. L. Braun *et al.*, "Charge-induced disorder controls the thermal conductivity of entropy-stabilized oxides," *Advanced Materials*, vol. 30, no. 51, pp. 1–8, 2018, doi: 10.1002/adma.201805004.

[17] R. Z. Zhang, F. Gucci, H. Zhu, K. Chen, and M. J. Reece, "Data-Driven Design of Ecofriendly Thermoelectric High-Entropy Sulfides," *Inorganic Chemistry*, vol. 57, no. 20, pp. 13027–13033, 2018, doi: 10.1021/acs.inorgchem.8b02379.

[18] R. Liu *et al.*, "Entropy as a Gene-Like Performance Indicator Promoting Thermoelectric Materials," *Advanced Materials*, vol. 29, no. 38, pp. 1–7, 2017, doi: 10.1002/adma.201702712.

[19] W. Hong, F. Chen, Q. Shen, Y. H. Han, W. G. Fahrenholtz, and L. Zhang, "Microstructural evolution and mechanical properties of (Mg,Co,Ni,Cu,Zn)O high-entropy ceramics," *Journal of the American Ceramic Society*, vol. 102, no. 4, pp. 2228–2237, 2019, doi: 10.1111/jace.16075.

[20] K. Jin and H. Bei, "Single-phase concentrated solid-solution alloys: Bridging intrinsic transport properties and irradiation resistance," *Frontiers in Materials*, vol. 5, no. April, pp. 1–11, 2018, doi: 10.3389/fmats.2018.00026.

[21] A. J. Wright, Q. Wang, C. Huang, A. Nieto, R. Chen, and J. Luo, "From high-entropy ceramics to compositionally-complex ceramics: A case study of fluorite oxides," *Journal of the European Ceramic Society*, vol. 40, no. 5, pp. 2120–2129, 2020, doi: 10.1016/j.jeurceramsoc.2020.01.015.

[22] S. Jiang *et al.*, "A new class of high-entropy perovskite oxides," *Scripta Materialia*, vol. 142, pp. 116–120, 2018, doi: 10.1016/j.scriptamat.2017.08.040.

[23] T. J. Harrington *et al.*, "Phase stability and mechanical properties of novel high entropy transition metal carbides," *Acta Materialia*, vol. 166, pp. 271–280, 2019, doi: 10.1016/j.actamat.2018.12.054.

[24] K. Balasubramanian, S. V. Khare, and D. Gall, "Valence electron concentration as an indicator for mechanical properties in rocksalt structure nitrides, carbides and carbonitrides," *Acta Materialia*, vol. 152, pp. 175–185, 2018, doi: 10.1016/j.actamat.2018.04.033.

[25] B. Cantor, I. T. H. Chang, P. Knight, and A. J. B. Vincent, "Microstructural development in equiatomic multicomponent alloys," *Materials Science and Engineering A*, vol. 375–377, no. 1-2 SPEC. ISS., pp. 213–218, 2004, doi: 10.1016/j.msea.2003.10.257.

[26] B.S. Murty; J.W. Yeh; S. Ranganathan; P.P Batta, *High-Entropy Alloys*. 2011. doi: 10.1016/B978-0-08-043152-9.02274-0.

[27] J. W. Yeh, "Alloy design strategies and future trends in high-entropy alloys," *Jom*, vol. 65, no. 12, pp. 1759–1771, 2013, doi: 10.1007/s11837-013-0761-6.

[28] L. R. Owen, E. J. Pickering, H. Y. Playford, H. J. Stone, M. G. Tucker, and N. G. Jones, "An assessment of the lattice strain in the CrMnFeCoNi high-entropy alloy," *Acta Materialia*, vol. 122, pp. 11–18, 2017, doi: 10.1016/j.actamat.2016.09.032.

[29] G. Tallarita, R. Licheri, S. Garroni, R. Orrù, and G. Cao, "Novel processing route for the fabrication of bulk high-entropy metal diborides," *Scripta Materialia*, vol. 158, pp. 100–104, 2019, doi: 10.1016/j.scriptamat.2018.08.039.

[30] Y. F. Kao, S. K. Chen, T. J. Chen, P. C. Chu, J. W. Yeh, and S. J. Lin, "Electrical, magnetic, and Hall properties of AlxCoCrFeNi high-entropy alloys," *Journal of Alloys and Compounds*, vol. 509, no. 5, pp. 1607–1614, 2011, doi: 10.1016/j.jallcom.2010.10.210.

[31] O. N. Senkov, G. B. Wilks, D. B. Miracle, C. P. Chuang, and P. K. Liaw, "Refractory high-entropy alloys," *Intermetallics*, vol. 18, no. 9, pp. 1758–1765, 2010, doi: 10.1016/j.intermet.2010.05.014.

[32] X. P. Zhang and L. N. Y. Wong, "Loading rate effects on cracking behavior of flaw-contained specimens under uniaxial compression," *International Journal of Fracture*, vol. 180, no. 1, pp. 93–110, 2013, doi: 10.1007/s10704-012-9803-2.

[33] K. Balasubramanian, S. Khare, and D. Gall, "Vacancy-induced mechanical stabilization of cubic tungsten nitride," *Physical Review B*, vol. 94, no. 17, pp. 36–38, 2016, doi: 10.1103/PhysRevB.94.174111.

[34] K. Y. Tsai, M. H. Tsai, and J. W. Yeh, "Sluggish diffusion in Co-Cr-Fe-Mn-Ni high-entropy alloys," *Acta Materialia*, vol. 61, no. 13, pp. 4887–4897, 2013, doi: 10.1016/j.actamat.2013.04.058.

[35] B. X. Cao, C. Wang, T. Yang, and C. T. Liu, "Cocktail effects in understanding the stability and properties of face-centered-cubic high-entropy alloys at ambient and cryogenic temperatures," *Scripta Materialia*, vol. 187, pp. 250–255, 2020, doi: 10.1016/j.scriptamat.2020.06.008.

[36] Y. Zhang, X. Yang, and P. K. Liaw, "Alloy design and properties optimization of high-entropy alloys," *Jom*, vol. 64, no. 7, pp. 830–838, 2012, doi: 10.1007/s11837-012-0366-5.

[37] J. W. Yeh, "Recent progress in high-entropy alloys," *Annales de Chimie: Science des Materiaux*, vol. 31, no. 6, pp. 633–648, 2006, doi: 10.3166/acsm.31.633-648.

[38] O. N. Senkov, S. V. Senkova, D. M. Dimiduk, C. Woodward, and D. B. Miracle, "Oxidation behavior of a refractory NbCrMo 0.5Ta 0.5TiZr alloy," *Journal of Materials Science*, vol. 47, no. 18, pp. 6522–6534, 2012, doi: 10.1007/s10853-012-6582-0.

[39] M. H. Tsai and J. W. Yeh, "High-entropy alloys: A critical review," *Materials Research Letters*, vol. 2, no. 3, pp. 107–123, 2014, doi: 10.1080/21663831.2014.912690.

[40] K. G. Pradeep, N. Wanderka, P. Choi, J. Banhart, B. S. Murty, and D. Raabe, "Atomic-scale compositional characterization of a nanocrystalline AlCrCuFeNiZn high-entropy alloy using atom probe tomography," *Acta Materialia*, vol. 61, no. 12, pp. 4696–4706, 2013, doi: 10.1016/j.actamat.2013.04.059.

[41] F. Otto, Y. Yang, H. Bei, and E. P. George, "Relative effects of enthalpy and entropy on the phase stability of equiatomic high-entropy alloys," *Acta Materialia*, vol. 61, no. 7, pp. 2628–2638, 2013, doi: 10.1016/j.actamat.2013.01.042.

[42] S. Singh, N. Wanderka, B. S. Murty, U. Glatzel, and J. Banhart, "Decomposition in multi-component AlCoCrCuFeNi high-entropy alloy," *Acta Materialia*, vol. 59, no. 1, pp. 182–190, 2011, doi: 10.1016/j.actamat.2010.09.023.

[43] S. Singh, N. Wanderka, K. Kiefer, K. Siemensmeyer, and J. Banhart, "Effect of decomposition of the Cr-Fe-Co rich phase of AlCoCrCuFeNi high entropy alloy on magnetic properties," *Ultramicroscopy*, vol. 111, no. 6, pp. 619–622, 2011, doi: 10.1016/j.ultramic.2010.12.001.

[44] T. T. Shun, L. Y. Chang, and M. H. Shiu, "Microstructure and mechanical properties of multiprincipal component CoCrFeNiMo x alloys," *Materials Characterization*, vol. 70, pp. 63–67, 2012, doi: 10.1016/j.matchar.2012.05.005.

[45] M. J. Yao, K. G. Pradeep, C. C. Tasan, and D. Raabe, "A novel, single phase, non-equiatomic FeMnNiCoCr high-entropy alloy with exceptional phase stability and tensile ductility," *Scripta Materialia*, vol. 72–73, pp. 5–8, 2014, doi: 10.1016/j.scriptamat.2013.09.030.

[46] C. C. Tasan, Y. Deng, K. G. Pradeep, M. J. Yao, H. Springer, and D. Raabe, "Composition Dependence of Phase Stability, Deformation Mechanisms, and Mechanical Properties of the CoCrFeMnNi High-Entropy Alloy System," *Jom*, vol. 66, no. 10, pp. 1993–2001, 2014, doi: 10.1007/s11837-014-1133-6.

[47] T. Borkar *et al.*, "Hierarchical multi-scale microstructural evolution in an as-cast Al2CuCrFeNi2 complex concentrated alloy," *Intermetallics*, vol. 71, pp. 31–42, 2016, doi: 10.1016/j.intermet.2015.12.013.

[48] X. Yang, S. Y. Chen, J. D. Cotton, and Y. Zhang, "Phase Stability of Low-Density, Multiprincipal Component Alloys Containing Aluminum, Magnesium, and Lithium," *Jom*, vol. 66, no. 10, pp. 2009–2020, 2014, doi: 10.1007/s11837-014-1059-z.

[49] H. Y. Diao, R. Feng, K. A. Dahmen, and P. K. Liaw, "Fundamental deformation behavior in high-entropy alloys: An overview," *Current Opinion in Solid State and Materials Science*, vol. 21, no. 5, pp. 252–266, 2017, doi: 10.1016/j.cossms.2017.08.003.

[50] V. Soni *et al.*, "Phase inversion in a two-phase, BCC+B2, refractory high entropy alloy," *Acta Materialia*, vol. 185, pp. 89–97, 2020, doi: 10.1016/j.actamat.2019.12.004.

[51] S. Praveen, B. S. Murty, and R. S. Kottada, "Alloying behavior in multi-component AlCoCrCuFe and NiCoCrCuFe high entropy alloys," *Materials Science and Engineering A*, vol. 534, pp. 83–89, 2012, doi: 10.1016/j.msea.2011.11.044.

[52] D. Li *et al.*, "High-entropy Al0.3CoCrFeNi alloy fibers with high tensile strength and ductility at ambient and cryogenic temperatures," *Acta Materialia*, vol. 123, pp. 285–294, 2017, doi: 10.1016/j.actamat.2016.10.038.

[53] V. Soni, O. N. Senkov, B. Gwalani, D. B. Miracle, and R. Banerjee, "Microstructural Design for Improving Ductility of An Initially Brittle Refractory High Entropy Alloy," *Scientific Reports*, vol. 8, no. 1, pp. 1–10, 2018, doi: 10.1038/s41598-018-27144-3.

[54] S. Dasari, B. Gwalani, A. Jagetia, V. Soni, S. Gorsse, and R. Banerjee, "Hierarchical Eutectoid Nano-lamellar Decomposition in an Al0.3CoFeNi Complex Concentrated Alloy," *Scientific Reports*, vol. 10, no. 1, pp. 1–15, 2020, doi: 10.1038/s41598-020-61538-6.

[55] J. W. Yeh *et al.*, "Nanostructured high-entropy alloys with multiple principal elements: Novel alloy design concepts and outcomes," *Advanced Engineering Materials*, vol. 6, no. 5, pp. 299–303, 2004, doi: 10.1002/adem.200300567.

[56] Y. Tong *et al.*, "Outstanding tensile properties of a precipitation-strengthened FeCoNiCrTi0.2 high-entropy alloy at room and cryogenic temperatures," *Acta Materialia*, vol. 165, pp. 228–240, 2019, doi: 10.1016/j.actamat.2018.11.049.

[57] W. Li, D. Xie, D. Li, Y. Zhang, Y. Gao, and P. K. Liaw, "Mechanical behavior of high-entropy alloys," *Progress in Materials Science*, vol. 118, no. December 2020, p. 100777, 2021, doi: 10.1016/j.pmatsci.2021.100777.

[58] M. A. Hemphill *et al.*, "Fatigue behavior of Al 0.5CoCrCuFeNi high entropy alloys," *Acta Materialia*, vol. 60, no. 16, pp. 5723–5734, 2012, doi: 10.1016/j.actamat.2012.06.046.

[59] W. Shen, M. Tsai, and J. Yeh, "Machining Performance of Sputter-Deposited (Al0.34Cr0.22Nb0.11Si0.11Ti0.22)50N50 High-Entropy Nitride Coatings," pp. 312–325, 2015, doi: 10.3390/coatings5030312.

[60] M. Srikanth, A. Raja Annamalai, A. Muthuchamy, and C. P. Jen, "A review of the latest developments in the field of refractory high-entropy alloys," *Crystals*, vol. 11, no. 6, pp. 1–15, 2021, doi: 10.3390/cryst11060612.

[61] D. B. Miracle, M. H. Tsai, O. N. Senkov, V. Soni, and R. Banerjee, "Refractory high entropy superalloys (RSAs)," *Scripta Materialia*, vol. 187, pp. 445–452, 2020, doi: 10.1016/j.scriptamat.2020.06.048.

[62] M. Vaidya, G. M. Muralikrishna, and B. S. Murty, "High-entropy alloys by mechanical alloying: A review," *Journal of Materials Research*, vol. 34, no. 5, pp. 664–686, 2019, doi: 10.1557/jmr.2019.37.

[63] Y. Zhang *et al.*, "Microstructures and properties of high-entropy alloys," *Progress in Materials Science*, vol. 61, no. October 2013, pp. 1–93, 2014, doi: 10.1016/j.pmatsci.2013.10.001.

[64] A. Laszczyńska, J. Winiarski, B. Szczygieł, and I. Szczygieł, "Electrodeposition and characterization of Ni-Mo-ZrO 2 composite coatings," *Applied Surface Science*, vol. 369, pp. 224–231, 2016, doi: 10.1016/j.apsusc.2016.02.086.

[65] Y. Dong, K. Ren, Y. Lu, Q. Wang, J. Liu, and Y. Wang, "High-entropy environmental barrier coating for the ceramic matrix composites," *Journal of the European Ceramic Society*, vol. 39, no. 7, pp. 2574–2579, 2019, doi: 10.1016/j.jeurceramsoc.2019.02.022.

[66] X. Chang, M. Zeng, K. Liu, and L. Fu, "Phase Engineering of High-Entropy Alloys," *Advanced Materials*, vol. 32, no. 14, 2020, doi: 10.1002/adma.201907226.

[67] Y. F. Ye, Q. Wang, J. Lu, C. T. Liu, and Y. Yang, "High-entropy alloy: challenges and prospects," *Materials Today*, vol. 19, no. 6, pp. 349–362, 2016, doi: 10.1016/j.mattod.2015.11.026.

[68] S. Dasari *et al.*, "Highly tunable magnetic and mechanical properties in an Al0.3CoFeNi complex concentrated alloy," *Materialia*, vol. 12, no. May, 2020, doi: 10.1016/j.mtla.2020.100755.

[69] R. K. Mishra, P. P. Sahay, and R. R. Shahi, "Alloying, magnetic and corrosion behavior of AlCrFeMnNiTi high entropy alloy," *Journal of Materials Science*, vol. 54, no. 5, pp. 4433–4443, 2019, doi: 10.1007/s10853-018-3153-z.

[70] B. M. Moshtaghioun, D. Gómez-García, and A. Domínguez-Rodríguez, "Spark plasma sintering of titanium nitride in nitrogen: Does it affect the sinterability and the mechanical properties?," *Journal of the European Ceramic Society*, vol. 38, no. 4, pp. 1190–1196, 2018, doi: 10.1016/j.jeurceramsoc.2017.12.029.

[71] D. Demirskyi, H. Borodianska, T. S. Suzuki, Y. Sakka, K. Yoshimi, and O. Vasylkiv, "High-temperature flexural strength performance of ternary high-entropy carbide consolidated via spark plasma sintering of TaC, ZrC and NbC," *Scripta Materialia*, vol. 164, pp. 12–16, 2019, doi: 10.1016/j.scriptamat.2019.01.024.

[72] B. Gwalani *et al.*, "Strengthening of Al0.3CoCrFeMnNi-based ODS high entropy alloys with incremental changes in the concentration of Y2O3," *Scripta Materialia*, vol. 162, pp. 477–481, 2019, doi: 10.1016/j.scriptamat.2018.12.021.

[73] V. Soni, O. N. Senkov, J. P. Couzinie, Y. Zheng, B. Gwalani, and R. Banerjee, "Phase stability and microstructure evolution in a ductile refractory high entropy alloy Al10Nb15Ta5Ti30Zr40," *Materialia*, vol. 9, no. October 2019, p. 100569, 2020, doi: 10.1016/j.mtla.2019.100569.

[74] Y. Qiu *et al.*, "A lightweight single-phase AlTiVCr compositionally complex alloy," *Acta Materialia*, vol. 123, pp. 115–124, 2017, doi: 10.1016/j.actamat.2016.10.037.

[75] K. Balasubramanian, S. V. Khare, and D. Gall, "Energetics of point defects in rocksalt structure transition metal nitrides: Thermodynamic reasons for deviations from stoichiometry," *Acta Materialia*, vol. 159, pp. 77–88, 2018, doi: 10.1016/j.actamat.2018.07.074.

[76] G. Lee *et al.*, "Densification of zirconium nitride by spark plasma sintering and high voltage electric discharge consolidation: A comparative analysis," *Ceramics International*, vol. 41, no. 10, pp. 14973–14987, 2015, doi: 10.1016/j.ceramint.2015.08.042.

[77] M. S. Lucas *et al.*, "Magnetic and vibrational properties of high-entropy alloys," *Journal of Applied Physics*, vol. 109, no. 7, 2011, doi: 10.1063/1.3538936.

[78] E. S. Panina, N. Y. Yurchenko, S. V. Zherebtsov, M. A. Tikhonovsky, M. V. Mishunin, and N. D. Stepanov, "Structures and mechanical properties of Ti-Nb-Cr-V-Ni-Al refractory high entropy alloys," *Materials Science and Engineering A*, vol. 786, no. March, p. 139409, 2020, doi: 10.1016/j.msea.2020.139409.

[79] W. Guo *et al.*, "Microstructures and mechanical properties of ductile NbTaTiV refractory high entropy alloy prepared by powder metallurgy," *Journal of Alloys and Compounds*, vol. 776, pp. 428–436, 2019, doi: 10.1016/j.jallcom.2018.10.230.

[80] Z. Q. Xu, Z. L. Ma, M. Wang, Y. W. Chen, Y. D. Tan, and X. W. Cheng, "Design of novel low-density refractory high entropy alloys for high-temperature applications," *Materials Science and Engineering A*, vol. 755, no. March, pp. 318–322, 2019, doi: 10.1016/j.msea.2019.03.054.

[81] T. Yang *et al.*, "Multicomponent intermetallic nanoparticles and superb mechanical behaviors of complex alloys," *Science*, vol. 362, no. 6417, pp. 933–937, 2018, doi: 10.1126/science.aas8815.

[82] O. N. Senkov, S. V. Senkova, C. Woodward, and D. B. Miracle, "Low-density, refractory multi-principal element alloys of the Cr-Nb-Ti-V-Zr system:

Microstructure and phase analysis," *Acta Materialia*, vol. 61, no. 5, pp. 1545–1557, 2013, doi: 10.1016/j.actamat.2012.11.032.

[83] O. N. Senkov, C. Woodward, and D. B. Miracle, "Microstructure and Properties of Aluminum-Containing Refractory High-Entropy Alloys," *Jom*, vol. 66, no. 10, pp. 2030–2042, 2014, doi: 10.1007/s11837-014-1066-0.

[84] B. Gwalani *et al.*, "Influence of fine-scale B2 precipitation on dynamic compression and wear properties in hypo-eutectic Al0.5CoCrFeNi high-entropy alloy," *Journal of Alloys and Compounds*, vol. 853, p. 157126, 2021, doi: 10.1016/j.jallcom.2020.157126.

[85] C. S. babu, K. Sivaprasad, V. Muthupandi, and Jerzy. A. Szpunar, "Characterization of Nanocrystalline AlCoCrCuNiFeZn High Entropy Alloy Produced by Mechanical Alloying," *Procedia Materials Science*, vol. 5, pp. 1020–1026, 2014, doi: 10.1016/j.mspro.2014.07.392.

[86] P. Chauhan, S. Yebaji, V. N. Nadakuduru, and T. Shanmugasundaram, "Development of a novel light weight Al35Cr14Mg6Ti35V10 high entropy alloy using mechanical alloying and spark plasma sintering," *Journal of Alloys and Compounds*, vol. 820, p. 153367, 2020, doi: 10.1016/j.jallcom.2019.153367.

[87] K. M. Youssef, A. J. Zaddach, C. Niu, D. L. Irving, and C. C. Koch, "A novel low-density, high-hardness, high-entropy alloy with close-packed single-phase nanocrystalline structures," *Materials Research Letters*, vol. 3, no. 2, pp. 95–99, 2014, doi: 10.1080/21663831.2014.985855.

[88] X. Yang, Y. Zhang, and P. K. Liaw, "Microstructure and compressive properties of NbTiVTaAlx high entropy alloys," *Procedia Engineering*, vol. 36, pp. 292–298, 2012, doi: 10.1016/j.proeng.2012.03.043.

[89] S. Y. Chen, X. Yang, K. A. Dahmen, P. K. Liaw, and Y. Zhang, "Microstructures and crackling noise of AlxNbTiMoV high entropy alloys," *Entropy*, vol. 16, no. 2, pp. 870–884, 2014, doi: 10.3390/e16020870.

[90] W. R. Wang, W. L. Wang, and J. W. Yeh, "Phases, microstructure and mechanical properties of AlxCoCrFeNi high-entropy alloys at elevated temperatures," *Journal of Alloys and Compounds*, vol. 589, pp. 143–152, 2014, doi: 10.1016/j.jallcom.2013.11.084.

[91] N. D. Stepanov, N. Yu Yurchenko, D. G. Shaysultanov, G. A. Salishchev, and M. A. Tikhonovsky, "Effect of Al on structure and mechanical properties of AlxNbTiVZr (x = 0, 0.5, 1, 1.5) high entropy alloys," *Materials Science and Technology (United Kingdom)*, vol. 31, no. 10, pp. 1184–1193, 2015, doi: 10.1179/1743284715Y.0000000032.

[92] N. D. Stepanov, D. G. Shaysultanov, G. A. Salishchev, and M. A. Tikhonovsky, "Structure and mechanical properties of a light-weight AlNbTiV high entropy alloy," *Materials Letters*, vol. 142, pp. 153–155, 2015, doi: 10.1016/j.matlet.2014.11.162.

[93] X. Yan and Y. Zhang, "A body-centered cubic Zr50Ti35Nb15 medium-entropy alloy with unique properties," *Scripta Materialia*, vol. 178, pp. 329–333, 2020, doi: 10.1016/j.scriptamat.2019.11.059.

[94] X. Yan, P. K. Liaw, and Y. Zhang, "Ultrastrong and ductile BCC high-entropy alloys with low-density via dislocation regulation and nanoprecipitates," *Journal of Materials Science and Technology*, vol. 110, pp. 109–116, 2022, doi: 10.1016/j.jmst.2021.08.034.

[95] O. A. Waseem and H. J. Ryu, "Combinatorial development of the low-density high-entropy alloy Al10Cr20Mo20Nb20Ti20Zr10 having gigapascal strength at 1000 °C," *Journal of Alloys and Compounds*, vol. 845, p. 155700, 2020, doi: 10.1016/j.jallcom.2020.155700.

[96] B. Kang, J. Lee, H. J. Ryu, and S. H. Hong, "Microstructure, mechanical property and Hall-Petch relationship of a light-weight refractory Al0.1CrNbVMo high entropy alloy fabricated by powder metallurgical process," *Journal of Alloys and Compounds*, vol. 767, pp. 1012–1021, 2018, doi: 10.1016/j.jallcom.2018.07.145.

[97] Y. Liu *et al.*, "Microstructure and mechanical properties of refractory HfMo0.5NbTiV0.5Sixhigh-entropy composites," *Journal of Alloys and Compounds*, vol. 694, pp. 869–876, 2017, doi: 10.1016/j.jallcom.2016.10.014.

[98] W. G. Fahrenholtz and G. E. Hilmas, "Ultra-high temperature ceramics: Materials for extreme environments," *Scripta Materialia*, vol. 129, pp. 94–99, 2017, doi: 10.1016/j.scriptamat.2016.10.018.

[99] B. R. Golla, A. Mukhopadhyay, B. Basu, and S. K. Thimmappa, "Review on ultra-high temperature boride ceramics," *Progress in Materials Science*, vol. 111, no. December 2015, p. 100651, 2020, doi: 10.1016/j.pmatsci.2020.100651.

[100] J. Zhou, J. Zhang, F. Zhang, B. Niu, L. Lei, and W. Wang, "High-entropy carbide: A novel class of multicomponent ceramics," *Ceramics International*, vol. 44, no. 17, pp. 22014–22018, 2018, doi: 10.1016/j.ceramint.2018.08.100.

[101] D. O. Moskovskikh *et al.*, "High-entropy (HfTaTiNbZr)C and (HfTaTiNbMo)C carbides fabricated through reactive high-energy ball milling and spark plasma sintering," *Ceramics International*, vol. 46, no. 11, pp. 19008–19014, 2020, doi: 10.1016/j.ceramint.2020.04.230.

[102] J. Cabrero, F. Audubert, and R. Pailler, "Fabrication and characterization of sintered TiC-SiC composites," *Journal of the European Ceramic Society*, vol. 31, no. 3, pp. 313–320, 2011, doi: 10.1016/j.jeurceramsoc.2010.10.010.

[103] Q. Sun *et al.*, "Single-phase (Hf-Mo-Nb-Ta-Ti)C high-entropy ceramic: A potential high temperature anti-wear material," *Tribology International*, vol. 157, no. January, p. 106883, 2021, doi: 10.1016/j.triboint.2021.106883.

[104] S. Akrami, P. Edalati, M. Fuji, and K. Edalati, "High-entropy ceramics: Review of principles, production and applications," *Materials Science and Engineering R: Reports*, vol. 146, no. October, p. 100644, 2021, doi: 10.1016/j.mser.2021.100644.

[105] H. Chen, H. Xiang, F. Z. Dai, J. Liu, and Y. Zhou, "Porous high entropy (Zr0.2Hf0.2Ti0.2Nb0.2Ta0.2)B2: A novel strategy towards making ultrahigh temperature ceramics thermal insulating," *Journal of Materials Science and Technology*, vol. 35, no. 10, pp. 2404–2408, 2019, doi: 10.1016/j.jmst.2019.05.059.

[106] S. Failla, P. Galizia, S. Fu, S. Grasso, and D. Sciti, "Formation of high entropy metal diborides using arc-melting and combinatorial approach to study quinary and

quaternary solid solutions," *Journal of the European Ceramic Society*, vol. 40, no. 3, pp. 588–593, 2020, doi: 10.1016/j.jeurceramsoc.2019.10.051.

[107] E. Castle, T. Csanádi, S. Grasso, J. Dusza, and M. Reece, "Processing and Properties of High-Entropy Ultra-High Temperature Carbides," *Scientific Reports*, vol. 8, no. 1, pp. 1–12, 2018, doi: 10.1038/s41598-018-26827-1.

[108] J. Gild *et al.*, "High-Entropy Metal Diborides: A New Class of High-Entropy Materials and a New Type of Ultrahigh Temperature Ceramics," *Scientific Reports*, vol. 6, no. July, pp. 2–11, 2016, doi: 10.1038/srep37946.

[109] Y. Zhang *et al.*, "Dense high-entropy boride ceramics with ultra-high hardness," *Scripta Materialia*, vol. 164, pp. 135–139, 2019, doi: 10.1016/j.scriptamat.2019.01.021.

[110] F. Monteverde and F. Saraga, "Entropy stabilized single-phase (Hf,Nb,Ta,Ti,Zr)B2 solid solution powders obtained via carbo/boro-thermal reduction," *Journal of Alloys and Compounds*, vol. 824, 2020, doi: 10.1016/j.jallcom.2020.153930.

[111] C. Suryanarayana, "Suryanarayana_2001_Progress-in-Materials-Science.pdf," *Progress in Materials Science*, vol. 46, 2001, doi: 10.1016/S0079-6425(99)00010-9.

[112] Walunj Ganesh; Bearden Antonny; Patil Amit; Larimian Taban; Christudasjustus Jijo ; Gupta Rajiv; Borkar Tushar, "The Effect of Titanium Carbide and Spark Plasma Sintering Processing on Nickel–Titanium Carbide Composites."

[113] R. Orrù, R. Licheri, A. M. Locci, A. Cincotti, and G. Cao, "Consolidation/synthesis of materials by electric current activated/assisted

sintering," *Materials Science and Engineering R: Reports*, vol. 63, no. 4–6, pp. 127–287, 2009, doi: 10.1016/j.mser.2008.09.003.

[114] Z. A. Munir, D. V. Quach, and M. Ohyanagi, "Electric current activation of sintering: A review of the pulsed electric current sintering process," *Journal of the American Ceramic Society*, vol. 94, no. 1, pp. 1–19, 2011, doi: 10.1111/j.1551-2916.2010.04210.x.

[115] A. International, "G99-17: Standard Test Method for Wear Testing with a Pin-on-Disk Apparatus," *Annual Book of ASTM Standards*, vol. 05, no. 2016, pp. 1–6, 2017, doi: 10.1520/G0099-17.Copyright.

[116] J. W. Yeh *et al.*, "Nanostructured high-entropy alloys with multiple principal elements: Novel alloy design concepts and outcomes," *Advanced Engineering Materials*, vol. 6, no. 5, pp. 299–303, 2004, doi: 10.1002/adem.200300567.

[117] B. Gludovatz *et al.*, "Exceptional damage-tolerance of a medium-entropy alloy CrCoNi at cryogenic temperatures," *Nature Communications*, vol. 7, pp. 1–8, 2016, doi: 10.1038/ncomms10602.

[118] Y. Li, R. Li, and Y. Zhang, "Effects of Si Addition on Microstructure, Properties and Serration Behaviors of Lightweight Al-Mg-Zn-Cu Medium-entropy Alloys," *Research and Application of Materials Science*, vol. 1, no. 1, pp. 10–17, 2019, doi: 10.33142/msra.v1i1.666.

[119] B. Gwalani *et al.*, "Microstructure and wear resistance of an intermetallic-based Al0.25Ti0.75CoCrFeNi high entropy alloy," *Materials Chemistry and Physics*, vol. 210, pp. 197–206, 2018, doi: 10.1016/j.matchemphys.2017.06.034.

[120] M. Chen, W. Li, M. Shen, S. Zhu, and F. Wang, "Glass-ceramic coatings on titanium alloys for high temperature oxidation protection: Oxidation kinetics and microstructure," *Corrosion Science*, vol. 74, pp. 178–186, 2013, doi: 10.1016/j.corsci.2013.04.041.

[121] X. Sun, Z. Jiang, Z. Yao, and X. Zhang, "The effects of anodic and cathodic processes on the characteristics of ceramic coatings formed on titanium alloy through the MAO coating technology," *Applied Surface Science*, vol. 252, no. 2, pp. 441–447, 2005, doi: 10.1016/j.apsusc.2005.01.023.

[122] T. L. Alzubaydi, S. S. Alameer, T. Ismaeel, A. Y. Alhijazi, and M. Geetha, "In vivo studies of the ceramic coated titanium alloy for enhanced osseointegration in dental applications," *Journal of Materials Science: Materials in Medicine*, vol. 20, no. SUPPL. 1, pp. 35–42, 2009, doi: 10.1007/s10856-008-3479-1.

[123] H. Zhou, F. Li, B. He, J. Wang, and B. de Sun, "Air plasma sprayed thermal barrier coatings on titanium alloy substrates," *Surface and Coatings Technology*, vol. 201, no. 16–17, pp. 7360–7367, 2007, doi: 10.1016/j.surfcoat.2007.02.010.

[124] L. E. Murr *et al.*, "Fabrication of metal and alloy components by additive manufacturing: Examples of 3D materials science," *Journal of Materials Research and Technology*, vol. 1, no. 1, pp. 42–54, 2012, doi: 10.1016/S2238-7854(12)70009-1.

[125] A. Zhecheva, W. Sha, S. Malinov, and A. Long, "Enhancing the microstructure and properties of titanium alloys through nitriding and other surface engineering methods," *Surface and Coatings Technology*, vol. 200, no. 7, pp. 2192–2207, 2005, doi: 10.1016/j.surfcoat.2004.07.115.

[126] R. Feng *et al.*, "Design of light-weight high-entropy alloys," *Entropy*, vol. 18, no. 9, pp. 16–29, 2016, doi: 10.3390/e18090333.

[127] A. Kumar and M. Gupta, "An insight into evolution of light weight high entropy alloys: A review," *Metals*, vol. 6, no. 9, 2016, doi: 10.3390/met6090199.

[128] J. M. Sanchez, I. Vicario, J. Albizuri, T. Guraya, and J. C. Garcia, "Phase prediction, microstructure and high hardness of novel light-weight high entropy alloys," *Journal of Materials Research and Technology*, vol. 8, no. 1, pp. 795–803, 2019, doi: 10.1016/j.jmrt.2018.06.010.

[129] R. Feng *et al.*, "Phase stability and transformation in a light-weight high-entropy alloy," *Acta Materialia*, vol. 146, pp. 280–293, 2018, doi: 10.1016/j.actamat.2017.12.061.

[130] B. Gwalani, R. Salloom, T. Alam, S. V. Grace, S. Srinivasan, and R. Banerjee, "Investigation of Clusters and Their Effect on Grain Growth in Single Phase AlxCoCrFeNi High Entropy Alloys," *Microscopy and Microanalysis*, vol. 24, no. S1, pp. 2214–2215, 2018, doi: 10.1017/s1431927618011558.

[131] T. Borkar *et al.*, "A Combinatorial Approach for Assessing the Magnetic Properties of High Entropy Alloys: Role of Cr in AlCoxCr1–xFeNi," *Advanced Engineering Materials*, vol. 19, no. 8, pp. 1–13, 2017, doi: 10.1002/adem.201700048.

[132] R. Feng *et al.*, "lightweight high-entropy alloys," *Nature Communications*, vol. 12, no. 4329, pp. 6–15, 2021, doi: 10.1038/s41467-021-24523-9.

[133] M. Palm and J. Lacaze, "Assessment of the Al e Fe e Ti system," *Intermetallics*, vol. 14, pp. 1291–1303, 2006, doi: 10.1016/j.intermet.2005.11.026.

[134] P. R. Alonso, P. H. Gargano, P. B. Bozzano, G. E. Ramírez-caballero, P. B. Balbuena, and G. H. Rubiolo, "Intermetallics Combined ab initio and experimental study of A2 þ L2 1 coherent equilibria in the Fe e Al e X (X ¼ Ti , Nb , V) systems," *Intermetallics*, vol. 19, pp. 1157–1167, 2011, doi: 10.1016/j.intermet.2011.03.025.

[135] D. E. Fontaine and R. I. O. May, "ANALYSIS OF CLUSTERING AND ORDERING STABILITY," *j.phys.chem.solids*, vol. 33, no. 1, pp. 297–310, 1972.

[136] G. Song, Z. Sun, J. D. Poplawsky, Y. Gao, and P. K. Liaw, "Microstructural evolution of single Ni2TiAl or hierarchical NiAl/Ni2TiAl precipitates in Fe-Ni-Al-Cr-Ti ferritic alloys during thermal treatment for elevated-temperature applications," *Acta Materialia*, vol. 127, pp. 1–16, Apr. 2017, doi: 10.1016/j.actamat.2017.01.011.

[137] S. Jiang *et al.*, "Ultrastrong steel via minimal lattice misfit and high-density nanoprecipitation," *Nature*, vol. 544, no. 7651, pp. 460–464, Apr. 2017, doi: 10.1038/nature22032.

[138] J. Douglas Eshelby and B. J. D EsHELBY, "Mathematical and physical sciences," *Proceedings of the Royal Society of London. Series A*, p. 241, 1957, doi: 10.1098/rspa.1957.0133ï.

[139] H. S. Seo, T. Y. Lee, J. G. Wen, I. Petrov, J. E. Greene, and D. Gall, "Growth and physical properties of epitaxial HfN layers on MgO(001)," *Journal of Applied Physics*, vol. 96, no. 1, pp. 878–884, 2004, doi: 10.1063/1.1759783.

[140] K. Zhang *et al.*, "Growth and mechanical properties of epitaxial NbN(001) films on MgO(001)," *Surface and Coatings Technology*, vol. 288, pp. 105–114, 2016, doi: 10.1016/j.surfcoat.2016.01.009.

[141] C. S. Shin *et al.*, "Growth and physical properties of epitaxial metastable cubic TaN(001)," *Applied Physics Letters*, vol. 75, no. 24, pp. 3808–3810, 1999, doi: 10.1063/1.125463.

[142] J. E. Sundgren, "Structure and properties of TiN coatings," *Thin Solid Films*, vol. 128, no. 1–2, pp. 21–44, 1985, doi: 10.1016/0040-6090(85)90333-5.

[143] A. B. Mei *et al.*, "Physical properties of epitaxial ZrN/MgO(001) layers grown by reactive magnetron sputtering," *Journal of Vacuum Science & Technology A: Vacuum, Surfaces, and Films*, vol. 31, no. 6, p. 061516, 2013, doi: 10.1116/1.4825349.

[144] B. D. Ozsdolay, K. Balasubramanian, and D. Gall, "Cation and anion vacancies in cubic molybdenum nitride," *Journal of Alloys and Compounds*, vol. 705, pp. 631–637, 2017, doi: 10.1016/j.jallcom.2017.02.072.

[145] B. D. Ozsdolay, C. P. Mulligan, K. Balasubramanian, L. Huang, S. V. Khare, and D. Gall, "Cubic β-WNx layers: Growth and properties vs N-to-W ratio," *Surface and Coatings Technology*, vol. 304, pp. 98–107, 2016, doi: 10.1016/j.surfcoat.2016.06.079.

[146] L. Rissanen, M. Neubauer, K. P. Lieb, and P. Schaaf, "The new cubic iron-nitride phase FeN prepared by reactive magnetron sputtering," *Journal of Alloys and Compounds*, vol. 274, no. 1–2, pp. 74–82, 1998, doi: 10.1016/S0925-8388(98)00594-5.

[147] A. B. Mei *et al.*, "Elastic constants, Poisson ratios, and the elastic anisotropy of VN(001), (011), and (111) epitaxial layers grown by reactive magnetron sputter deposition," *Journal of Applied Physics*, vol. 115, no. 21, 2014, doi: 10.1063/1.4881817.

[148] D. Moskovskikh *et al.*, "Extremely hard and tough high entropy nitride ceramics," *Scientific Reports*, vol. 10, no. 1, pp. 1–8, 2020, doi: 10.1038/s41598-020-76945-y.

[149] R. Z. Zhang and M. J. Reece, "Review of high entropy ceramics: design, synthesis, structure and properties," *Journal of Materials Chemistry A*, vol. 7, no. 39, pp. 22148–22162, 2019, doi: 10.1039/c9ta05698j.

[150] K. A. Kane, B. A. Pint, D. Mitchell, and J. A. Haynes, "Journal of the European Ceramic Society Oxidation of ultrahigh temperature ceramics : kinetics , mechanisms , and applications," *Journal of the European Ceramic Society*, vol. 41, no. 13, pp. 6130–6150, 2021, doi: 10.1016/j.jeurceramsoc.2021.05.055.

[151] S. H. Jhi, S. G. Louie, M. L. Cohen, and J. Ihm, "Vacancy hardening and softening in transition metal carbides and nitrides," *Physical Review Letters*, vol. 86, no. 15, pp. 3348–3351, 2001, doi: 10.1103/PhysRevLett.86.3348.

[152] T. Csanádi, E. Castle, M. J. Reece, and J. Dusza, "Strength enhancement and slip behaviour of high-entropy carbide grains during micro-compression," *Scientific Reports*, vol. 9, no. 1, pp. 1–14, 2019, doi: 10.1038/s41598-019-46614-w.

[153] F. Z. Dai, B. Wen, Y. Sun, H. Xiang, and Y. Zhou, "Theoretical prediction on thermal and mechanical properties of high entropy (Zr0.2Hf0.2Ti0.2Nb0.2Ta0.2)C by deep learning potential," *Journal of Materials Science and Technology*, vol. 43, pp. 168–174, 2020, doi: 10.1016/j.jmst.2020.01.005.

[154] B. Ye, T. Wen, and Y. Chu, "High-temperature oxidation behavior of (Hf0.2Zr0.2Ta0.2Nb0.2Ti0.2)C high-entropy ceramics in air," *Journal of the American Ceramic Society*, vol. 103, no. 1, pp. 500–507, 2020, doi: 10.1111/jace.16725.

[155] H. Zhang, D. Hedman, P. Feng, G. Han, and F. Akhtar, "A high-entropy B4(HfMo2TaTi)C and SiC ceramic composite," *Dalton Transactions*, vol. 48, no. 16, pp. 5161–5167, 2019, doi: 10.1039/c8dt04555k.

[156] X. Li, Z. Ao, J. Liu, H. Sun, A. I. Rykov, and J. Wang, "Topotactic Transformation of Metal-Organic Frameworks to Graphene-Encapsulated Transition-Metal Nitrides as Efficient Fenton-like Catalysts," *ACS Nano*, vol. 10, no. 12, pp. 11532–11540, Dec. 2016, doi: 10.1021/acsnano.6b07522.

[157] E. Lewin, "Multi-component and high-entropy nitride coatings - A promising field in need of a novel approach," *Journal of Applied Physics*, vol. 127, no. 16. 2020. doi: 10.1063/1.5144154.

[158] F. H. (Sam)Froes, C. Suryanarayana, K. Russell, and C.-G. Li, "Synthesis of intermetallics by mechanical alloying," *Materials Science and Engineering: A*, vol. 192–193, pp. 612–623, Feb. 1995, doi: 10.1016/0921-5093(94)03285-8.

[159] C. Suryanarayana, "Mechanical alloying and milling," *Progress in Materials Science*, vol. 46, 2001, doi: 10.1016/S0079-6425(99)00010-9.

[160] U. Jansson and E. Lewin, "Sputter deposition of transition-metal carbide films - A critical review from a chemical perspective," *Thin Solid Films*, vol. 536, pp. 1–24, 2013, doi: 10.1016/j.tsf.2013.02.019.

[161] I. Milošev, H. H. Strehblow, and B. Navinšek, "Comparison of TiN, ZrN and CrN hard nitride coatings: Electrochemical and thermal oxidation," *Thin Solid Films*, vol. 303, no. 1–2, pp. 246–254, 1997, doi: 10.1016/S0040-6090(97)00069-2.

[162] K. Zhang *et al.*, "Growth and mechanical properties of epitaxial NbN(001) films on MgO(001)," *Surface and Coatings Technology*, vol. 288, pp. 105–114, 2016, doi: 10.1016/j.surfcoat.2016.01.009.

[163] B. D. Ozsdolay, C. P. Mulligan, M. Guerette, L. Huang, and D. Gall, "Epitaxial growth and properties of cubic WN on MgO(001), MgO(111), and Al2O3(0001)," *Thin Solid Films*, vol. 590, pp. 276–283, 2015, doi: 10.1016/j.tsf.2015.08.002.

[164] X. Yan, L. Constantin, Y. Lu, J. F. Silvain, M. Nastasi, and B. Cui, "(Hf0.2Zr0.2Ta0.2Nb0.2Ti0.2)C high-entropy ceramics with low thermal conductivity," *Journal of the American Ceramic Society*, vol. 101, no. 10, pp. 4486–4491, 2018, doi: 10.1111/jace.15779.

[165] D. Demirskyi, O. Vasylkiv, and K. Yoshimi, "Allotropic strengthening and in situ phase transformations during ultra-high-temperature flexure of bulk tantalum nitride," *Materials Science and Engineering A*, vol. 826, no. August, p. 141954, 2021, doi: 10.1016/j.msea.2021.141954.

[166] S. Ran and L. Gao, "Spark plasma sintering of nanocrystalline niobium nitride powders," *Journal of the American Ceramic Society*, vol. 91, no. 2, pp. 599–602, 2008, doi: 10.1111/j.1551-2916.2007.02183.x.

[167] Y. Ahn, N. G. Cho, S. H. Lee, and D. Lee, "Lateral crack in abrasive wear of brittle materials," *JSME International Journal, Series A: Solid Mechanics and*

Material Engineering, vol. 46, no. 2. pp. 140–144, 2003. doi: 10.1299/jsmea.46.140.

[168] C. Hu *et al.*, "Negative effect of vacancies on cubic symmetry, hardness and conductivity in hafnium nitride films," *Scripta Materialia*, vol. 108, pp. 141–146, 2015, doi: 10.1016/j.scriptamat.2015.07.002.

[169] Y. N. Chang and F. I. Wei, "High temperature oxidation of low alloy steels," *Journal of Materials Science*, vol. 24, no. 1, pp. 14–22, 1989, doi: 10.1007/BF00660927.

[170] A. Nisar, C. Zhang, B. Boesl, and A. Agarwal, "A perspective on challenges and opportunities in developing high entropy-ultra high temperature ceramics," *Ceramics International*, no. June, pp. 1–9, 2020, doi: 10.1016/j.ceramint.2020.07.066.

Appendix

PUBLICATION

• **G. Walunj** et al., "Mechanical and Tribological Behavior of Mechanically Alloyed Ni-TiC Composites Processed via Spark Plasma Sintering." Materials 2020, 13, 5306

• **G. Walunj,** U. S. Waware, A. M. S. Hamouda, and T. Borkar, "Electrodeposition of Duplex Ni–B–Zn/Co Composite Coatings," Jom, vol. 72, no. 12, pp. 4296–4304, 2020.

• **G. Walunj** et al., "The Effect of Titanium Carbide and Spark Plasma Sintering Processing on Nickel–Titanium Carbide Composites". In: Srivatsan T.S., Harrigan, Jr. W.C., Hunyadi Murph S. (eds) Metal-Matrix Composites. The Minerals, Metals & Materials Series. Springer, Cham 2021, vol. 0, no. 0, pp. 65-73

• A. Patil, **G. Walunj** et al., " Tribological Behavior of in situ Processed NI-Ti-C Nanocomposites ," Tribol. Trans., vol. 0, no. 0, pp. 1– 13, 2020.

• A. Patil, **G. Walunj**, F. Ozdemir, R. K. Gupta, and T. Borkar, "Tribological Behavior of Carbon-Based Nanomaterial-Reinforced Nickel Metal Matrix Composites" *Materials* 14, no. 13: 3536, 2021.

• A. Patil, **G. Walunj** et al., "The Mechanical Performance of In Situ Processed Nickel-Titanium-Graphite Metal Matrix Composites: Influence of Processing", In: Srivatsan T.S., Harrigan, Jr. W.C., Hunyadi Murph S. (eds) Metal-Matrix Composites. The Minerals, Metals & Materials Series. Springer, Cham. 2021, vol. 0, no. 0, pp. 3-15

• R. Gorla, M. K. Pallikonda, **G.Walunj**, "Use of Rayleigh Distribution Method for Assessment of Wind Energy Output in Cleveland-Ohio," vol. 1, no. 1, pp. 11–18, 2020.

• L. Esteves, C.S. Witharamage, J. Christudasjustus, **G. Walunj** et al., "Corrosion behavior of AA5083 produced by high-energy ball milling," J. Alloys Compd., vol. 857, p. 158268, 2021.

• T. Larimian, B. AlMangour, D. Grzesiak, **G. Walunj**, and T. Borkar, "Effect of Laser Spot Size, Scanning Strategy, Scanning Speed, and Laser Power on Microstructure and Mechanical Behavior of 316L Stainless Steel Fabricated via Selective Laser Melting," J. Mater. Eng. Perform., no. Ref 10, 2021.

• L. Esteves, J. Christudasjustus, S.P. O'Brien, C.S. Witharamage, A.A. Darwish, **G. Walunj**, P. Stack, T. Borkar, R.E. Akans, R.K. Gupta, "Effect of V content on corrosion behavior of high-energy ball milled AA5083", Corrosion Science, Volume 186, 2021, 109465, ISSN 0010-938X